VNIVERSITAT DE VALÈNCIA

Departamento de Física Teórica

Cosmological implications of Standard Model extensions

Ph.D. Thesis

Manuel Peña Jiménez

Supervisor

Dr. Nuria Rius Dionis

Valencia, December 2012.

NURIA RIUS DIONIS, Profesora Titular del Departamento de Física Teórica de la Universitat de València,

CERTIFICA:
Que la presente memoria "COSMOLOGICAL IMPLICATIONS OF STANDARD MODEL EXTENSIONS" ha sido realizada bajo su dirección en el Departamento de Física Teórica de la Universitat de València, por MANUEL PEÑA JIMENEZ y constituye su Tesis para optar al grado de Doctor en Física.

Y para que así conste, en cumplimiento de la legislación vigente, presenta en el Departamento de Física Teórica de la Universitat de València la referida Tesis Doctoral, y firma el presente certificado.

Valencia, a 27 de Diciembre de 2012.

Nuria Rius Dionis

A mi família

Agradecimientos-Aknoledgements

Tantas cosas que decir, a tanta gente que agradecer tanto, y me falta tiempo, y por qué no admitirlo, ganas. Muy a mi pesar estos agradecimientos se me han quedado un poco escuetos, pero sinceramente debe y quiero acabar ya ;).

Esta tesis se ha escrito gracias al apoyo de mi tutora, Nuria Rius Dionís, y es a ella a quien primero quiero agradecer de todo corazón el tiempo y dedicación que ella me ha prestado. Y aunque alguna vez hayamos tenido discrepancias (he de confesar que no soy el estudiante modelo que todo profesor puede querer), sin su apoyo esta tesis nunca habría visto la luz. Ha sido un verdadero placer trabajar contigo, Nuria.

Mi segunda dedicatoria va a parar a mi familia, en especial a mi padre y a mi tía Angelita, pero también al resto de mis tíos y primos. He de confesar que me siento muy unido a mi familia, así que para mí, su apoyo incondicional ha sido muy importante. Cabe destacar que mi padre, pese a desear que yo fuese psicólogo (aún no sé por qué), y pese a no tener ni idea de lo que hago siempre ha estado a mi lado, a las duras y a las maduras. Mención especial para la persona con la que vivo, mi tía Angelita, que a parte de comprenderme, ha sabido buscar y enterarse de qué es lo que hago. Y eso teniendo 71 años, que no son pocos.

Retomando el hilo dedicado puramente a la ciencia, la siguiente persona a la que quería agradecer su ayuda es a Olga Mena. Siempre se ha interesado por el desarrollo de mi trabajo, dándome ánimos cuando los necesitaba y ofreciéndome la posibilidad de trabajar junto a ella en una ocasión, tiempo en el que me pude dar cuenta de lo inmensamente trabajadora que es. Además de todo ello, ella me ha ayudado en la escritura de mi tesis, cosa por la que le estoy profundamente agradecido.

Por supuesto he de agradecer a Carlos Peña su dedicación a mi trabajo. Siempre se ha preocupado por el desarrollo de mi tesis y ha intentado empujarme hacia delante siempre que me he estancado. Bajo su supervisión realizé el trabajo de final de máster y, aunque nuestros gustos personales en lo referente a ciéncia no nos han llevado a trabajar conjuntamente, siempre ha intentado ayudar en la medida de lo posible, incluso fuera de marco de la física.

Throughout the PhD I realized two short visits to foreign centers. In such visits I was pleased to work with David Wands in Portsmouth and Mark Wyman in Chicago. I am very thankful with both of them for taking me for several months and, although there was no final publications of the works done in any of these stays, I consider I learned a lot about inflationary theories, thing that has been useful for the development of my thesis. Also I

must confess I met with such great people (that finally I have come to call them friends) in my time off the office in both places. I thank them also for the time spent with me and, why not, for the beers had in that time.

Nel corso del mio lavoro di tesi, un ruolo di grande importanza è stato assunto da Paolo Criminelli. Durante i mesi di istanza a Trieste, mi ha dato la possibilità di lavorare con lui, un suo studente di dottorato, Marko Simonovic, e un suo collaboratore, Jorge Noreña, sullo studio di un modello inflazionario. Senza il loro contributo la mia tesi non sarebbe risultata così completa. Lavorando a stretto contatto con lui, mi sono reso conto di quanto sia una persona dedita al suo lavoro e ai suoi studenti. Per questo gli sono profandamente riconoscente e lo ringrazio per il tempo che mi ha dedicato.

Esto no serían unos agradecimientos dignos si no se incluyesen en ellos las personas con las que he compartido algo más que ciencia ya sea en el mundo de la física o fuera. No quiero dar nombre porque he de reconocer que afortunadamente he compartido mi vida con mucha gente y, no pudiendo nombrarlos a todos, me ha parecido mas correcto no nombrar a ninguno. Pero si te sientes aludido/a, tranquilo/a, estás en esta lista. Muchas gracias por estar ahí, de verdad, a TODOS!

Resumen

Los modelos estándar tanto de partículas como de Cosmología son capaces de describir una gran cantidad de datos experimentales con una increíble precisión. Sin embargo, en ciertas áreas de estos modelos aún existen discrepancias frente a lo descrito teóricamente y lo observado en la naturaleza. En concreto, el modelo estándar de partículas es incapaz de dar una explicación del patrón de masas y mezclas observadas en las partículas conocidas (siendo de suma importancia la masa de los neutrinos) o por qué el Universo está formado por partículas, sin presencial sustancial de antipartículas (asimetría bariónica). Desde un punto de vista Cosmógico, tampoco es posible explicar el contenido energético de nuestro Universo. Únicamente el 4% de la densidad de energía del Universo está formada por partículas del modelo estándar. El resto está, en un 23% en forma de materia no conocida y con una interacción débil, conocida como materia oscura, y en un 73% en forma de un fluido con una ecuación de estado aproximadamente igual a la de la energí de vacío de cualquier teoría cuántica de campos ($p = -\rho$). Además, el modelo Cosmológico del Big Bang es incapaz de dar una interpretación clara de las excepcionalmente precisas condiciones iniciales que debe tener el Universo para poder dar una explicación de las observaciones, en concreto, de la homogeneidad y la isotropía presentes en el Universo conocido.

En esta tesis nos vamos a centrar en dos marcos teóricos desarrollados para intentar dar una solucón a algunos de los problemas encionados con anterioridad. Dichos marcos se conocen como *Inflación* y *Leptogénesis*. El primero supone un periodo de expansión acelerada en los inicios de nuestro Universo mediante el cual se pueden solucionar los problemas de homogeneidad e isotropía, así como otros no mencionados como la generación de las perturbaciones iniciales que dieron lugar a a las estructuras actuales del Universo, o la ausencia de *relics*, objetos predichos por ciertas teorías más allá del modelo estándar de partículas que en caso de estar presentes habrían modificado la estructura o evolución del Universo considerablemente. En su versión más simple, dicha expansión acelerada es provocada por un campo escalar que evoluciona al mínimo de su potencial muy lentamente, debido a que el potencial es extremadamente plano. La ecuación de estado asociada a ese campo es aproximadamente igual a la de la energía de vacío, causando una expansión acelerada. El segundo de ellos, Leptogénesis, da una explicación a la asimetría bariónica a través de la conversión parcial de una previa asimetría leptónica mediante los procesos denominados *esfalerones*. Dicho marco se engloba dentro de las teorías *seesaw*, en donde el modelo estándar de partículas se amplía con al menos dos neutrinos pesados de Majorana. Estas teorías sirven para dar una interpretación de la diminuta masa de los neutrinos ligeros. En

los modelos de Leptogénesis, la asimetría leptónica es provocada por la desintegración de algunos de dichos neutrinos pesados en partículas del modelo estándar.

Después de una breve reseña a los acontecimientos más importantes en la historia del Universo en el Capítulo 1, los Capítulos 2 y 3 están dedicados a una introducción a la Cosmología actual y a los métodos observacionales más importantes para obtener los parámetros cosmológicos. En los subsecuentes Capítulos (4, 5 y 6) se expone la base de los modelos de Inflación y Leptogénesis que más tarde se utilizará en los trabajos realizados (Capítulos 7, 8 y 9). Por último se presentan las conclusiones más destacables de la tesis, Capítulo 10.

Una de las características mas reseñables de los modelos inflacionarios es que predicen un *power spectrum* que es prácticamente invariante bajo un cambio de escala. Esta predicción ha sido confirmada por las diferentes observaciones de las perturbaciones del fondo cósmico de microondas. Dicha invariancia es debida a la simetría bajo translación temporal presente en las teorías de Inflación ($t \to \tilde{t} = t + c$), siendo c una constante, por lo que cualquier teoría inflacionaria ha de contar con esa simetría aproximada. En [1] nos planteamos la posibilidad de extender dicha invariancia a una simetría de reparametrización temporal completa ($t \to \tilde{t} = \tilde{t}(t)$). La implementación de esta provoca que los términos permitidos en el lagrangiano de perturbaciones son ahora muchos menos. Como consecuencia se observa que las funciones de onda de las perturbaciones del campo que provoca Inflación se comportan como si estuviesen en un espacio de Minkowsky. Sin embargo, la correcta generación de perturbaciones clásicas se obtiene al tener en cuenta que esta fase debe desembocar en un Universo de Friedmann-Robertson-Walker. Otro aspecto destacable de la teoría es que todas las funciones de correlación a cualquier orden están fijadas por únicamente dos parámetros, la amplitud del *power spectrum* y la velocidad del sonido de las perturbaciones.

El estudio de las perturbaciones del fondo cósmico de microondas ha logrado obtener una precisión inimaginable tan solo 20 años atrás acerca de muchos parámetros cosmológicos, relacionados por ejemplo con el contenido de materia y energía de nuestro Universo, o su geometría espacial. De especial importancia para nuestro trabajo son los parámetros relacionados con Inflación. Cantidades como la amplitud del *power spectrum* de las perturbaciones escalares y tensoriales o su desviación de la invariancia de escala, medida por su *spectral index* han podido ser medidas o acotadas extraordinariamente, dando una información muy importante sobre el proceso mismo de Inflación. No obstante, para la extracción de esos valores, as como de tantos otros a través del estudio de las perturbaciones del fondo cósmico de microondas, algunas suposiciones han sido hechas en la literatura. Como ejemplo, en el experimento WMAP se supone una reionización instantánea del Universo a un *redshift* z comprendido entre 6 y 28. Dado la falta de información acerca de los procesos exactos que dieron lugar a la reionización, en [2] nos preguntamos cual sería el efecto de un esquema de reionización más general, en el caso en el cual dicho proceso tuviera una duración no nula. La conclusión mas reseñable es la relajación de los límites en el valor del *running* α, que mide la variación respecto a la escala del *spectral index*. Teniendo en cuenta los nuevos límites, los modelos híbridos de Inflación, anteriormente excluidos, pasan a estar dentro de los límites.

En lo referente a Leptogénesis, para el caso estándar en el que existe una jerarquía fuerte en las masas de los neutrinos pesados que generan la asimetría ($M_1 \ll M_2 \ll M_3$), existe un límite en la cantidad de asimetría CP que dicha desintegración puede generar, que a su vez se traduce en un límite a la masa del neutrino más ligero de los tres del orden de $M_1 \gtrsim 10^9$ GeV, el as conocido como límite de Davidson-Ibarra. Es necesario entonces que la temperatura de *reheating* que alcanza el Universo después de Inflación sea como mínimo algo superior a 10^9 GeV para as poder generar los neutrinos pesados térmicamente. En caso contrario, Leptogénesis no podría tener lugar en este contexto. Esta temperatura mínima a su vez genera ciertas dificultades en teorías más allá del modelo estándar de partículas. Es de especial importancia el caso de Supersimetría y la generación de gravitinos en el Universo primitivo. Con una temperatura de *reheating* tan elevada, en el contexto de supersimetría, en los origines de nuestro Universo se hubiese generado una cantidad tal de gravitinos que su desintegración tardía hubiese comprometido la Nucleosntesis primordial. Sin embargo, el caso del gravitino no es el único que entra en conflicto con elevadas temperaturas de *reheating*. La presencia sustancial de monopólos magnéticos o de *cosmic strings* también hubiesen tenido consecuencias muy improtantes en la evolución del Universo que no se obtienen de las observaciones. Una posible solución al problema es suponer dos neutrinos muy degenerados ($M_2 - M_1 \sim \Gamma_N$). En este caso, la asimetría CP puede ser mucho más grande, y Leptogénesis puede ser viable a temperaturas del orden de ~ 1 TeV. Este escenario ha sido ampliamente estudiado en la literatura. Otra posible solución aparece cuando los operadores que causan la asimetría CP son diferentes de los que dan masa a los neutrinos ligeros. Dichos operadores escapan del límite de Davidson-Ibarra, sin embargo al orden mas bajo, estos operadores conservan el número leptónico total L. Es por ello que es necesario que los efectos de sabor sean importantes para obtener suficiente asimetría leptónica.

En [3] estudiamos precisamente este último caso, centrándonos en la parte que conserva el número leptónico. Encontramos que Leptogénesis es viable para masas del neutrino pesado más ligero del orden de 10^6 GeV, aliviando los problemas relacionados con altas temperaturas de *reheating*, en especial el del gravitino.

Introduction

The standard models of both particle physics and Cosmology are the fundamental tool from which we can explain, on one hand, the interactions among particles and on the other hand, the structure and evolution of our Universe. In the Standard Model (SM) of particles, the matter contents are quarks and leptons, replicated in three families. The strong interaction, described by the Quantum Cromodynamics (QCD) and based on the $SU(3)$ group, is present only in the quark sector. Meanwhile, electromagnetic and weak interactions affect both sectors (quarks and leptons). Electromagnetic interaction affects any particle with electric charge. Therefore, only the neutral leptons, called neutrinos, do not feel the electromagnetic interaction. Weak interactions affect all the known particles and it is the only one affecting neutrinos. Electromagnetic and weak interactions become one unified interaction at energies larger than 246 GeV, giving rise to what is known as the electroweak interaction, based on the group $SU(2)_L \times U(1)_Y$. In addition, the Cosmological Model, based on the General Relativity theory and on the Cosmological Principle, describes the evolution of the Universe at large scales given its matter content. The matter content of the Universe varies as the Universe evolves, and this variation depends on both the evolution of the Universe and the interactions among the particles. For this reason, the Cosmological Model needs a good knowledge of the particle theory and their interactions.

Despite the correct and quite accurate description of most of the experiments and observations, there are some open problems in Nature which cannot be explained within the particle physics and cosmological models. Regarding the SM of particles, there is the flavour puzzle, *i.e.*, the lack of understanding of the observed pattern of masses and mixings of the SM particles. From a cosmological point of view, the particle physics and cosmological models cannot give an answer about the origin of the baryon asymmetry of the Universe, namely, the difference among the number of baryons and antibaryons present in the Universe. Futhermore, only a 4% of the total energy density of the Universe is explained in terms of Standard Model particles. The rest is in the form of non visible (and not or almost not interacting) matter, usually called *dark matter*, whose total amount represents about the 23% of the total energy, and the remaining 73% is in the form of a fluid with an equation of state $p \approx -\rho$, close to the equation of state of a vacuum energy ($p = -\rho$). This fluid is known as *dark energy* and it is the responsible of the current acceleration of the expansion of the Universe. Both kinds of matter and energy have a totally unknown origin. Regarding only the Cosmological Model, there is no physical reasons why the Universe should look extremely homogeneous and isotropic on large scales, as seen by observations of the cosmic

microwave background (CMB). Despite being that homogeneos, the Universe presented tiny perturbations in the last scattering surface, when it was $380,000$ years old, which have no other reason to appear unless you suppose they were present since the beginning of the Universe. To try to address these questions, several extensions of both standard models have been proposed. In the development of this thesis we have focussed on two of them, namely *Inflation* and *Leptogenesis*. The first one is meant to solve the problem of the homogeneity and isotropy of the Universe and also the generation of the perturbations present at early times, among other questions that will be explained. The second one ties together the explanation for the tiny mass of the light neutrinos and the generation of the baryon asymmetry.

The Universe seems to be very homogeneous and isotropic at large scales. CMB observations show that when the Universe was $380,000$ years old, density fluctuations were about 10^{-5} of the mean value. This fact comes into conflict with the standard Cosmological Model, since it is easy to show that the Universe was made of about a thousand causally disconnected regions at the CMB time and hence, there is no physical reason why all these regions were so similar if they had not had time to communicate one to each other. This problem is known as the *horizon problem*. Together with it, there exists another problem in the Cosmological Model, the so called, *flatness problem*. The Universe today seems to be spatially flat. The energy density associated to the curvature component is constrained to be less the 1% of the total energy density of the Universe. Considering that the curvature component grows with cosmic time compared to matter and/or radiation, at earlier times, this deviation with respect to zero is getting smaller. This means that at the beginning of the Universe that deviation from a purely flat Universe should have been negligible. As an example, at the Planck scale the energy associated with the curvature term could represent at most one part in 10^{61} of the total energy.

Both problems, among some others that will be explained in this thesis, can be solved by means of a mechanism known as *Inflation*. In that mechanism, there is a period at very early times when the Universe suffered from an accelerated expansion, caused in the simplest models by a single scalar field, the *inflaton*, with a potential shape extremely flat. As we will see, this hypothetical acceleration, *i.e.*, Inflation, can solve all the mentioned problems, as well as the generation of the small perturbations which seed the structures we observe today in the Universe.

Primordial nucleosynthesis and the recent measurement of the cosmic microwave background (CMB) imply that the baryon to photon density ratio in the Universe is $(6.1 \pm 0.3) \times 10^{-10}$. The dynamical production mechanism of this baryon asymmetry is known as Baryogenesis. Although the Standard Model contains all the necessary ingredients to produce the baryon asymmetry during the electroweak phase transition, it predicts a value which is several orders of magnitude smaller than the measured one. Therefore, if we want to explain the baryon asymmetry of the Universe, some extension of the Standard Model must be considered. Another evidence of Physics beyond the SM are the masses of the light neutrinos. Both problems are naturally explained in the context of the seesaw mechanism. In type I seesaw models, the SM is extended with at least two singlet Majorana neutrinos

which can produce the observed baryon asymmetry via Leptogenesis. In this framework, the decay out of equilibrium of the heavy Majorana neutrinos leads to a lepton asymmetry, partially converted into a baryon asymmetry via the sphaleron interactions.

Our major goal is to develop theoretical models of both Inflation and Leptogenesis scenarios, which carry new ideas yet unexplored and/or can alleviate some tension or discrepancy still present in these frameworks. We now expose briefly the works done in this thesis.

In the case of single-field slow-roll Inflation, the flatness of the potential of the inflaton induces an approximate symmetry of the lagrangian under time translation. In Ref. [1] we analyze the consequences of extending that symmetry to a full time-diffeomorphism symmetry, in the context of effective field theory. This "upgraded" symmetry implies that not all the terms included in the lagrangian in usual slow-roll Inflation, with just the time-translation symmetry, are now allowed. As a consequence, it can be shown that during Inflation, the mode wavefunctions have the same form as in Minkowsky. However, the correct generation of scalar perturbations is protected since this symmetric phase must be broken and the standard behavior is recovered. Another important feature of this model is that all correlation functions of the curvature perturbation, ζ, at lowest order in derivatives are fixed by two coefficients, giving the model a great prediction power.

Step aside from the purely model building, it is also very important to understand how the different cosmological parameters are obtained, and which are the approximations made to obtain them. In that sense, in [2] we move to the extraction of information of different inflationary parameters by means of the study of the CMB perturbations, relaxing some usual assumptions made in the literature.

The constraints of some inflationary parameters given by the WMAP collaboration are computed supposing a sudden reionization scenario occurred about $z \sim 6 - 28$. In Ref. [2] we want to find out what are the consequences of a more general reionization scenario. The most remarkable fact is the relaxation of the constraints in the running of the scalar power spectrum α. As a consequence, hybrid models of Inflation, previously excluded with the sudden reionization approximation, reenter in the game. This indicates that a better knowledge of the reionization processes in the Universe is mandatory.

With respect to Leptogenesis, in the presence of three heavy Majorana neutrinos with a very hierarchical specrtrum, $M_1 \ll M_2 \ll M_3$, there exists a lower bound on the mass of the lightest singlet, M_1 of $\sim 10^9$ GeV in order to produce a large enough baryon asymmetry, the so called Davidson-Ibarra bound. This minimum value for the mass M_1 has been found when the same operators that generate the needed CP asymmetry are responsible for the generation of the mass of the light neutrinos. Further studies have found similar results for non very hierarchical masses, outside the resonant regime (when at least two of the neutrinos are very degenerate, such that $M_2 - M_1 \sim \Gamma_N$). This bound implies a bound on the reheating temperature T_{RH} of the same order. This temperature would have implied also the thermal production of gravitinos in supersymmetric theories in the very early Universe. It turns out that the late decay of such gravitinos could jeopardize successful nucleosyntesis. One possible way out of this conflict is to suppose at least two strongly degenerated heavy

neutrinos. In this scenario, Leptogenesis is possible at temperatures as low as $T \sim \mathcal{O}(1\ \text{TeV})$, solving the gravitino problem. Other possible solutions might appear when flavour effects are important. In this case, if the operators leading Leptogenesis are not the same as the ones giving mass to the light neutrinos, it is possible to lower the value of M_1 since these operators escape from the Davidson-Ibarra bound. These operators at lowest order are lepton number (L) conserving but lepton flavour changing. This is the reason why it is mandatory to have flavour effects at work in Leptogenesis.

In [3] we analyze Leptogenesis in the context of seesaw models with almost conserved lepton number, focusing on the L-conserving contribution and far enough from the resonant regime, which has been already broadly studied. We find that successful Leptogenesis is feasible for masses of the lightest heavy neutrino as low as $M_1 \sim 10^6$ GeV. This lower limit renders thermal Leptogenesis compatible with the gravitino bound in supersymmetric scenarios.

This thesis is organized as follows: In Chapter 1 we revise very briefly the thermal history of the Universe. Some general aspects of the Standard Cosmology are explained en Chapter 2. The connection among the most important cosmological parameters for this thesis and the observations is made in Chapter 3. Chapters 4 and 5 introduce the basis of inflationary theories while Chapter 6 is meant to describe the Leptogenesis scenario. Our Scientific Research, Refs: [1] [2] and [3], is developed in Chapters 7, 8 and 9 respectively. Finally the most important results and conclusions are drawn in 10.

Contents

Part I

Cosmology Overview

Chapter 1

Brief history of the Universe

The expansion of the Universe has been confirmed by some different and independent observations: the spectra of light coming to us from distant sources is inevitably redshifted away during its travel across the Universe [4], the present abundances of light elements such as H, He and Li matches perfectly with the predictions of Big Bang Nucleosyntesis (BBN) [5] and the only convincing explanation for the Cosmic Microwave Background (CMB) is a relic radiation from a hot early Universe [6].

Thus a hotter and hotter and a smaller and smaller Universe as we go backwards in time seems to be the only convincing explanation for the observations. There are two major facts to have in mind regarding particle physics in that context. As the Universe is cooling down, species of particles are decoupling from the thermal bath and evolving independently at lower temperatures. The way to estimate this decoupling is by comparing the Hubble or expansion rate with the interaction rate. When the second drops below the first, the particle specie freezes out. The second fact is that broken symmetries can be restored as the energy of the Universe increases at early times.

In Table 1.1 we give a brief summary of the major events in the History of our Universe. The physical processes from 10^{-10} seconds onwards are well under control thanks to laboratory experiments that have come to achieve energy scales comparable to the energy of the particles in the Universe at that time ($\sim$ 100 GeV). Let us start the study of these events by the energy scale in this specific moment of time. Above this energy scale, electroweak symmetry is restored and all known gauge bosons are massless. All interaction rates are fast enough to maintain quarks and leptons in thermal equilibrium. Once the particle's "soup" temperature cools down to that value, the symmetry breaks down and the Z, W^+ and W^- bosons acquire a non zero mass. The cross section of weak interactions decreases with the temperature. As a result, at around 1 MeV, neutrino decouple from the thermal bath of particles. In between these two scales there are two important events regarding the strong interaction: the confinement of the quarks into hadrons, called hadronization and the freeze out of the strong interaction. The growing of the running coupling at low energies makes very plausible that the QCD dynamics generates the required confinement of quarks

Table 1.1: Major Events in the History of the Universe (Extracted from [7]).

	Time	Energy	
Planck Scale	$< 10^{-43}$ s	10^{18} GeV	
String Scale	$\gtrsim 10^{-43}$ s	$\lesssim 10^{18}$ GeV	
Grand Unification	$\sim 10^{-36}$ s	10^{15} GeV	
Inflation	$\gtrsim 10^{-34}$ s	$\lesssim 10^{14}$ GeV	
SUSY Breaking	$< 10^{-10}$ s	> 100 GeV	
Baryogenesis	$< 10^{-10}$ s	> 100 GeV	
Electroweak Unification	10^{-10} s	100 GeV	
Quark-Hadron Transition	10^{-4} s	10^{2} MeV	
Nucleon Freeze-Out	0.01 s	10 MeV	
Neutrino Decoupling	1 s	1 MeV	
BBN	3 min	0.1 MeV	
			Redshift
Matter-Radiation Equality	10^{4} yrs	1 eV	10^{4}
Recombination	10^{5} yrs	0.1 eV	1,100
Dark Ages	$10^{5} - 10^{8}$ yrs		> 25
Reionization	10^{8} yrs		25-6
Galaxy Formation	$\sim 6 \times 10^{8}$ yrs		~ 10
Dark Energy Domination	$\sim 10^{9}$ yrs		~ 2
Solar System Formation	8×10^{9} yrs		0.5
Albert Einstein born	14×10^{9} yrs	1 meV	0

and gluons into colour-singlet hadronic states. A rigorous proof of this property is, however, still lacking. At this moment, the dynamical details of hadronization are completely unknown.Concerning the freeze out of the strong interaction, once the interactions among baryons and the rest of species are out of equilibrium, baryons and anti-baryons annihilate and only a small fraction of baryons survive due to a previous and tiny asymmetry of 1 part into a billion.

Shortly after the neutrino decoupling, the temperature drops bellow the electron rest mass and the interactions $\gamma\gamma \rightarrow e^+e^-$ begin to be inefficient. As it happened previously with baryons and anti-baryons, the electrons and positrons annihilate and only a tiny portion of the total amount of electrons remains. The resulting photon-baryon plasma is in equilibrium. As we go decreasing the temperature, strong interactions become more and more important and at 0.1 MeV protons and neutrons combine into light elements (H, He, Li) during the so called Big Bang Nucleosynthesis ($\sim$ 200 s). The successful prediction of H, He and Li abundances is one of the most striking consequences of Big Bang Theory. In the subsequent years until the energy is around 0.1 eV, the plasma is mainly made of photons plus charged particles. In that context, electromagnetic interactions strongly couple this soup of particles and fluctuations on it propagate as sound waves. At 0.1 eV (380.000 yrs) the last charged particles, protons and electrons, combine into neutral hydrogen making the plasma electrically neutral and leading the photon gas propagating freely. 13.7 billion years later this radiation, known as the Cosmic Microwave Background (CMB), will give us the first image of our Universe.

That CMB shows small density perturbations, $\rho(\vec{x},t) = \bar{\rho}(t)[1+\delta(\vec{x},t)]$, which will grow via gravitational collapse to form the large structures observed in the late Universe. The growth details depend on the contents of the Universe, and hence they are changing as the Universe evolves. During radiation domination the growth is slow, $\delta \sim \ln a$, being $a(t)$ the scale factor of the Universe (see section 2.1), becoming more efficient after matter begins to dominate the background density (at a redshift $z \sim 10^4$, defined as $1+z = a^{-1}$), $\delta \sim a$. Small scales become non linear first ($\delta \geq 1$) and form gravitationally bound objects that decouple from the overall expansion. This leads to a picture of hierarchical structure formation with small scale structures (like stars and galaxies) forming first and then merging into larger objects such as clusters and superclusters of galaxies.

As we have anticipated, after recombination the Universe is completely dark in the sense that no light is emitted from any source. This period, known as Dark Ages, comes to its end around redshift $z \sim 25$, when the first and most massive stars are formed. The radiation coming from these stars begins to ionize the hydrogen present in the intergalactic medium. This process of 'reionization' is completed at $z \approx 6$. Meanwhile, the most massive stars run out of nuclear fuel and explode as 'supernovae'. In these explosions the heavy elements (C, O, ...) necessary for the formation of life are created. At $z \approx 1$, a negative pressure 'dark energy' comes to dominate the energy density of the Universe. The background spacetime is accelerating and the growth of structure ceases, $\delta \sim constant$.

We have analyzed the most important events in the history of the Universe from $t \sim 10^{-10}$

s until now, from a Cosmological and particle physics point of view. At earlier times, the energy density of the Universe and hence, the theories describing the interaction among particles, have not been tested in laboratory experiments. We can distinguish three epochs.

- $10^{-10} - 10^{-14}$ s ($T \sim 100\,\text{GeV} - 10\,\text{TeV}$). This range of energy scales can still be probed by accelerators. The SM of electroweak and strong interactions appears to be applicable here. As already commented, above ~ 100 GeV, the electroweak symmetry is restored. As a consequence of this symmetry, fermion and baryon numbers are strongly violated in topological transitions above the restoration-symmetry scale. Some theories beyond the SM predict the appearance of new particles at this energy range.

- $10^{-14} - 10^{-43}$ s ($10\,\text{TeV} - 10^{19}\,\text{GeV}$). This energy range will probably not be reached by accelerators in the near future. The study of the early Universe becomes the only option we are left to learn particle physics at these scales of energy. The main uncertainty here is the matter composition of the Universe. In principle, there could be many more particle species present at that energies, as predicted by extensions of the SM of particles.

  The origin of *baryon asymmetry* in the Universe should be related to physics beyond the SM, most probably happening in this energy range. In the same way as it happens with electromagnetic and weak interactions at energies above ~ 100 GeV, it is expected a *Grand Unification* of the electroweak and strong forces at energies about 10^{16} GeV. This Grand Unification can generate topological defects such as cosmic strings or monopoles that might play some role in the early Universe. However, although these topological defects were originally proposed as the origin of cosmological structure, their contributions to the CMB anisotropy have been constrained to be less than 10% of the total [8, 9].

  One of the most interesting phenomena in the above energy range is the accelerated expansion of the Universe - *Inflation* - which probably occurs somewhere near Grand Unification scales. It is remarkable and fortunate that the most important robust predictions of Inflation do not depend substantially on the details of the underlying particle physics. Therefore, the existence of such a stage may be observationally verified in the near future.

- $\sim 10^{-43}$ s ($10^{19}\,\text{GeV}$). It is this scale when nonperturbative quantum gravity dominates and general relativity can no longer be trusted. The most important problem is the initial singularity problem in general relativity. It is expected that this problem will be properly addressed in an as yet unknown nonperturbative string/quantum gravity theory.

Chapter 2

Standard Cosmology

The standard cosmological model is based upon the Einstein's theory of Gravity (see for instance [10]) and the assumptions that the Universe is homogeneous and isotropic everywhere, on scales larger than 100 Mpc (1 Mpc $\approx 3.26 \times 10^6$ light years $\approx 3.08 \times 10^{24}$ cm). Those assumptions, known as *The Cosmological Principle*, are firmly accepted by the majority of the cosmology community since many independent observations seem to point towards this direction. There are in addition some other important and well established properties of our Universe worthy to be mentioned here [11].

Concerning the matter composition of the Universe:

- *it is pervaded by thermal microwave background radiation with temperature* $T \approx 2.73$ **K***;*
- *there is baryonic matter, roughly one baryon per* 10^9 *photons, but no substantial amount of antimatter;*
- *the chemical composition of baryonic matter is about* 75% *hydrogen,* 25% *helium, plus trace amounts of heavier elements;*
- *baryons contribute only a small percentage of the total energy density, around* 4%*; the rest appears as a dark component, which seems to be composed of cold dark matter with negligible pressure* ($\sim 23\%$) *and dark energy with negative pressure* ($\sim 73\%$)*.*

Observations of the fluctuations in the cosmic microwave background radiation suggest that:

- *there were only small fluctuations of order* 10^{-5} *in the energy density distribution when the volume of the Universe was* $\sim 10^9$ *smaller than now.*

In this Chapter we will review the basic equations for our expanding Universe.

2.1 Friedmann-Robertson-Walker metric and Friedmann equations

Einstein's General Relativity [12] gives us the framework in where we build up the standard theory of Cosmology. The basic equations are

$$G_{\mu\nu} \equiv R_{\mu\nu} - \frac{1}{2} g_{\mu\nu} R = \frac{8\pi G}{c^4} T_{\mu\nu}{}^{[1]}, \tag{2.1}$$

where the left-hand side of (2.1) describes the geometry of the Universe while the right hand side relates that geometry with the matter components that fulfill the Universe. $g_{\mu\nu}$ is the space-time metric and takes upon the geometry. $R_{\mu\nu}$ is the Ricci tensor which measures the curvature of the Universe defined in terms of the Christoffel symbols $\Gamma^{\alpha}_{\mu\nu} = \frac{1}{2} g^{\alpha\beta}(\partial_\mu g_{\beta\nu} + \partial_\nu g_{\beta\mu} - \partial_\alpha g_{\mu\nu})$[2]:

$$R_{\mu\nu} = \partial_\alpha \Gamma^{\alpha}_{\mu\nu} - \partial_\mu \Gamma^{\alpha}_{\alpha\nu} + \Gamma^{\alpha}_{\mu\nu}\Gamma^{\beta}_{\alpha\beta} - \Gamma^{\alpha}_{\beta\nu}\Gamma^{\beta}_{\alpha\mu}. \tag{2.2}$$

and $T_{\mu\nu}$ is the global stress-enegy tensor which is constructed in terms of the matter components of the Universe in the following way

$$T_{\mu\nu} \equiv -\frac{2}{\sqrt{-g}} \frac{\delta(\sqrt{g}\mathcal{L}_m)}{\delta g^{\mu\nu}}, \tag{2.3}$$

being $\mathcal{L}_m$ the matter lagrangian density and g the determinant of $g_{\mu\nu}$.

These equations relate the structure and evolution of space and time, encoded in $g_{\mu\nu}$, with the energy components of the Universe given in $T_{\mu\nu}$. Unluckily, these are in general 10 coupled differential equations with partial derivatives, together with 4 constraints[3], fact that makes impossible to treat them analytically. But as we will see imposing homogeneity and isotropy will simplify enormously the problem.

Einstein, in its first attempt to formulate a cosmological theory [13], tried to describe a Universe static, homogeneous and isotropic. This was clearly impossible only with the ingredients mentioned above, since gravity acts as an attractive force for matter and, even starting with a completely static Universe, its effect should have been to compress every form of matter (from lonely hydrogen and helium atoms to clusters and superclusters of galaxies) to a single point. The solution to this problem given by Einstein, afterwards named by himself his biggest mistake, was to include in the equation a constant, Λ, which would give a net repulsive force acting in every point of the space with the same magnitude, and introduced in the equations as:

[1] For simplicity we will set $c = 1$ from now on.

[2] $g^{\alpha\beta}$ is the inverse of the metric $g_{\mu\nu}$ ($g^{\alpha\beta} g_{\beta\mu} = \delta^{\alpha}_{\mu}$), and $\partial_\alpha \equiv \partial/\partial x^\alpha$.

[3] $g_{\mu\nu}$ is a 4×4 symmetric matrix with 10 independent components. Bianchi identities ($G^{;\nu}_{\mu\nu} = 0$) give 4 constraints which reduces the independent variables to be 6.

$$G_{\mu\nu}^{new} = 8\pi G T_{\mu\nu} + \Lambda g_{\mu\nu}. \tag{2.4}$$

Obviously, even in the case that this constant Λ had taken the exact value to cancel the contribution of the background value of the matter component contained in $T_{\mu\nu}$ and hence, given a zero net force for this background, positive small perturbations around it would have evolved with a positive attraction force and hence, with enough time finally would have collapsed to single points. Consequently, in this framework, with General Relativity being the theory describing the evolution of the Universe, there is no way to make it static.

In 1929 Hubble discovered an expansion of the Universe, needed to explain the observed recession of nearby galaxies and ruled out completely the belief of an static Universe [4].

It was Friedmann who first gave a cosmological solution for an expanding, homogeneous and isotropic Universe [14].

2.1.1 Friedmann-Robertson-Walker metric

Like any geometric theory, Friedmann Cosmology is based on a mathematical object describing how distances between two different objects are measured, i. e. the metric $g_{\mu\nu}$. Its definition in General Relativity reads

$$\mathrm{d}s^2 = g_{\mu\nu}\mathrm{d}x^\mu \mathrm{d}x^\nu, \tag{2.5}$$

being ds the space-time distance between two events A and B with coordinates $x_A^\mu = (t_A, x_A, y_A, z_A)$ and $x_B^\mu = (t_B, x_B, y_B, z_B)$, so $\mathrm{d}x^\mu = x_A^\mu - x_B^\nu$.

Following Section 1.1 of Ref. [15] let us begin with the geometry of a three-dimensional homogeneous and isotropic space $\mathrm{d}s^2 \equiv g_{ij}\mathrm{d}x^i\mathrm{d}x^j$. The simplest possibility is the flat space, with line element

$$\mathrm{d}s^2 = \mathrm{d}\mathbf{x}^2. \tag{2.6}$$

Altogether with the flat space, we find another obvious possibility, a spherical surface in 4D with radius a.

$$\mathrm{d}s^2 = \mathrm{d}\mathbf{x}^2 + \mathrm{d}w^2, \qquad w^2 + \mathbf{x}^2 = a^2, \tag{2.7}$$

and of course another extension will be a hyperspherical surface in 4D with line element:

$$\mathrm{d}s^2 = \mathrm{d}\mathbf{x}^2 - \mathrm{d}w^2, \qquad w^2 - \mathbf{x}^2 = a^2, \tag{2.8}$$

where a^2 is so far an arbitrary positive constant. It is possible to show (See Ref. [16] Sec. 13.2) that these three spatial metrics are the only ones describing a homogeneous and isotropic space in 3D. Let us rescale coordinates so that $w^2 \pm \mathbf{x}'^2 = 1$.

$$\mathbf{x}' \equiv a\mathbf{x}, \qquad w' \equiv aw \qquad \Rightarrow \qquad \mathrm{d}s^2 = a^2\left[\mathrm{d}\mathbf{x}'^2 \pm \mathrm{d}w'^2\right]. \tag{2.9}$$

Dropping primes for simplicity, the differential of the equation $w^2 \pm \mathbf{x}^2 = 1$ gives $wdw = \mp\mathbf{x}\cdot d\mathbf{x}$ so

$$\mathrm{d}s^2 = a^2\left[\mathrm{d}\mathbf{x}^2 \pm \frac{(\mathbf{x}\cdot\mathrm{d}\mathbf{x})^2}{1\mp\mathbf{x}^2}\right]. \tag{2.10}$$

The Euclidean flat case can be reincorporated by introducing a new factor k:

$$\mathrm{d}s^2 = a^2\left[\mathrm{d}\mathbf{x}^2 + k\frac{(\mathbf{x}\cdot\mathrm{d}\mathbf{x})^2}{1-k\mathbf{x}^2}\right]. \tag{2.11}$$

where

$$k = \begin{cases} +1 & \text{spherical,} \\ -1 & \text{hyperspherical,} \\ 0 & \text{Euclidean.} \end{cases} \tag{2.12}$$

So far, we have only cared about the spatial part of the metric. There is an obvious way to embed this metric into the geometry of spacetime; by including the time component on it. Homogeneity and isotropy prevent a in Eq. (2.11) to depend on spatial coordinates, but nothing prevents that number, from now on known as the scale factor, to depend on time $a = a(t)$:

$$\mathrm{d}s^2 \equiv g_{\mu\nu}(x)\mathrm{d}x^\mu\mathrm{d}x^\nu = -\mathrm{d}t^2 + a^2(t)\left[\mathrm{d}\mathbf{x}^2 + k\frac{(\mathbf{x}\cdot\mathrm{d}\mathbf{x})^2}{1-k\mathbf{x}^2}\right]. \tag{2.13}$$

The $g_{\mu\nu}$ extracted from Eq. (2.13) is known as the Friedmann-Robertson-Walker (FRW) metric. It is possible to show that this is the unique metric (up to a coordinate transformation) if the Universe appears spherically symmetric and isotropic to a set of freely falling observers. Instead of *quasi-Cartesian* coordinates, we can use the more common spherical-polar coordinates and rewrite Eq. (2.13) in its usual form:

$$\mathrm{d}s^2 = -\mathrm{d}t^2 + a^2(t)\left[\frac{\mathrm{d}r^2}{1-kr^2} + r^2\mathrm{d}\Omega\right], \qquad \text{with} \qquad \mathrm{d}\Omega \equiv \mathrm{d}\theta^2 + \sin^2\theta\,\mathrm{d}\phi^2. \tag{2.14}$$

The inclusion of the scale factor $a(t)$ separates the dynamics and evolution of the Universe as a whole, which is described in the time evolution of the scale factor, with the particular movements of objects like stars or galaxies due to the gravitational attraction to the rest of the objects in their surroundings. In that sense, the coordinates (x, y, z) in Eq. (2.13) or (r, θ, ϕ) in Eq. (2.14) are usually called co-moving coordinates since for any object with no

motion caused by gravitational interaction will remain "at rest" in these coordinate systems, *i.e.* their co-moving coordinates will be always the same.

Let us now compute the first and second Friedmann equations (see Refs. [11] or [15] for more details)

2.1.2 Friedmann equations

The geometric part (left hand side of Eq. (2.1)) can now be worked out by using the metric given in Eq. (2.14). In addition we need to write down the form of the stress-energy tensor $T_{\mu\nu}$. The exact definition for this tensor as we have seen in Eq. (2.3) reads:

$$T_{\mu\nu} \equiv -\frac{2}{\sqrt{-g}}\frac{\delta(\sqrt{g}\mathcal{L}_m)}{\delta g^{\mu\nu}}, \tag{2.15}$$

being $\mathcal{L}_m$ the matter lagrangian density. Nevertheless, for our purposes it is a good approximation, and evidently more useful, to describe the matter and energy components of the Universe as a perfect fluid. Then, homogeneity and isotropy forces $T_{\mu\nu}$ for any free falling observer to be:

$$T_{\mu\nu} = \begin{pmatrix} \rho & 0 & 0 & 0 \\ 0 & -p & 0 & 0 \\ 0 & 0 & -p & 0 \\ 0 & 0 & 0 & -p \end{pmatrix}, \tag{2.16}$$

with ρ the energy density of the fluid and p its pressure.

The first Friedmann equation is nothing but the first of the Einstein's equations, i.e. the equation $G_{00} = 8\pi G\, T_{00}$. Computing this equation in the *flat* FRW gauge (i.e., using Eq. (2.14) with $k = 0$) we find:

$$3\left(\frac{\dot{a}}{a}\right)^2 = 8\pi G\rho(t). \tag{2.17}$$

Thus, in order to compute the evolution of the expansion of the Universe, encoded in $a(t)$, we need to determine the energy density of each of the different components of the Universe such as ordinary matter, radiation... . As we will see below, the evolution of the energy density of the radiation in an expanding Universe is $\rho_r \propto a^{-4}$. As a result, in radiation domination (from shortly after Inflation to $z \sim 10^4$ *i.e.*, $a/a_0 \sim 10^{-4}$, where $a_0 \equiv a(t_0)$ is the scale factor today), the energy density evolves like $\rho(t) \approx \rho_I/a^4$, being ρ_I the value of the energy density after Inflation. Whereas in matter domination (from $z \sim 10^4$ to $z \sim 2$) the evolution is determined to a good approximation by the evolution of non relativistic matter $\rho_m \propto a^{-3}$. Nowadays it is widely accepted that we are in a phase of accelerated expansion of the Universe, similar to Inflation (see Chapter 4), characterized most probably by a constant energy density, coming from the term $\Lambda g_{\mu\nu}$ in Eq. (2.4).

In order to better understand the evolution of the Universe, we can rewrite the Friedmann equation when these three components are present:

$$\left(\frac{\dot{a}}{a}\right)^2 = \frac{8\pi G}{3}\left[\frac{\rho_r^0}{a^4} + \frac{\rho_m^0}{a^3} + \frac{\Lambda}{8\pi G}\right], \tag{2.18}$$

where ρ_r^0 and ρ_m^0 refer to the energy density of radiation and matter today. The only assumption in computing last equation is that the interactions between the different fluids are small, like if the whole fluid was a perfect fluid; if this does not apply the interactions among them must be taken into account.

Depending on which component of the energy density is the dominant one in the Universe at any time, the time evolution of the scale-factor $a(t)$ will be different. For instance, in the early Universe, when radiation dominates the energy component, $a(t) \propto t^{1/2}$. When matter overpasses radiation as the dominant energy component, Eq. (2.18) tells us that the evolution of the scale factor is $a(t) \propto t^{2/3}$, while at late times, when the dark energy starts dominating (and even more in the future, if the dark energy is really due to a constant in the Einstein Equations) $a(t)|_{t\to\infty} \propto e^{\sqrt{\Lambda/3}t}$. This late time evolution is often called the de-Sitter solution since it is the evolution obtained from the Einstein-de Sitter cosmology [17].

Introducing the *Hubble parameter* $H \equiv \dot{a}/a$, connected with the expansion rate, the critical density today $\rho_c^0 = 3H_0^2/8\pi G$, where $H_0 = H(t_0)$ [4] is the present value of the Hubble parameter or *Hubble constant*, and $\Omega_i(t_0) = \rho_i^0/\rho_c^0$, Eq. (2.18) can also be expressed as

$$\left(\frac{H}{H_0}\right)^2 = \frac{\Omega_r(t_0)}{a^4} + \frac{\Omega_m(t_0)}{a^3} + \Omega_\Lambda \tag{2.19}$$

where Ω_Λ is constant.

If we now relax the assumption of flat Universe and use the more general line element

$$\mathrm{d}s^2 = -\mathrm{d}t^2 + a^2(t)\left[\frac{\mathrm{d}r^2}{1-kr^2} + r^2\mathrm{d}\Omega^2\right], \tag{2.20}$$

the presence of a non zero value of k modifies the first Friedmann equation (2.19) in the following way

$$\left(\frac{H}{H_0}\right)^2 = \frac{\Omega_r(t_0)}{a^4} + \frac{\Omega_m(t_0)}{a^3} + \Omega_\Lambda - \frac{k}{H_0^2 a^2} = \frac{\Omega_r(t_0)}{a^4} + \frac{\Omega_m(t_0)}{a^3} + \Omega_\Lambda + \frac{\Omega_k(t_0)}{a^2}. \tag{2.21}$$

[4] Current observations indicate $H_0 \approx 73$ km/(s Mpc) [18]. In astronomy it is commonly used the dimensionless parameter h instead, defined as $H_0 = 100\ h$ km/(s Mpc), with $h \approx 0.7$.

Considering Eq. (2.21) at present time ($H = H_0$ and $a = a_0 = 1$ [5]) we find the following relation among the different density fractions

$$1 - \Omega_k^0 = \Omega_r^0 + \Omega_m^0 + \Omega_\Lambda. \tag{2.22}$$

Therefore it is possible to infer the curvature sign and value from the total energy density of the Universe at present time $\rho_T^0 = \rho_r^0 + \rho_m^0 + \rho_\Lambda^0$:

- $\rho_T^0 > \rho_c^0 \rightarrow \Omega_k < 0$ closed Universe.
- $\rho_T^0 < \rho_c^0 \rightarrow \Omega_k > 0$ open Universe.
- $\rho_T^0 = \rho_c^0 \rightarrow \Omega_k = 0$ flat Universe.

Currently, Ω_k is well constrained to be close to zero ($-0.01 \leq \Omega_k(t_0) \leq 0.01$, see Ref. [19]), which means that our Universe seems to have a spatially flat geometry.

Up to now, we have only considered the 00 component of the Einstein equations (2.1). Taking into account the spacial components $G_{ij} = 8\pi G T_{ij}$ and tracing them we obtain the following equality:

$$\frac{\ddot{a}}{a} + 2\left(\frac{\dot{a}}{a}\right)^2 + 2\frac{k}{a^2} = 4\pi G(\rho - p), \tag{2.23}$$

where we have directly considered a possible non negligible spacial curvature of the Universe, k. Using Eq. (2.21) to get rid of the k-term we obtain the second Friedmann equation:

$$\frac{\ddot{a}}{a} = -\frac{4\pi G}{3}(\rho + 3p). \tag{2.24}$$

The equation above tells us whether the expansion of the Universe is being accelerated or decelerated. For ordinary stuff like matter or radiation, with pressure equal to zero or $\rho/3$ respectively, $\ddot{a} < 0$, meaning that the gravitational force generated by it is always attractive, as we already knew. To get a repulsive gravity force we need something with a relation between pressure and energy density that satisfies $p < -\rho/3$, like the cosmological constant term, with $p_\Lambda = -\rho_\Lambda$, or as we will see in Chapter 4 a scalar field ϕ with a potential energy larger than its kinetic energy ($p_\phi \gtrsim -\rho_\phi$). In fact, this is the basis of a very early inflationary phase, believed to happen in the very early Universe ($t \sim 10^{-34}$ sec).

There is a third useful equation coming from the conservation of the stress-energy tensor $\nabla^\mu T_{\mu\nu} = 0$. Considering the 0 component of this equation, we find the so called continuity equation:

$$\frac{d\rho}{dt} + \frac{3\dot{a}}{a}(p + \rho) = 0. \tag{2.25}$$

[5] It is widely accepted to consider $a(t_0) = 1$, being t_0 today. From now on we will follow that prescription.

It is also possible to find it using both first and second Friedmann equations. Indeed, deriving Eq. (2.21) with respect to time and substituting it back in Eq. (2.24) we finally get Eq. (2.25).

Using a generic equation of state $p = w(a)\rho$ and plugging it back in the continuity equation leads to

$$\frac{d\rho}{dt} = -\frac{3\dot{a}}{a}\rho(1+w) \rightarrow \rho = \begin{cases} \rho^0 e^{3\int_a^1 \frac{(1+w(a))}{a}\mathrm{d}a} & \text{for } w = w(a), \\ \frac{\rho^0}{a^{3(1+w)}} & \text{if } w = \text{const.} \end{cases} \tag{2.26}$$

Equations (2.21) and (2.24), together with the equation of state $\rho(t) = w(t)p(t)$ describing the behavior of the fluid allocated throughout the Universe, characterize completely the time evolution of the scale factor $a(t)$ and hence the evolution of the whole Universe.

2.2 Propagation of light and redshift

Most of the physical information obtained from our Universe is coming to us in form of light. It is therefore mandatory to understand not only the light emission by astrophysical objects but also the propagation of it throughout the Universe from the source to us.

One of the most important properties of an expanding Universe is that this expansion modifies the frequency of photons traveling across it. The equation describing the path followed by any particle is called *the geodesic equation*. In Special Relativity the geodesic equation for a massles particle traveling at the speed of light is simply $\mathrm{d}s^2 = 0$. This must be true in General Relativity for any local inertial coordinate frame. Since $\mathrm{d}s$ is invariant under any coordinate transformation $\mathrm{d}s^2 = 0$ is the geodesic equation for a light ray. Let us consider a FRW coordinate system in which we are at the center and a light ray is coming to us along the radial direction. Using Eq. (2.14) we find for such ray

$$\mathrm{d}t = -a(t)\frac{\mathrm{d}r}{\sqrt{1-kr^2}}, \tag{2.27}$$

where we have implicitly considered that for a light ray coming from a distant source, r decreases as t increases choosing the minus sign in Eq. (2.27). Let us integrate Eq. (2.27) from a distant point with co-moving coordinates r_1 and t_1 to the origin $r = 0$ at a later time t_0

$$\int_{t_1}^{t_0} \frac{\mathrm{d}t}{a(t)} = \int_0^{r_1} \frac{\mathrm{d}r}{\sqrt{1-kr^2}}. \tag{2.28}$$

From last equation we can infer what is the total time $t_0 - t_1$ taken by a light ray to us $r = 0$ from a distant source r_1. Now consider a subsequent light ray emitted in r_1 shortly after the first one was emitted at time $t_1 + \delta t_1$. This second light ray will arrive at Earth at

time $t_0 + \delta t_0$. Integrating again Eq. (2.27) for its path recalling that the radial coordinate r_1 of co-moving sources is time-independent, we have

$$\int_{t_1+\delta t_1}^{t_0+\delta t_0} \frac{\mathrm{d}t}{a(t)} = \int_0^{r_1} \frac{\mathrm{d}r}{\sqrt{1-kr^2}} = \int_{t_1}^{t_0} \frac{\mathrm{d}t}{a(t)}, \tag{2.29}$$

which can be read as

$$\frac{\delta t_1}{a(t_1)} = \frac{\delta t_0}{a(t_0)}. \tag{2.30}$$

Assuming the two "signals" correspond to two consecutive wave crests, the emitted and the observed frequencies are $\nu_1 = 1/\delta t_1$ and $\nu_0 = 1/\delta t_0$ respectively, so

$$\frac{\nu_0}{\nu_1} = \frac{a(t_1)}{a(t_0)}. \tag{2.31}$$

Under this interpretation a photon emitted at time t_1 with energy $E_1 = h\nu_1$, will reach the Earth at time t_0 with an energy $E_0 = h\nu_0 = E_1 a(t_1)/a(t_0)$.

Conventionally it has been used the relative difference z in the observed and emitted wavelengths, so called redshift, instead of the frequency

$$z = \frac{\lambda_{\mathrm{obs}} - \lambda_{\mathrm{em}}}{\lambda_{\mathrm{em}}} \rightarrow 1 + z = \frac{a(t_0)}{a(t_1)}, \tag{2.32}$$

where λ_{obs} is the photon wavelength observed on Earth and λ_{em} is the emitted wavelength.

For an expanding Universe, $a(t_1) < a(t_0) = 1$, we observe an increase in the measured wavelength or redshift encoded in a positive z (on the contrary if the Universe were contracting the light wavelength would decrease going towards a bluer spectrum, or equivalently $z < 0$).

Although there were some previous hints that seemed to indicate an observed redshift for nearby nebulae [20, 21], interpreted as a possible proof of an expanding Universe, it was Hubble who first gave a convincing observational proof for this hypothesis. In 1929 he announced he had found a "roughly linear" relation between redshift and distance [4]. In the early 1930s, these observations were strongly improved by Hubble himself, including data from galaxies out to the Coma clusters, located at $z \sim 0.02$, supporting the idea of an expanding Universe.

The reason why it took that much to accept the data as a proof for an expanding Universe is because of the presence of "peculiar" velocities in the galaxies measured. Real galaxies do not move only with the general expansion or contraction of the Universe; in addition they have velocities of hundreds of kilometers per second, caused by gravitational attraction due to nearby galaxies and intergalactic matter. It is necessary to go to redshifts $z \gg 10^{-3}$, whose cosmological velocities zc (with c the speed of light) are thousands of kilometers per second, to get rid of the spurious effects of these "peculiar" velocities.

2.3 Distances and horizon definitions

According to Einstein's Special Relativity Theory, any signal can travel through any medium at most at the speed of light c. This fixed quantity, together with a given cosmology, allows us to measure distances in the Universe. For instance, the *proper distance* at time t from the origin of one system of reference to a co-moving object at radial coordinate r reads

$$d(r,t) = a(t)\int_0^r \frac{\mathrm{d}r}{\sqrt{1-kr^2}} = a(t)\times\begin{cases}\sin^{-1} r & k=+1,\\ \sinh^{-1} r & k=-1,\\ r & k=0.\end{cases}$$

This quantity can be expressed in terms of the energy components of the Universe in the following way

$$d(r,t) = \frac{a(t)}{H_0}\int_{1/(1+z)}^1 \frac{\mathrm{d}a}{\sqrt{\Omega_r(t_0)+\Omega_m(t_0)a+\Omega_\Lambda a^4+\Omega_k(t_0)a^2}}, \tag{2.33}$$

and hence can be used to infer the values of the different cosmological parameters.

Another useful distance measurement is what is known as the *angular diameter distance*. An object at an angular diameter distance d_A is an object which subtends an angle θ observed from the Earth, whose light was emitted in t_1, and has a proper distance $s = a(t_1)r_1\theta$ normal to the line of sight. In other words, the angular diameter distance d_A is defined so that θ is given by the usual relation of Euclidean geometry

$$\theta = s/d_A, \tag{2.34}$$

from where we can read

$$d_A = a(t_1)r_1. \tag{2.35}$$

The finite speed of light imposes a fundamental limit on how far we can see. The distance traveled by a photon since the origin of the Universe, called *particle horizon*, is the maximum distance form which we can get any kind of information. According to Eq. (2.28) if the Big Bang started at time $t = 0$ the maximum value $r_{max}(t)$ of the Robertson-Walker radial coordinate from which an observer at time t will be able to receive signals traveling at the speed of light is given by the condition

$$\tau \equiv \int_0^t \frac{\mathrm{d}t'}{a(t')} = \int_0^{r_{max}(t)} \frac{\mathrm{d}r}{\sqrt{1-kr^2}}, \tag{2.36}$$

where τ represents the maximum comoving distance a light ray between time 0 and time t, and from now on we will refer to it as the *comoving particle horizon*.

The *particle horizon* at a time t is thus defined as

$$d_{max}(t) = a(t)\int_0^{r_{max}(t)} \frac{\mathrm{d}r}{\sqrt{1-kr^2}} = a(t)\int_0^t \frac{\mathrm{d}t'}{a(t')}. \tag{2.37}$$

For instance, as we have said above $a(t) \propto t^{1/2}$ in radiation dominance hence it is straightforward to show that $d_{max}(t) = 1/H(t)$. The exact solution for the *particle horizon* at late times can be computed using Eq. (2.21):

$$\begin{aligned} d_{max}(t_0) &= \frac{1}{H_0}\int_0^1 \frac{\mathrm{d}x}{x^2\sqrt{\Omega_\Lambda + \Omega_k(t_0)x^{-2} + \Omega_m(t_0)x^{-3} + \Omega_r(t_0)x^{-4}}} \\ &\approx \frac{1}{H_0}\int_0^1 \frac{\mathrm{d}x}{x^2\sqrt{\Omega_\Lambda + \Omega_m(t_0)x^{-3}}}, \end{aligned} \tag{2.38}$$

where the last approximation holds since matter and dark energy are the dominant contributions in the integral.

It is possible that in the near future we will be able to detect and to study gravitational waves or even neutrinos coming from the very early Universe. Nevertheless, so far the most antique piece of information is coming to us from recombination when the first "free" photons were emitted. This "last scattering surface" represents indeed the observable horizon up to now, commonly called optical horizon:

$$d_{opt}(t_0) = \frac{1}{H_0}\int_{a_{LS}}^1 \frac{\mathrm{d}x}{x^2\sqrt{\Omega_\Lambda + \Omega_k(t_0)x^{-2} + \Omega_m(t_0)x^{-3} + \Omega_r(t_0)x^{-4}}}. \tag{2.39}$$

Chapter 3

Cosmological parameters and observational methods

The quantities of greatest cosmological interest are *averages*. As we will discuss in Chapter 4, for anisotropies that arise form quantum fluctuations in the very early Universe, these averages are related to quantum mechanical expectation values. By studying them we can extract some information about the underlying physics that caused these primordial perturbations. Moreover, different sets of values of the cosmological parameters lead to different statistical distributions of the anisotropies in the CMB. For this reason, the analysis of the statistical properties of those anisotropies can be used to constrain the value of the cosmological parameters.

In this Section we briefly summarize the most important observational methods, from which we can extract the most accurate values of the cosmological parameters related to this thesis, namely the parameters related to Inflation and Leptogenesis. The best methods for these purposes study the perturbations in the matter content of the Universe at different times and scales. We will focus here in Cosmic Microwave Background (CMB) and Large Scale Structure (LSS) observations, which describe these perturbations at different redshifts, starting in the last scattering surface ($z_{LS} \sim 1000$), the moment in time when the radiation became free. .

3.1 CMB

Studies of the distribution of the anisotropies in the CMB have allowed the determination of the cosmological parameters with an unprecedented precision. Here we present a brief summary of the basics of this method.

According to the Big Bang model, as we go backwards in time, the Universe was hotter and hotter and denser and denser. It is therefore obvious to imagine an early time where the Universe was too hot for electrons to be bounded into atoms. At that times, when electrons

were free, Thompson scattering among photons and free electrons was fast enough to keep photons in thermal equilibrium with the hot dense matter. The number density of photons in equilibrium with matter at temperature T and photon frequency between ν and $\nu + \mathrm{d}\nu$ is given by the *black-body spectrum*:

$$n_T(\nu)\mathrm{d}\nu = \frac{8\pi\nu^2\mathrm{d}\nu}{\exp(h\nu/k_{\mathcal{B}}T) - 1}, \tag{3.1}$$

where h is the original Planck's constant and $k_{\mathcal{B}}$ is the Boltzmann's constant [1].

As time passed, the matter became cooler and less dense, and eventually free electrons and nucleons combined into single Hydrogen atoms and the radiation began a free expansion, conserving the form of its spectrum, but with different temperature, reduced by the redshift factor:

$$n_T(\nu)\mathrm{d}\nu = \frac{8\pi\nu^2\mathrm{d}\nu}{\exp(h\nu/k_{\mathcal{B}}T(t)) - 1} = n_{T(t)}(\nu)\mathrm{d}\nu, \tag{3.2}$$

where

$$T(t) = T(t_{LS})a(t_{LS})/a(t) = T(t_{LS})\frac{1 + z(t)}{1 + z(t_{LS})}. \tag{3.3}$$

Due to the redshift caused by the expansion of the Universe, the black body temperature for this radiation has been reduced from $T(t_{LS}) \approx 3,000$ K at last scattering surface to $T_0 = 2.725$ K today.

The temperature of this background of microwaves is not perfectly homogeneous, but it presents tiny deviations of about one part in 10^5. The primary temperature anisotropies in the CMB, $\Delta T(\hat{n}) \equiv T(\hat{n}) - T_0$, where T_0 is the mean value for the temperature of the CMB, seem to be Gaussian to a good accuracy. They arise from different reasons:

- Intrinsic temperature fluctuations in the electron-nucleon-photon plasma at the last scattering surface ($z \sim 1,090$).
- The Doppler effect caused by velocity fluctuations in the plasma at last scattering.
- Fluctuations in the gravitational potential at last scattering where photons were emitted. This is known as the *Sachs-Wolfe effect*.
- Gravitational redshifts or blueshifts due to time-dependent fluctuations in the gravitational potential between the time of last scattering and the present time: *Integrated Sachs-Wolfe effect*.

[1] Recall that we are using units with $c = 1$.

It is convenient to expand $\Delta T(\hat{n})$ in spherical harmonics Y_l^m

$$\Delta T(\hat{n}) = T(\hat{n}) - T_0 = \sum_{lm} a_{lm} Y_l^m(\hat{n}), \quad T_0 = \frac{1}{4\pi} \int \mathrm{d}^2\hat{n}\; T(\hat{n}). \tag{3.4}$$

Assuming rotational invariance of our Universe, all averages $\langle \Delta T(\hat{n}_1)\Delta T(\hat{n}_2)\Delta T(\hat{n}_3)\cdots\rangle$ are rotationally invariant functions of the directions $\hat{n}_1$, $\hat{n}_2$, $\hat{n}_3$, etc. This means that $\langle \Delta T(\hat{n})\rangle$ must vanish.

The simplest non-trivial quantity characterizing the distribution of the anisotropies in the CMB is given by the mean value of the product of two $\Delta T(\widehat{n})$:

$$\langle \Delta T(\hat{n})\Delta T(\hat{n}')\rangle = \sum_{lm} C_l Y_l^m(\hat{n}) Y_l^{-m}(\hat{n}') = \sum_l C_l \left(\frac{2l+1}{4\pi}\right) P_l(\hat{n}\cdot\hat{n}'), \tag{3.5}$$

being P_l the Legendre polynomials, and we have made use of $\langle a_{lm} a_{l'm'}\rangle = \delta_{ll'}\delta_{m-m'} C_l$, consequence of the condition that the Universe is rotationally invariant. It is possible to invert Eq. (3.5) to find C_l

$$C_l = \frac{1}{4\pi} \int \mathrm{d}^2\hat{n}\mathrm{d}^2\hat{n}' P_l(\hat{n}\cdot\hat{n}')\langle \Delta T(\hat{n})\Delta T(\hat{n}')\rangle. \tag{3.6}$$

Observationally it is impossible to average over all the positions from which the CMB is seen. What we can directly observe are quantities averaged over the m's, not over position:

$$C_l^{\mathrm{obs}} \equiv \frac{1}{2l+1} \sum_m a_{lm} a_{l-m} = \frac{1}{4\pi} \int \mathrm{d}^2\hat{n}\mathrm{d}^2\hat{n}' P_l(\hat{n}\cdot\hat{n}')\Delta T(\hat{n})\Delta T(\hat{n}'). \tag{3.7}$$

The relative difference between C_l and C_l^{obs} is known as the *cosmic variance*. For Gaussian perturbations, the mean square of the cosmic variance decreases with l:

$$\left\langle \left(\frac{C_l - C_l^{\mathrm{obs}}}{C_l}\right)^2 \right\rangle = \frac{2}{2l+1}. \tag{3.8}$$

As we will see in Chapter 5, the perturbations present in the CMB are nearly Gaussian, hence, to a good approximation we can make use of C_l^{obs} instead of C_l to extract the information.

Figure 3.1 shows the value of C_l^{obs} as a function of the multipole moment l as measured from five different experiments; Wilkinson Microwave Anisotropy Probe (WMAP), Arcminute Cosmology Bolometer Array Receiver (Acbar), Balloon Observations Of Millimetric Extragalactic Radiation ANd Geophysics (Boomerang), Cosmic Background Imager (CBI) and Very Small Array (VSA) from the CMB. That plot represents the correlations between temperature anisotropies separated by an angle equal to θ, where $\theta \approx \pi/l$. As can be seen from Fig. 3.1, there are several peaks in the graphic, indicating the presence

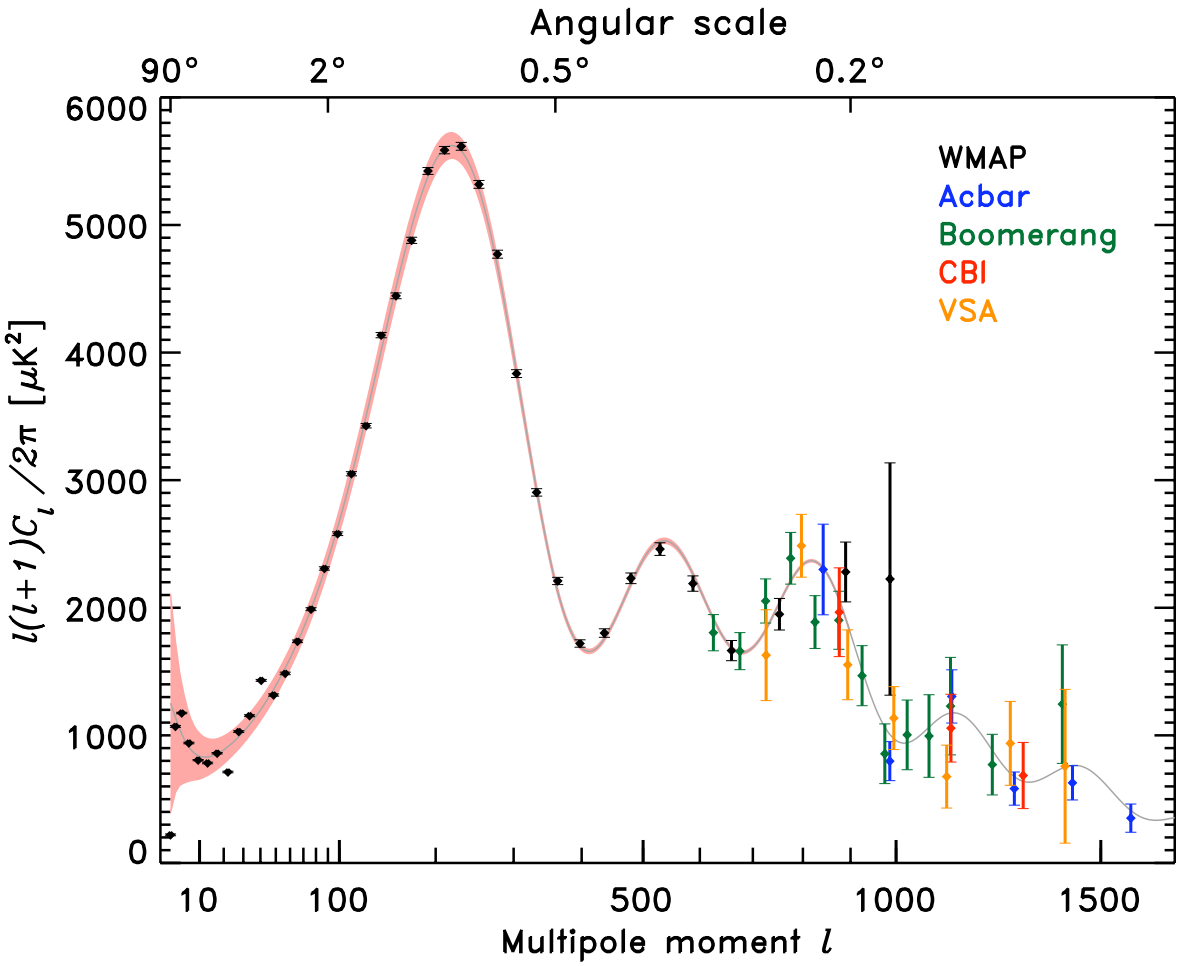

Figure 3.1: C_l^{obs} versus the multipole moment l for data taken with five different instruments; WMAP, Acbar, Boomerang, CBI and VSA from the cosmic microwave background. (Taken from http://en.wikipedia.org/wiki/File:PowerSpectrumExt.svg)

of correlations at different angular locations in the CMB. Physically these peaks represent the acoustic waves in the photon-baryon plasma of the primordial Universe. Those waves were originated from the primordial inhomogeneities in the distribution of dark matter as the result of the competition between two forces: on one hand radiation pressure acts as a repulsive force, on the other hand gravity tries to compress matter.

The study of the positions and sizes of these peaks gives us important information about the different cosmological parameters in a given cosmology. For instance, the first peak corresponds to an acoustic wave which was compressed only once before decoupling. Its position gives a measurement of the size of the horizon at the time of decoupling, namely the last scattering surface, providing information about the geometry of the Universe. This position is compatible with a spatially flat or nearly flat Universe. The second peak contains information about the fraction of baryons in the Universe, and some information regarding the fraction of dark matter in the Universe is enclosed in the third peak.

It is important to notice that, due to cosmic variance (appearing in the plot as a pink shadow over the observational points and the best fit), measurements of multipoles with $l < 5$, purely dominated by it, cannot be taken into account. For $l > 2,000$ we are entirely dominated by foreground effects, such as the *Sunyaev-Zel'dovich effect* [22]. The interesting region is constrained then among $10 \lesssim l \lesssim 1,500$. Fortunately the most important effects are encoded in the acoustic peaks present in that region.

3.2 LSS

CMB measurements show a nearly homogeneous Universe with tiny deviations of order 10^{-5} at redshift $z \sim 1,090$, believed to be the seeds that generate the structures observed today in our Universe. An analysis of some statistical properties of these structures at low redshift ($z \sim 0.5-1$), such as the distribution of the galaxies or the observed number of clusters, can give us valuable information about the properties of our Universe. Combining it with CMB measurements it is possible to accurately extract the value of some cosmological parameters. In addition we can better understand the evolution of these primordial seeds, merging to form larger objects that lead to the observed Universe today.

In this Section we describe the standard methods used to study the distribution of matter in the Universe and how the cosmological parameters can be inferred from them.

Let us begin by the introduction of the so called *correlation function*, ξ. For a continuous field it is defined as

$$\xi(|\mathbf{r} - \mathbf{r}'|) = \langle \delta(\mathbf{r}) \delta(\mathbf{r}') \rangle \,, \tag{3.9}$$

while for a discrete field it is defined via

$$\mathrm{d}P = \bar{n}^2 (1 + \xi(r_{12})) \mathrm{d}V_1 \mathrm{d}V_2. \tag{3.10}$$

For a galaxy catalog $\mathrm{d}P$ is the probability to find a pair of galaxies enclosed in two volumes $\mathrm{d}V_1$ and $\mathrm{d}V_2$, each one centered in one galaxy, separated by a distance r_{12}. $\bar{n}$ is the mean number of galaxies in the catalog. Note that in Eq. (3.9) and in Eq. (3.10), the correlation function depends only on the modulus, not on the direction of the vector. This is because we consider that the Universe is rotationally invariant.

Widely used in cosmology and enclosing the same information as the correlation function, the *power spectrum* $P(k)$ is defined as the fourier transform of the correlation function:

$$P(\mathbf{k}) = \int \xi(\mathbf{r}) e^{i\mathbf{k}\cdot\mathbf{r}} \mathrm{d}^3\mathbf{r} \qquad \xi(\mathbf{r}) = \int P(\mathbf{k}) e^{-i\mathbf{k}\cdot\mathbf{r}} \frac{\mathrm{d}^3\mathbf{k}}{(2\pi)^3}, \tag{3.11}$$

where k indicates the scale of the perturbation λ as $\lambda = 2\pi/k$. Using galaxy catalogs, the power spectrum can be reconstructed, at least in a range of k's (see for example [23, 24, 25]). The use of complementary methods such as the CMB, or the Lyman-α forest has the potential to reconstruct the power spectrum in a wide range of k, allowing a much better measurement of the cosmological parameters.

Figure 3.2 shows the correlation function extracted from the SDSS galaxy survey. An important feature of this plot is the presence of an excess at about 100 h^{-1} Mpc. The existence of this peak, physically connected to the existence of several oscillations in the power spectrum of the CMB (see Fig. 3.1) is an unambiguous proof of the presence of baryonic acoustic oscillations (BAO) in the primordial particle plasma before recombination. As previously stated, in the early Universe, before electrons and nucleons recombined into H atoms, there were two forces in competition acting on the particles in the plasma. On one hand the excess of matter in a given place acts as an attractive force while the pressure of photons due to Thompson scattering results in a repulsive force. The balance between these two effects induce acoustic waves which propagate through the plasma with a velocity

$$c_s = \frac{1}{[3(1 + 3\rho_b/4\rho_\gamma)]^{-1/2}}, \tag{3.12}$$

where ρ_b and ρ_γ are the energy densities of baryons and photons, which is approximately equal to $c/2$, creating density variations. Those waves left a pattern in the distribution of baryons that is measurable by galaxy surveys.

The baryonic acoustic oscillations represent a cosmological standard ruler, whose size is fixed by simple physics and it is related to the value of the Hubble parameter, $H(t)$, and to the value of the angular diameter distance, $d_A(t)$, at a given time t.

We end this chapter by showing in Fig. 3.3 the latest cosmological parameters derived from studies of CMB, BAO and some other methods like supernovae, that have not been explained here for the sake of simplicity.

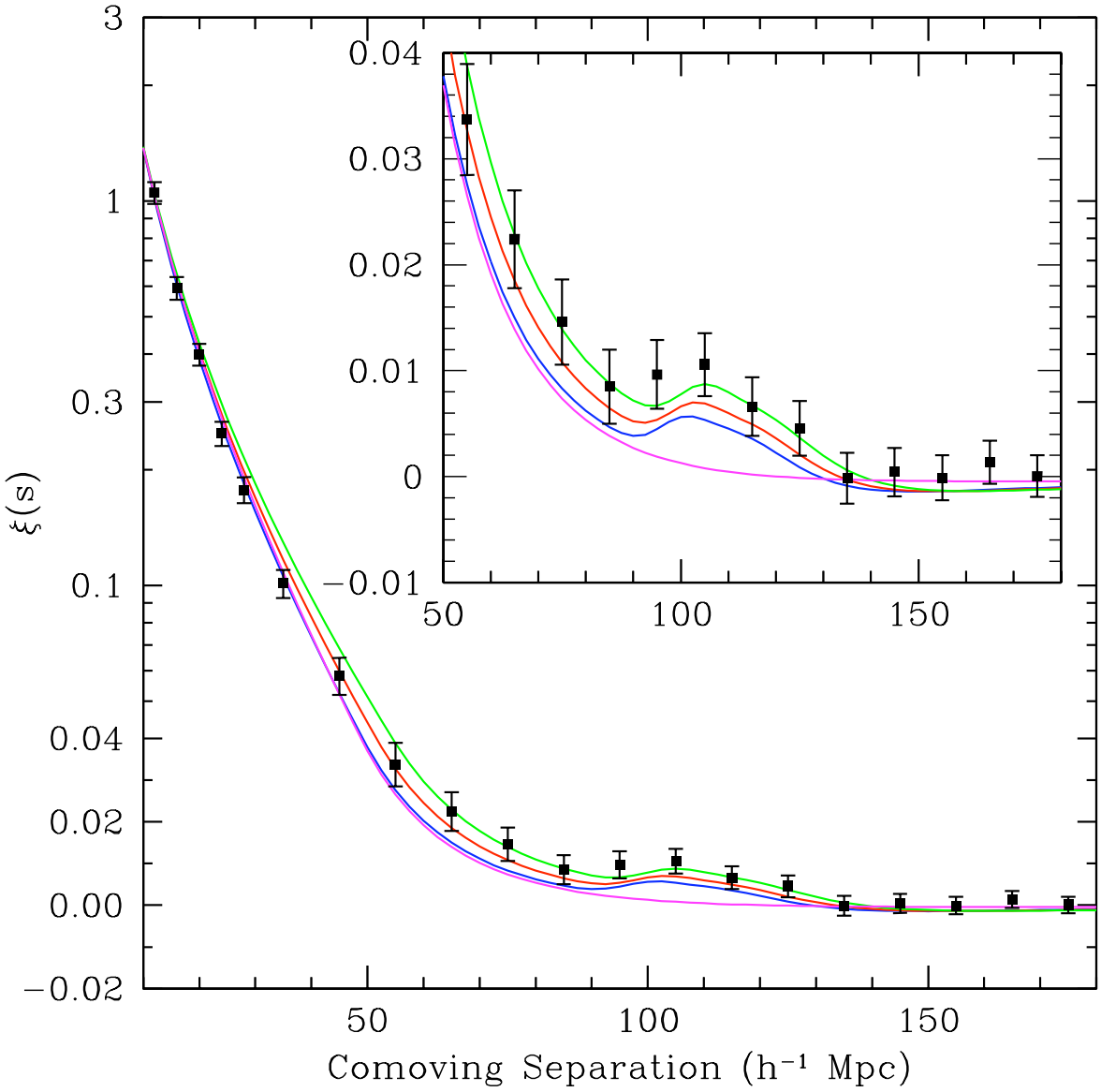

Figure 3.2: Correlation function extracted from the SDSS galaxy catalog. In the Figure, it is visible an excess of correlation at about 100 h^{-1}Mpc, showing the presence of the first acoustic peak. The colored solid lines represent the theoretical prediction of the correlation function for the following cases: green, red and blue, all of them have $\Omega_b h^2 = 0.024$ and $\Omega_m h^2 = 0.12,\ 0.13,\ 0.14$ respectively while the purple line represents a pure CDM universe, without baryons, and $\Omega_m h^2 = 0.105$. (Image taken from the reference [26])

.

WMAP Cosmological Parameters Model: lcdm+sz+lens Data: wmap7+bao+h0			
$10^2\Omega_b h^2$	2.260 ± 0.053	$1 - n_s$	0.037 ± 0.012
$1 - n_s$	$0.013 < 1 - n_s < 0.061$ (95% CL)	$A_{\rm BAO}(z = 0.35)$	0.468 ± 0.011
C_{220}	5762^{+38}_{-37}	$d_A(z_{\rm eq})$	14238^{+128}_{-129} Mpc
$d_A(z_*)$	14073^{+129}_{-130} Mpc	$\Delta^2_{\mathcal{R}}$	$(2.441^{+0.088}_{-0.092}) \times 10^{-9}$
h	$0.704^{+0.013}_{-0.014}$	H_0	$70.4^{+1.3}_{-1.4}$ km/s/Mpc
$k_{\rm eq}$	0.00985 ± 0.00026	$\ell_{\rm eq}$	$138.6^{+2.6}_{-2.5}$
ℓ_*	302.40 ± 0.73	n_s	0.963 ± 0.012
Ω_b	0.0456 ± 0.0016	$\Omega_b h^2$	0.02260 ± 0.00053
Ω_c	0.227 ± 0.014	$\Omega_c h^2$	0.1123 ± 0.0035
Ω_Λ	$0.728^{+0.015}_{-0.016}$	Ω_m	$0.272^{+0.016}_{-0.015}$
$\Omega_m h^2$	0.1349 ± 0.0036	$r_{\rm hor}(z_{\rm dec})$	284.6 ± 1.9 Mpc
$r_s(z_d)$	152.7 ± 1.3 Mpc	$r_s(z_d)/D_v(z = 0.2)$	$0.1904^{+0.0037}_{-0.0038}$
$r_s(z_d)/D_v(z = 0.35)$	0.1143 ± 0.0020	$r_s(z_*)$	146.2 ± 1.1 Mpc
R	$1.7239^{+0.0100}_{-0.0099}$	σ_8	0.809 ± 0.024
$A_{\rm SZ}$	$0.96^{+0.69}_{-0.96}$	t_0	13.75 ± 0.11 Gyr
τ	0.087 ± 0.014	θ_*	0.010389 ± 0.000025
θ_*	0.5953 ± 0.0014 °	t_*	377730^{+3205}_{-3200} yr
$z_{\rm dec}$	1088.2 ± 1.1	z_d	1020.5 ± 1.3
$z_{\rm eq}$	3232 ± 87	$z_{\rm reion}$	10.4 ± 1.2
z_*	$1090.89^{+0.68}_{-0.69}$		

Figure 3.3: Cosmological parameters derived from data from CMB anisotropies (WMAP), together with BAO and supernovae (H_0). (File taken from http://map.gsfc.nasa.gov/)

Chapter 4

Basics of Inflation

As we have anticipated in the previous chapters, Inflation is a hypothetical scenario in the very early Universe ($t \sim 10^{-34}$ s) in which the Universe undergoes a period of accelerated expansion, nearly exponential, leading to an increase of the scale factor of more than twenty orders of magnitude. This simple idea can explain by itself many of the problems of the Hot Big Bang model, although it is not free of some difficulties, especially concerning the construction of a reliable theoretical framework capable of driving such a period. In this Chapter we will briefly summarize the basics of the theory of Inflation, while perturbations will be extensively studied in the following Chapter.

4.1 Problems in the standard cosmological model

At the time when the Inflationary hypothesis came out, the Hot Big Bang scenario was an extremely successful idea that could account for several observational facts like the expansion of the Universe, the CMB or the abundances of light elements. Nevertheless, it suffered from several problems that we are going to describe in the present Section, being the lack of an explanation for the rather peculiar initial conditions needed to explain the Universe we observe today the most important one.

In this Chapter we explain some of the problems of the Hot Big Bang scenario, focusing mainly on the ones regarding the initial conditions, namely the *horizon* and the *flatness problems*.

4.1.1 Horizon problem

CMB observations show a nearly perfect homogeneous Universe at $z \sim 1,090$, corresponding to $t \sim 380,000$ years. At first glance, this is somehow surprising since we are looking at

almost the whole part of the Universe causally connected today[1] but when it was only $t \sim 380,000$ years old. Therefore, the causally connected regions at that time were much smaller than the observed portion of the Universe we observe at the CMB.

In Section 2.3 we defined the comoving particle horizon τ as the maximum distance a light signal is able to travel between time 0 and time t:

$$\tau \equiv \int_0^t \frac{\mathrm{d}t'}{a(t')} = \int_0^{a(t)} \frac{\mathrm{d}a}{Ha^2} \propto \begin{cases} a & \text{RD}, \\ a^{1/2} & \text{MD}. \end{cases} \tag{4.1}$$

This means that both in radiation and in matter dominance, the comoving horizon grows monotonically with time and hence at the time of last scattering the comoving horizon was much smaller than the portion of the sky we can observe today, or basically the portion seen at the CMB. In other words, there were many causally disconnected regions at last scattering surface. Nevertheless all the radiation coming from the last scattering surface is extremely homogeneous in temperature, no matter which part of that surface the radiation is coming from. In the Hot Big Bang model there is no a priory any reason why two causally disconnected regions must be that similar in energy density and in temperature. This fact is translated into an extreme fine tuning on the initial conditions of the energy density of the Universe, as this energy density should have had the same exact value in every part of it.

4.1.2 Flatness problem

In Section 2.1.2 it was shown the current constraints in the parameter $\Omega_k(a) \equiv 1 - \Omega(a)$ [2] taken from [19] are

$$-0.01 \leq \Omega_k(t_0) \leq 0.01 \tag{4.2}$$

which seem to indicate that we live in a nearly flat Universe with an energy density $\rho(t)$ very close to $\rho_c = 3H^2/(8\pi G)$. To be more precise let us quantify the problem in time. The Friedmann Equation reads

$$H^2 = \frac{8\pi G}{3}\rho(a) - \frac{k}{a^2}, \tag{4.3}$$

and it can be written as

$$\Omega_k(a) \equiv 1 - \Omega(a) = \frac{-k}{a^2 H^2}. \tag{4.4}$$

[1] We are observing photons coming to us from the last scattering surface, namely, the largest distance a free photon may have traveled since almost the beginning of the Universe.

[2] All the energy density components like the matter, radiation and dark energy components are encoded in $\Omega(a)$.

In standard cosmology, when the Universe is mainly filled of matter or radiation, the comoving Hubble radius, $(aH)^{-1}$, grows with time and so does $|\Omega_k(a)|$. Therefore, in standard Big Bang cosmology, the near-flatness observed today, $\Omega(a_0) \sim 1$, requires an extreme fine-tuning of Ω close to 1 in the early Universe. More specifically, one finds that the deviation from flatness at Big Bang Nucleosyntesis (BBN), during the GUT era and at the Plank scale, respectively has to satisfy the following conditions

$$\begin{aligned} |\Omega(a_{\rm BBN}) - 1| &\leq \mathcal{O}(10^{-16}), \\ |\Omega(a_{\rm GUT}) - 1| &\leq \mathcal{O}(10^{-55}), \\ |\Omega(a_{\rm Pl}) - 1| &\leq \mathcal{O}(10^{-61}). \end{aligned} \tag{4.5}$$

4.1.3 Some other problems

On top of those two main problems there were some other open questions in the Hot Big Bang cosmology. Here we list some of them [27]. It is important to notice that there exist problems which are model dependent, usually associated to some extensions of the Standard Model of particle physics, and others which are completely general and independent of the Cosmological and particle physics theories considered. For instance, the two problems discussed above are nearly model independent[3] as they refer to the initial conditions after the Big Bang.

- *Structure formation*

  Despite the high level of homogeneity observed in the early Universe, small perturbations were present giving rise to the current structures (such as stars and galaxies). For a long time, the origin of such density inhomogeneities remained completely obscure. As the horizon and flatness problems, the structure formation problem is also model independent.

  Probably the major success of inflationary theories is the elegant explanation of the origin of such perturbations, generated in the incredible amplification of quantum fluctuations of the inflationary field ϕ during Inflation. We will come back to this in Chapter 5.

- *The monopole problem*

  As already mentioned in Chapter 1, as the Universe cooled down, initial symmetries are expected to get broken, as it happens with the electroweak symmetry. These phase transitions could, in some cases, generate harmful structures capable of destroying some widely accepted epochs of the Universe. Perhaps, the most important effect is the creation of superheavy t'Hooft-Polyakov magnetic monopoles [28, 29], which

[3] There are cosmological theories that try to explain these two problems relying on the existence of the Universe before the Big Bang. It is easy to show that in these models, both problems are not present.

should be copiously produced in practically all of the grand unified theories [30]. In such theories, it has been shown [31] that the monopole density number at present should be comparable to the baryon number density. If that were the case, the Universe would have collapsed long ago since the typical monopole mass is around 16 orders of magnitude larger than the proton one.

- *The domain wall problem*

  Phase transitions due to spontaneous breaking of a discrete symmetry give rise to other undesirable effects. These discrete symmetries once broken generate different vacuum states where the fields driving them get different values. Domains filled by the field with an arbitrary vacuum value are separated from those with some other different value by domain walls. In turns out that the energy density of these walls is so high that the presence of a solely wall in any part of the observable Universe would lead to unacceptable consequences [32].

- *The primordial gravitino problem*

  An elegant and nice way to explain the hierarchy problem of unified field theories holds in supersymmetric theories. But as we know, supersymmetry must be broken and, in order to solve the hierarchy problem, the energy scale of this transition should be of the order of the electroweak scale. This in turn implies a mass for the gravitino of $m_{3/2} \sim m_{\rm W} \sim 10^2$ GeV [33]. However the rather slow decay of the gravitino for this mass range would spoil Big Bang Nucleosynthesis, and it is inconsistent with the observations [34, 35].

Contrarily to the first three ones, the monopole, domain wall and gravitino problems are, of course model dependent, and one can get rid of them by simply saying that these theories are not a good description of the physics beyond the Standard Model. Nevertheless one would like to be as general as possible, and to be able to include all possible extensions of the SM at high energy scales, which can be very helpful for other reasons, as already commented by the case of the gravitino.

We shall remark that the problems listed above are not the only ones but the most related to the work we will develop here.

4.2 Inflation. A first look

It is the scope of this Chapter and the next one to show how the problems listed in Section 4.1 might be solved within the framework of inflationary cosmology.

Let us focus specifically on two of them, namely the horizon and flatness problems. Both of them are intrinsically related to the evolution of the Hubble radius $(aH)^{-1}$ with the expansion of the Universe and arise since in the conventional cosmology the comoving Hubble radius is strictly increasing. If, on contrary, there was a period in the early Universe

where the Hubble radius decreased by a significant amount both problems can be relaxed or even solved completely.

- *Flatness problem solved qualitatively*

  Equation (4.4) shows that for a monotonically increasing Hubble radius $\Omega_k = 1-\Omega \to 1$ and only with an extreme fine tuning of initial conditions we would be able to explain the present value of Ω_k, compatible with zero. However, if somehow $(aH(a))^{-1}$ decreases, then, in that period $\Omega_k = 1 - \Omega \to 0$ and it is therefore possible to explain the tiny values listed in Eq. 4.5.

- *Horizon problem solved qualitatively*

  Figure 4.1 shows the evolution of the Hubble radius in the Hot Big Bang scenario together with an hypothetical period in the very early Universe in which $(aH(a))^{-1}$ decreases. In that scenario, a perturbation whose comoving scale k is plotted in blue, entering inside the Hubble radius some time not too far from today, could have already been inside it. That statement could explain why the greatest scales in the Universe appear with the same temperature, since in this scenario those scales could have come from a causally connected patch of the very early Universe.

Those facts suggest that a period in the very early Universe satisfying the condition

$$\frac{d(aH)^{-1}}{dt} < 0, \tag{4.6}$$

could solve the horizon and flatness problems. Such period is extensively known as *Inflation*. Indeed, as we will see, this hypothesis can solve not only these two problems but all of the problems listed before.

From the relation

$$\frac{d(aH)^{-1}}{dt} = \frac{-\ddot{a}}{(aH)^2}, \tag{4.7}$$

the condition (4.6) can be read as

$$\frac{d^2a}{dt^2} > 0. \tag{4.8}$$

So, the most common definition for Inflation is the following:

Inflation is a stage of accelerated expansion occurred in the very early Universe

Obviously in order to get rid of the problems mentioned above, it is mandatory to have at least a minimum time with acceleration. To get a quantitative analysis about how much of acceleration we need let us study more carefully both the flatness and the horizon problems.

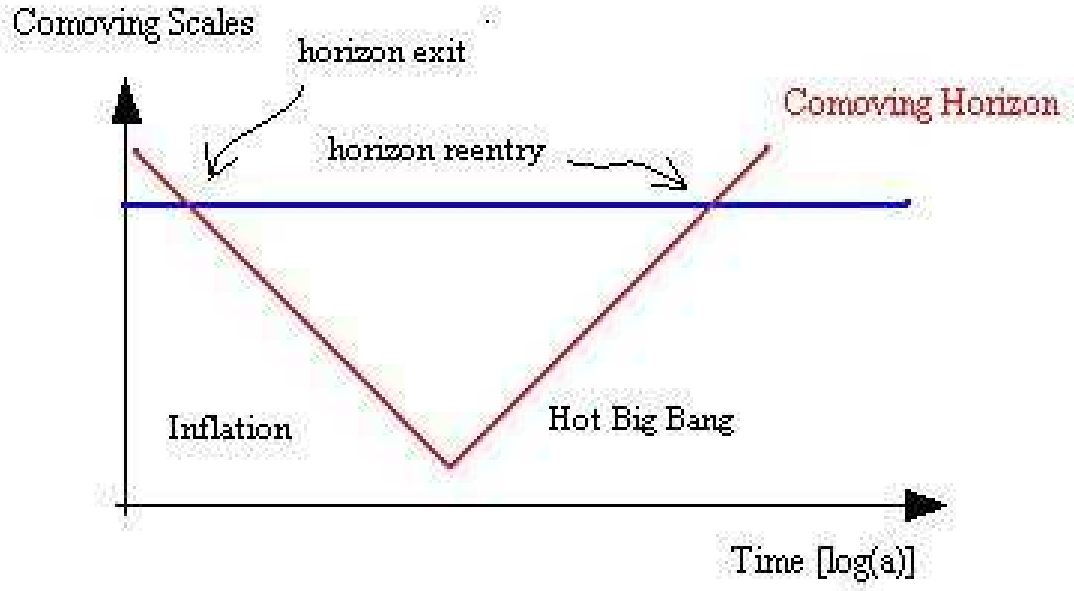

Figure 4.1: Evolution of the comoving Hubble radius during Inflation and the Hot Big Bang era (red line). The blue line represents a comoving scale inside the Hubble radius before Inflation started. During Inflation that scale went outside it and came back inside it in the last stages of the history of the Universe.

4.2.1 Flatness problem solved quantitatively

The hot Friedmann Universe is supposed to start shortly after Inflation ends. It is possible hence to infer what was the $\Omega_k(t_{end})$ when Inflation ended by relating it with the current value $\Omega_k(t_0) \lesssim 10^{-2}$. Indeed, following Eq. (4.4) such relation reads

$$\Omega_k(t_{end}) = \Omega_k(t_0)\frac{H_0^2}{a_{end}^2 H_{end}^2}, \tag{4.9}$$

where, as before, the subscript *end* refers to the end of Inflation. It is useful to refer everything to the matter-radiation equality ($z \sim 10^4$) since the value of the scale factor when $\Omega_m = \Omega_r$ is precisely $a_{eq} = \frac{\Omega_r(t_0)}{\Omega_m(t_0)}$ and to a good approximation the Hubble parameter at that time is well described by

$$\frac{H^2}{H_0^2} \approx \frac{\Omega_r(t_0)}{a^4} + \frac{\Omega_m(t_0)}{a^3}. \tag{4.10}$$

Evaluating H at matter-radiation equality we obtain from Eq. (4.10)

$$H_{eq}^2 \approx 2H_0^2\Omega_m(t_0)\left(\frac{\Omega_m(t_0)}{\Omega_r(t_0)}\right)^3. \tag{4.11}$$

Shortly after Inflation ends, it comes the era of radiation dominance. That fact allows us to relate H_{end} to H_{eq}. The relation is approximately equal to

$$H_{end}^2 \approx \frac{H_{eq}^2}{2}\left(\frac{a_{eq}}{a_{end}}\right)^4, \tag{4.12}$$

where we have divided by 2 considering that only 1/2 of H_{eq}^2 is actually coming from the radiation part. Putting Eqs. (4.9), (4.11) and (4.12) together we finally arrive to

$$\Omega_k(t_0) \approx \Omega_k(t_{end})\frac{H_{end}}{H_0}\sqrt{\Omega_r(t_0)}. \tag{4.13}$$

It will be useful for further discussions to relate $\Omega_k(t_{end})$ and $\Omega_k(t_{in})$ (at the end and at the beginning of Inflation respectively) in the following way,

$$\Omega_k(t_{in}) = e^{2C}\Omega_k(t_{end}), \tag{4.14}$$

where C is in principle the parameter we want to compute. Using the first Friedmann equation in the form

$$\frac{H^2}{H_0^2} = \frac{\rho}{\rho_0^c}(1+\Omega_k(t))^{-1} \Rightarrow \frac{H_{end}^2}{H_0^2} \simeq \frac{\rho_{end}}{\rho_0^c}, \tag{4.15}$$

Eq. (4.13) can be rewritten as

$$\Omega_k(t_0) \approx \Omega_k(t_{in}) e^{-2C} \sqrt{\frac{\rho_{end}\Omega_r(t_0)}{\rho_c^0}}, \tag{4.16}$$

where the critical density today is $(\rho_c^0)^{1/4} = 3^3 h^{1/2}$ eV, with $h \approx 0.7$ [19] and the total amount of radiation today can be expressed as

$$\Omega_r^0 = \Omega_\gamma (1 + 0.2271 N_{eff}), \tag{4.17}$$

with $\Omega_\gamma = 2.469 \times 10^{-5} h^{-2}$, $\Omega_k(t_0) \lesssim 10^{-2}$ [19]; and $N_{eff} = 3.046$ [36]. By substituting all the parameters and considering the energy scale after Inflation associated to ρ_{end} to be 2×10^{16} GeV [4], we find a value for C around 62 for the case $\Omega_k(t_{in}) \approx 1$.

A more useful formula for the value for this parameter C with free $\Omega_k(t_{in})$ and ρ_{end} is

$$C \simeq 26.5 + \frac{1}{2} \ln \frac{\Omega_k(t_{in})}{\Omega_k(t_0)} + \ln\, M_{end}[\text{GeV}], \tag{4.18}$$

where M_{end} is the energy scale after Inflation.

In order to relate C with Inflation let us assume a well motivated simplification discussed in Sec. 4.4.2, which is to consider a constant value for H through the whole period of Inflation. By doing so, we can easily relate the scale factor before and after Inflation

$$H \equiv \frac{\dot{a}}{a} \quad \Rightarrow \quad a_{end} = a_{in} e^{N_e}, \tag{4.19}$$

where N_e is the number of e-foldings that the Universe has expanded during Inflation and it is equal to

$$N_e \equiv \int_{t_{in}}^{t_{end}} H \mathrm{d}t \approx H \Delta t. \tag{4.20}$$

From Eq. (4.4) it follows that

$$\Omega_k(t_{in}) = \frac{a_{end}^2 H_{end}^2}{a_{in}^2 H_{in}^2} \Omega_k(t_{end}), \tag{4.21}$$

which together with Eq. (4.19) leads to

$$\Omega_k(t_{in}) = e^{2N_e} \Omega_k(t_{end}). \tag{4.22}$$

A direct comparison with Eq. (4.14) gives $C = N_e$.

[4] This is a typical energy density after Inflation for many models.

4.2.2 Horizon problem revised quantitatively

The Universe is observed to be homogeneous and isotropic everywhere at large scales with a high accuracy. In particular, CMB measurements show that deviations from homogeneity of one part in a hundred thousand. This is extremely surprising since at the last scattering surface, when the CMB was emitted, the Universe was only 380, 000 years old and according to the standard cosmological model, the particle horizon at that epoch was much smaller than the size of last scattering surface observed today, ~ 13 Gyr later, which is mainly the particle horizon today. To put some numbers let us compute the angle that the particle horizon at last scattering surface subtends for us.

The particle horizon at the time of last scattering d_{LS} is given by

$$d_{LS} = \frac{a_{LS}}{H_0}\int_0^{a_{LS}} \frac{\mathrm{d}a}{\sqrt{\Omega_r(t_0) + \Omega_m(t_0)a + \Omega_\Lambda a^4 + \Omega_k(t_0)a^2}}. \tag{4.23}$$

Assuming matter domination from last scattering surface until today $d_{LS} \approx H_0^{-1}(1 + z_{LS})^{-3/2}$. The angular distance of this surface $d_A(t_{LS}) = a(t_{LS})r_{LS}$ can be obtained by computing r_{LS} from the equality

$$\int_0^{r_{LS}} \frac{\mathrm{d}r}{\sqrt{1-kr^2}} = \frac{1}{H_0 a_{LS}}\int_{1/(1+z_{LS})}^{1} \frac{\mathrm{d}a}{\sqrt{\Omega_r(t_0) + \Omega_m(t_0)a + \Omega_\Lambda a^4 + \Omega_k(t_0)a^2}}, \tag{4.24}$$

which yields to

$$r_{LS} = \frac{1}{H_0\Omega_k(t_0)^{1/2}}\sinh\left[\int_{1/(1+z_{LS})}^{1} \frac{\Omega_k(t_0)^{1/2}\mathrm{d}a}{\sqrt{\Omega_r(t_0) + \Omega_m(t_0)a + \Omega_\Lambda a^4 + \Omega_k(t_0)a^2}}\right]. \tag{4.25}$$

This gives an approximate value for the angular distance of $H_0^{-1}a(t_{LS}) = H_0^{-1}(1+z_{LS})^{-1}$. Therefore, using Eq. (2.34) the angle subtended today by the particle horizon at the time of last scattering is roughly $\theta_{LS} \approx (1 + z_{LS})^{-1/2} \approx 1.6^o$, which means that there were about ten thousand causally disconnected regions in the last scattering surface.

The way to address the problem is, as before, by considering a period of Inflation which in turn would yield to an enhancement of the size of the particle horizon at the time of last scattering. The proper horizon distance at t_{LS} is

$$d_H(t_{LS}) \equiv a(t_{LS})\int_{t_{in}}^{t_{LS}} \frac{\mathrm{d}t}{a(t)}, \tag{4.26}$$

with t_{in} the beginning of the era of Inflation. Considering as before a constant value for H during Inflation and neglecting the contributions from the radiation and matter eras for d_H, which is negligible compared to what Inflation gives, we find

$$d_H(t_{LS}) = \frac{a(t_{LS})}{a_{end}H_{end}}(e^{N_e} - 1), \tag{4.27}$$

being N_e the number of e-foldings of Inflation defined in Eq. (4.19). Comparing Eq. (4.27) with the angular distance to the last scattering surface $d_A(t_{LS})$ we find that the condition $d_H(t_{LS}) > d_A(t_{LS})$ is satisfied if

$$e^{N_e} > \frac{a_{end}H_{end}}{H_0}, \tag{4.28}$$

which is the same condition that must be fulfilled to avoid the flatness problem[5].

4.2.3 Comments on the other problems

In the next Chapter we will explain how due to the inflationary mechanism, quantum fluctuations are magnified to macroscales driving the formation of the structures once they re-enter in the matter domination regime.

Concerning the rest of the problems, the stretching of the scales occurred during Inflation leads to an exponential decrease in the density of monopoles, domain walls, gravitinos, and other entities produced before or during Inflation. If T_R, the maximum temperature reached in the Universe once the radiation dominated era begins, is not high enough to produce monopoles, domain walls and gravitinos again, the corresponding problems disappear.

4.3 Historical notes about the origin of Inflation

Before going into detail on the study of the dynamics of Inflation, it is fare enough to write down some remarks about the different works that finally led to the born and development of the inflationary scenario.

From Eq.(2.24) we can extract the following information: To get an accelerated expansion in order to solve the problems already mentioned, we need a global fluid equation that satisfies the following condition

$$p < -\frac{\rho}{3}. \tag{4.29}$$

As we know both matter and radiation have equations of state that cannot accomplish Eq. (4.29). In the time Inflation was developed there was however a way to satisfy Eq. (4.29), which is the energy density coming from the lowest energy state or the vacuum of the theory (with $p = -\rho$). It was Zel'dovich [37] in 1968 who first noticed that within quantum

[5]Recall that $\Omega_k(t_{end}) = \Omega_k(t_0)\frac{H_0^2}{a_{end}^2 H_{end}^2} \approx e^{-2N_e}$ for $\Omega_k(t_{in}) \sim \mathcal{O}(1)$

mechanics, the vacuum certainly could have a nonzero energy density, produced by zero-point fluctuations. Following this idea, Kazanas [38] and Sato [39] both proposed a model with an accelerated expansion driven by the vacuum energy. Kazanas noted that the near exponential expansion could eliminate the particle horizon of the standard model and hence explain the observed homogeneity of the Universe. Sato tried to use his model to explain the observed asymmetry matter-antimatter, as a consequence of a spontaneous symmetry breaking that would have occurred with different signs in different regions, separated by domain walls. Nevertheless, both models failed in giving a natural exit to a FRW Universe. Parallel to these models, in 1979-1980 Starobinsky [40, 41] proposed an interesting scenario of the evolution of the Universe, in which the de Sitter metric is a solution of the Einstein equations with quantum corrections. It was Starobinsky who noticed that this solution is unstable, leading finally to a Friedmann Universe. The main objective pursued by Starobinsky was to solve the problem of the initial cosmological singularity[6], rather than the one of the initial conditions. Futhermore, the density inhomogeneities appearing after decay of the de Sitter space turned out to be too large [42, 43]. Despite the lack of a successful explanation for the initial conditions, Starobinsky model served as the first pillar to the inflationary idea and an improved version of it is indeed one of the most studied inflationary models (to be more precise the Chaotic Inflation scenario).

The necessity of considering scenarios of a quasiexponential accelerated expansion was only fully recognized after Guth's work [44]. In this scenario, the Universe initially is in a ultra-high temperature state, with a global global minimum for the potential at $\phi = 0$. As the Universe expands, the temperature falls off and the potential minimum is displaced to a different position, $\phi \neq 0$. Nonetheless, $\phi = 0$ is still a local minimum, and the field ϕ remains in that state for a long time. It is in this state where the temperature becomes negligible and so does the kinetic term for the inflaton, compared to its potential energy, inflating the Universe with a nearly exponential acceleration. Finally, Inflation ends sharply due to a first order phase transition to the true minimum ϕ_0 of the potential. This process forms bubbles with ϕ_0 surrounded with regions with $\phi = 0$. It is due to bubble collisions that the Universe finally heats up, leading to a hot Friendmann evolution.

Guth's version of Inflation was not free of some defects. It assumed a first order phase transition as the end of the Inflationary period. As Sato anticipated [45], this has the problem that the nucleation rate is estimated to be too slow to lead Inflation to an end. Also as noted by Guth himself collisions of walls should destroy homogeneity and isotropy created during the exponential expansion in an unacceptable level. Those problems were soon solved in the pictures developed by Linde [46, 47] and Albrecht and Steinhardt [48], in which the phase transition is of the second order, continuous but rapid enough to produce the amount of entropy needed. This so called *new Inflation scenario* generates the accelerated expansion not in a supercooled state $\phi = 0$ as in the previous case, but while the slow growth of the field ϕ from the origin to its real minimum ϕ_0. In order to inflate the Universe long enough, the time t taken for the field to reach the minimum must be much longer than

[6] In a Friedmann Robertson Walker Universe filled by matter or radiation there is a singularity at $t = 0$ since $a(t)\big|_{t\to 0} = 0$ and hence, the energy density of the Universe at that time should be infinite.

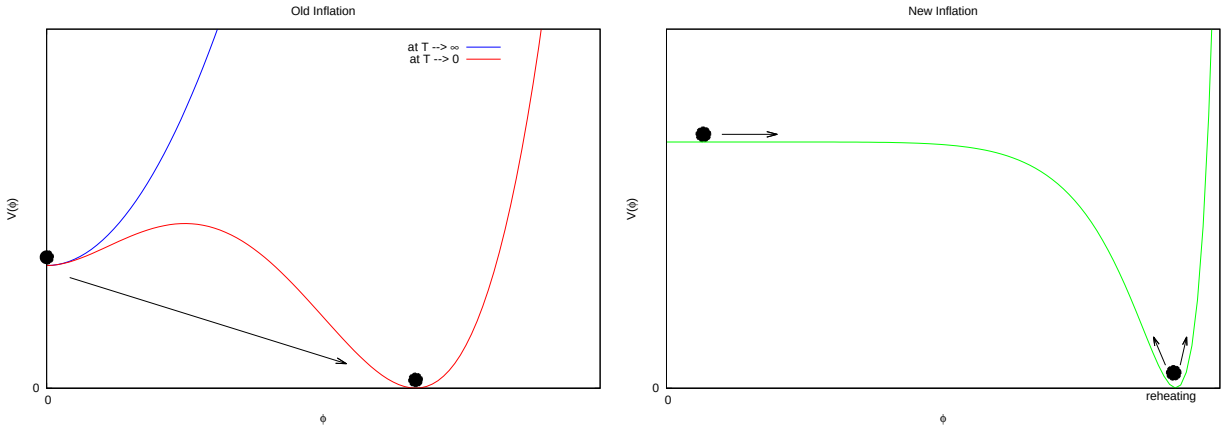

Figure 4.2: Typical potentials of the Inflationary field ϕ of both the old (left) and new (right) scenarios. It is shown that in the old scenario at high temperature the field is bound near its minimum around zero (blue curve) and the Universe expands exponentially fast due to the *vacuum-like* state provided by the potential energy of the ϕ field. Once the temperature falls down to 0 a new minimum appears (red curve) and the Inflatory field finally undergoes a first order phase transition to its real minumum. In the new scenario however, the quasi-exponential expansion is driven by the field ϕ but in a second order phase transition slow enough to give the Universe the needed expansion and finally the field reaches its minimum and starts *reheating* the Universe.

H^{-1} which can be satisfied for sufficiently flat potentials $V(\phi)$ near $\phi = 0$. In this scenario the Universe heats up not because of wall collisions, but due to particle creation by the classical field ϕ when it starts oscillating around its minimum. In this period commonly named *reheating*, the energy stored in the inflationary field is rapidly transfered to other particles (such as the standard model ones) and the temperature of the Universe heats up to values that typically are of the order of $T_{reh} \approx 10^{15}$ GeV [7].

Figure 4.2 shows two typical potentials that lead to both the old and the new Inflation scenarios, respectively.

In the next Section we will describe how Inflation may be driven by means of a single scalar field leaving the discussion of the generation of perturbations for Chapter 5

4.4 Dynamics of Inflation

So far we have discussed why we need a period like Inflation but not how to generate such period. In this Section we will briefly describe the dynamics of the simplest particle physics model from which we can generate an accelerated expansion for the Universe, namely, the *single field model*. Then we will summarize the most important models in the zoo of

[7] The subscript *reh* refers to the temperature reached once the reheating process is completed.

Inflationary scenarios present in the literature.

4.4.1 Single Field Inflation

Following [7], the simplest models of Inflation involving a single scalar field ϕ, the *Inflaton*, minimally coupled to gravity. Here, we do not specify the physical nature of the field ϕ, but simply use it as a "clock" to parametrize the time-evolution of the Inflationary energy density. The dynamics of that scalar field is governed by the action

$$S = \int \mathrm{d}^4x\sqrt{-g}\left[\frac{1}{2}R + \frac{1}{2}g^{\mu\nu}\partial_\mu\phi\partial_\nu\phi - V(\phi)\right] = S_{\rm EH} + S_\phi. \tag{4.30}$$

The action in Eq. (4.30) is the sum of the gravitational Einstein-Hilbert action, $S_{\rm EH}$, and the action of a scalar field with canonical kinetic term, S_ϕ. The potential $V(\phi)$ describes the self-interactions of the scalar field. The field equation of motion is

$$\frac{1}{\sqrt{-g}}\partial_\mu(\sqrt{-g}\partial^\mu\phi) + V_{,\phi} = 0, \tag{4.31}$$

where $V_{,\phi} = dV/d\phi$. On the other hand the energy momentum tensor for the scalar field is

$$T^{(\phi)}_{\mu\nu} \equiv -\frac{2}{\sqrt{-g}}\frac{\delta S_\phi}{\delta g^{\mu\nu}} = \partial_\mu\phi\partial_\nu\phi - g_{\mu\nu}\left(\frac{1}{2}\partial^\sigma\phi\partial_\sigma\phi + V(\phi)\right). \tag{4.32}$$

Assuming a FRW metric, Eq. (2.14), and restricting to the case of a homogeneous field $\phi(t,\mathbf{x}) \equiv \phi(t)$, the scalar energy-momentum tensor takes the form of a perfect fluid, Eq. (2.16), with

$$\rho_\phi = \frac{1}{2}\dot\phi^2 + V(\phi), \tag{4.33}$$

$$p_\phi = \frac{1}{2}\dot\phi^2 - V(\phi). \tag{4.34}$$

The resulting equation of state for that fluid reads

$$w_\phi \equiv \frac{p_\phi}{\rho_\phi} = \frac{\frac{1}{2}\dot\phi^2 - V(\phi)}{\frac{1}{2}\dot\phi^2 + V(\phi)}, \tag{4.35}$$

and shows that a scalar field can lead to an accelerated expansion ($w_\phi < -1/3$, see Eq. (2.24)) if the potential energy dominates over the kinetic energy (concretely, $V(\phi) > \dot\phi^2$). The dynamics of the (homogeneous) scalar field, Eq. (4.31), and the FRW geometry are determined by

$$\ddot\phi + 3H\dot\phi + V_{,\phi} = 0 \qquad \text{and} \qquad H^2 = \frac{8\pi G}{3}\left(\frac{1}{2}\dot\phi^2 + V(\phi)\right). \tag{4.36}$$

This set of two equations determines uniquely the evolution of the expansion of the Universe, encoded in the scale factor a, and the evolution of the homogeneous field ϕ.

4.4.2 Slow-roll approximation

In order to achieve an accelerated expansion of the Universe $\ddot{a} > 0$ it is enough to be dominated by a fluid with an equation of state satisfying $p < -1/3\ \rho$, which, in the case of a single scalar field, as we have seen in the previous Section, is translated into the condition $V(\phi) > \dot{\phi}^2$. Nevertheless the quasi-exponential expansion described in previous sections needs of an equation of state $p \approx -\rho$, or in other words, $V(\phi) \gg \dot{\phi}^2$ in single field Inflationary models, described above. Also it can be shown (see Sec 5.3 of [11]) that this condition must be satisfied to get a substantial amount of expansion, i.e. a sufficiently large number of e-folds.

In that case, the Hubble function can be well approximated by $H \approx \sqrt{\frac{8\pi G}{3}V(\phi)}$. It is well known that a large friction term damps the initial velocities and enforces a slow-roll regime where the acceleration can be neglected compared to the friction term. This means that in the first of Eqs. (4.36) we can drop $\ddot{\phi}$ and hence the equations describing this stage are now

$$3H\dot{\phi} + V_{,\phi} \approx 0 \qquad \text{and} \qquad H^2 \approx \frac{8\pi G}{3}V(\phi), \tag{4.37}$$

combining them we can translate the condition $\dot{\phi} \ll \sqrt{V(\phi)}$ into some other form

$$\sqrt{V(\phi)} \gg \dot{\phi} \approx -\frac{V_{,\phi}}{3H} \approx -\frac{V_{,\phi}}{\sqrt{24\pi G V(\phi)}} \qquad \Rightarrow \qquad \left|\frac{V_{,\phi}}{V}\right| \ll \sqrt{24\pi G}. \tag{4.38}$$

Another useful relation can be obtained deriving $\dot{\phi} \approx -\frac{V_{,\phi}}{3H}$ with respect to time

$$\ddot{\phi} \approx -\frac{V_{,,\phi}\dot{\phi}}{3H} + \frac{V_{,\phi}\dot{H}}{3H^2} \approx \frac{V_{,,\phi}V_{,\phi}}{9H^2} - \frac{V_{,\phi}^3}{48\pi G V(\phi)^2}. \tag{4.39}$$

Together with the condition $\ddot{\phi} \ll V_{,\phi}$, Eq. (4.39) leads to

$$\left|\frac{V_{,,\phi}}{V}\right| \ll 24\pi G, \tag{4.40}$$

where we have used Eq. (4.38). We can define now the so called slow-roll parameters ϵ_V and η_V

$$\epsilon_V \equiv \frac{M_P^2}{2}\left(\frac{V_{,\phi}}{V}\right)^2, \tag{4.41}$$

$$\eta_V \equiv M_P^2 \frac{V_{,,\phi}}{V}, \tag{4.42}$$

being $M_P = 1/\sqrt{4\pi G} \approx 10^{19}$ GeV the Planck mass. The slow-roll regime is accomplished if and only if $\epsilon_V \ll 1$ and $\eta_V \ll 1$ and this description breaks down when either $\epsilon_V \sim 1$ or $|\eta_V| \sim 1$. The subscript 'V' refers to the use of the potential in the definition. Indeed, these definitions are not the only ones to describe the slow-roll regime. The relation among H and $V(\phi)$ can be used to define another 2 slow-roll parameters, this time in terms of H.

$$\epsilon_H \equiv 2M_P^2 \left(\frac{H_{,\phi}}{H}\right)^2, \tag{4.43}$$

$$\eta_H \equiv 2M_P^2 \frac{H_{,,\phi}}{H}. \tag{4.44}$$

These last ones are usually called 'Hubble slow-roll parameters' to distinguish them from those of the Eqs. (4.41) and (4.42). It is easy to check that in the slow-roll regime the relations among them are

$$\epsilon_V \approx \epsilon_H \qquad \text{and} \qquad \eta_V - \epsilon_V \approx \eta_H \qquad \text{when} \qquad \epsilon_i,\ \eta_i \ll 1, \quad \text{being} \varepsilon i = V, H. \tag{4.45}$$

In Section 4.2.1 we introduced the number of e-folds N_e. Using the definition of ϵ_H we now obtain

$$N_e(t_{in}, t_{end}) \equiv \int_{t_{in}}^{t_{end}} H \mathrm{d}t = \int_{\phi_{in}}^{\phi_{end}} \frac{H}{\dot{\phi}} \mathrm{d}\phi = \frac{1}{M_P} \int_{\phi_{end}}^{\phi_{in}} \sqrt{\frac{2}{\epsilon_H}} \mathrm{d}\phi, \tag{4.46}$$

where in the las equality we have made use of the equation

$$\dot{H} = -\dot{\phi}^2, \tag{4.47}$$

obtained deriving the left part of Eq. (4.36) with respect to time and using its right part, together with $\dot{H} = H_{,\phi}\dot{\phi}$.

As a toy example we can study the case of a power-law potential of the form

$$V(\phi) = g\phi^\alpha, \tag{4.48}$$

with g and α arbitrary real parameters satisfying $g > 0$ and $|\alpha|$ not orders of magnitude bigger than 1. The slow-roll conditions, Eqs. (4.38) and (4.40), can be both satisfied for $|\alpha| \geqslant 2$ for values of the field $\phi \gg 1/\sqrt{6\pi G} = \sqrt{2/3} M_P$. This value should be taken as ϕ_{end} since it is the value that makes the acceleration of the scale factor $\ddot{a}$ go from positive to negative values, ending the Inflationary stage.

It is important to note that such large values of the scalar field do not necessarily mean that we should use a full quantum description of gravity. These quantum gravitational

effects can be neglected as long as the energy density involved in the problem, which is the potential of the field $V(\phi)$, is much smaller than the Planck energy density:

$$|V(\phi)| \ll \frac{1}{(4\pi G)^2}. \tag{4.49}$$

So for sufficiently small coupling constant g (see Eq. (4.48)) quantum effects are negligible and can be ignored.

From Eq. (4.46) it is possible to infer the value ϕ_{in} for a given N_e. For the potential given in Eq. (4.48) we find

$$\begin{aligned} N_e \approx \tfrac{2}{M_P^2}\int_{\phi_{end}}^{\phi_{in}}\left(\tfrac{V}{V_{,\phi}}\right)\mathrm{d}\phi = \tfrac{1}{\alpha}\left(\tfrac{\phi_{in}^2}{M_P^2}-\tfrac{2}{3}\right) \quad \Rightarrow \\ \Rightarrow \qquad \phi_{in} = \sqrt{(\tfrac{2}{3}+\alpha N_e)}M_P \approx \sqrt{\alpha N_e}M_P, \end{aligned} \tag{4.50}$$

where we have considered $N_e \approx 60$ and $|\alpha| \geqslant 2$ in the last equality.

4.5 Reheating

Once the inflaton field starts approaching the minimum of the potential, its velocity starts increasing and finally its kinetic energy is of the same order of the potential energy so that the condition $p_\phi < -\rho_\phi/3$, needed to have acceleration (see Eq. (2.24)), is no longer satisfied. After this period of Inflation, ϕ begins to oscillate around the minimum of the potential and to decay to other fields including the fields of ordinary matter and radiation. This period is known as *reheating*. It is this period when the entropy observed in the present Universe is supposed to be generated.

When coupling the inflaton to other fields, the energy density of the field ϕ decreases as

$$\rho_\phi(t) = \rho_\phi(t_{in})\left(\frac{a(t_{in})}{a(t)}\right)^3 e^{-\Gamma(t-t_{in})}, \tag{4.51}$$

where Γ is the decay rate of the ϕ quanta into other particles, and t_{in} is the time of the beginning of the inflaton oscillations and decay. The energy density ρ_M of the particles into which ϕ decays satisfies the equation:

$$\dot{\rho}_M + 3H(\rho_M + p_M) = \Gamma\rho_\phi. \tag{4.52}$$

Following [15] it is easy to compute the maximum energy density of the particles ϕ decays into in two extreme cases, $\Gamma \gg H(t_{in})$ and $\Gamma \ll H(t_{in})$, supposing that these particles are highly relativistic.

For $\Gamma \gg H(t_{in})$ we see that $\rho_{M,max} \approx \rho_\phi(t_{in})$, indicating that the decay is extremely efficient and fast, whereas for $\Gamma \ll H(t_{in})$ we have

$$\rho_{M,max} = 0.139 \left(\frac{\Gamma}{H(t_{in})}\right) \rho_\phi(t_{in}), \tag{4.53}$$

(see Eq. 4.2.31 of [15]). In this case the maximum energy density at the beginning of the radiation-dominated era would have been much less than the energy density in the inflaton filed at the end of inflation.

This maximum of the energy density $\rho_{M,max}$ gives as well the maximum temperature ever reached in our Universe, so called *reheating temperature* T_{RH}, which indicates what particle species could have been created after Inflation (those with bare mass less than T_{RH}, roughly) and which ones were not created ever. As explained in Section 4.2, in order to get rid of some problems regarding the creation of undesirable relics, we need this temperature to be not too high to avoid the thermal creation of such relics after Inflation.

4.6 Brief classification of Inflationary models

Giving the lack of knowledge on the concrete details of the inflationary period, many different theories have been used to describe it, leading to similar, and in many cases indistinguishable, results. In that sense, it has been useful to classify different models regarding some common properties they present in describing a period of acceleration.

For instance, for single field models[8] such as the already described above in the slow-roll regime, the shape of the potential $V(\phi)$ determines completely all the properties we are able to measure in observations of the CMB. The different possibilities for $V(\phi)$ can be classified by comparing the initial value of the field ϕ with respect to M_P. In that sense we find

- *Small-Field models*

  In these models, the value of the field ϕ is sub-Planckian all time during Inflation. It starts close to zero and evolves to greater values, to its real minimum. The potential that give rise to such small field evolution often arises in mechanisms of spontaneous symmetry breaking. This potential can be locally approximated by

  $$V(\phi) = V_0 \left[1 - \left(\frac{\phi}{\mu}\right)^p\right] + \ldots, \tag{4.54}$$

  where the dots account for terms that may become important in the last stages of Inflation or during the reheating process. A particle physics motivated model for the $p = 2$

[8] When we talk about single field models, we refer to models with only one field acting as the Inflaton, regardless whether that field is the only one present in the Universe at that time or not. In that sense, *hybrid models* are also single field models even though they have two scalar fields.

case is a pseudo-Nambu-Goldstone boson like the axion [49]. An important property of these models is that they do not produce strong enough primordial gravitational waves to be detected in future observations.

- *Large-Field models*

  In this case, the value of the field is super-Planckian at the beginning of Inflation and then evolves towards the minimum, which is placed at $\phi = 0$. They are usually characterized by *chaotic* initial conditions for ϕ and its derivatives [47].

  A typical potential is given by a single monomial term of the form

$$V(\phi) = \lambda_p M_P^{4-p} \phi^p. \tag{4.55}$$

  Even though the value of the field has to be above the Planck mass, the value of the self coupling must be very small to account for the small density perturbations generated during Inflation (see next Section), $\lambda_p \ll 1$. This automatically guaranties that the potential energy is sub-Planckian, $V \ll M_p^4$ and quantum gravity corrections can be ignored.

  One observational difference with respect to the small-field models is that, in this cases, the value for the amplitude of the primordial gravitational waves is sufficiently high to be observed in future experiments. Analyzing the curvature of the potential in the region of interest for small and large field models we find another difference: for the first ones $V'' > 0$ while for large field models $V'' < 0$.

- *Hybrid models*

  Normally, for small and large field models the energy density stored in the potential $V(\phi)$ after all the process is negligible. This is not the case in hybrid models. In this case, the inflaton keeps a significant amount of energy at the end, $V(\phi_{end}) \neq 0$. Inflation ends by means of the action of another scalar field χ.

  The simplest example of hybrid Inflation [50] presents a potential

$$V(\phi, \chi) = \frac{\lambda_1}{4}(\chi^2 - M^2)^2 + \frac{1}{2}m^2\phi^2 + \frac{1}{2}\lambda_2\phi^2\chi^2. \tag{4.56}$$

  For sufficiently large ϕ, the minimum of the potential is along the direction $\chi = 0$ but once ϕ falls off $\phi_0 = \lambda_1 M^2/\lambda_2$, the χ field stars rolling down to one of its two minima ($\chi = \pm M$ for $\phi = 0$). The field χ it is usually named a 'waterfall' since it is due to its presence that Inflation can terminate by allowing ϕ to end its evolution in the true minimum with $V = 0$.

  The effective potential for the ϕ field during Inflation can be read as

$$V_{eff}(\phi) = \frac{\lambda_1}{4}M^4 + \frac{1}{2}m^2\phi^2, \tag{4.57}$$

and in general these models work for sub-Planckian values of the field ϕ. However, they present a positive curvature of the potential $V'' > 0$. That is the reason why they are known as hybrid models.

Obviously single field slow-roll Inflation is not the end of the game. A large number of phenomenological models has been proposed with different theoretical motivations and observational predictions. An extensive summary of models of Inflation can be seen in [51]. Among the most extensively studied we find *Non-minimal coupling to gravity* models, models based on *Modified gravity* theories, models with *More than one field* active during Inflation and models with *Non-canonical kinetic terms* (related to our work in Chapter 7) that we will briefly describe in the following:

Non-canonical kinetic terms

One possible generalization of a typical action for the inflaton ϕ is to include non-canonical kinetic terms of the form:

$$\mathcal{L} = F(\phi, X) - V(\phi), \qquad X \equiv \frac{1}{2} g^{\mu\nu} \partial_\mu \phi \partial_\nu \phi. \tag{4.58}$$

It is possible then, that Inflation occurs out of the slow-roll regime, driven totally by the kinetic term.

In this Chapter we have reviewed the properties of the inflationary models given by the evolution of the homogeneous field $\phi(t)$. In the next Chapter we present the properties concerning the quantum fluctuations of that field and how they are translated into Cosmological Perturbations during Inflation.

Chapter 5

The origin of Cosmological Perturbations

Despite the successful realization of Inflation solving the problems described in the previous Chapter, the greatest goal achieved for the inflationary scenario has not been already described here. That is the simple but rather wise explanation for the generation of the Cosmological Perturbations, emerging from the amplification of quantum fluctuations present on the inflaton field ϕ due to the inflationary process. Here we present the computation of such perturbations in the simplest case of single-field slow-roll Inflation, and their relation with observables.

5.1 General description of perturbations and gauge invariant quantities

Despite the presence of inhomogeneous objects in our current Universe such as galaxies and clusters, observations of the CMB shows us a Universe extremely homogeneous at early times. We thus split any quantity $X(t, \mathbf{x})$ into its homogeneous part $\bar{X}(t)$ and the related perturbation

$$\delta X(t, \mathbf{x}) \equiv X(t, \mathbf{x}) - \bar{X}(t), \qquad \text{with} \quad \delta X(t, \mathbf{x}) \ll \bar{X}(t), \tag{5.1}$$

where the last condition in Eq. (5.1) allows us to work using linear theory.

5.1.1 Decomposition of perturbations

Rotational and translational invariance of the background can be used to classify perturbations in a useful way. To do so, it is easier to describe perturbations in Fourier space

$$X_{\mathbf{k}}(t) = \int \mathrm{d}^3\mathbf{x}\, X(t,\mathbf{x}) e^{i\mathbf{k}\cdot\mathbf{x}} \tag{5.2}$$

Translational invariance for the perturbations means that the different Fourier modes do not interact one to each other. Spatial rotational invariance of the background allows a decomposition of the metric and the stress-energy tensor perturbations into independent scalar, vector and tensor modes. Generally speaking, applying a rotation of the coordinate system of an angle φ changes the amplitude of a given perturbation by a factor $e^{im\varphi}$

$$X_{\mathbf{k}} \to e^{im\varphi} X_{\mathbf{k}}, \tag{5.3}$$

with m known as the helicity of the perturbation. Scalar, vector and tensor perturbations have helicity 0, ± 1 and ± 2 respectively. As already commented, scalar, vector and tensor perturbations evolve independently and can therefore, be treated independently.

Einstein equations (2.1) relate the matter components of the Universe with its geometry, encoded in the metric $g_{\mu\nu}$. We must decompose the metric as well as the stress-energy tensor $T_{\mu\nu}$ into their scalar, vectorial and tensorial components.

For the metric tensor, the decomposition in real space up to first order in the perturbations is done as follows

$$\begin{aligned} \mathrm{d}s^2 &= g_{\mu\nu}\mathrm{d}x^\mu \mathrm{d}x^\nu = \\ &= -(1+2\phi)\mathrm{d}t^2 + 2aB_i \mathrm{d}x^i \mathrm{d}t + a^2[(1-2\psi)\delta_{ij} + E_{ij}]\mathrm{d}x^i \mathrm{d}x^j, \end{aligned} \tag{5.4}$$

with

$$B_i \equiv \partial_i B - S_i, \qquad \text{where} \quad \partial^i S_i = 0, \tag{5.5}$$

and

$$E_{ij} \equiv 2\partial_i\partial_j E + 2\partial_{(i}F_{j)} + h_{ij}, \qquad \text{where} \quad \partial^i F_i = 0, \quad h^i_i = 0 \quad \text{and} \quad \partial^i h_{ij} = 0. \tag{5.6}$$

ϕ [1], ψ, B and E describe the scalar perturbations. In addition, S_i and F_i are the vectorial components of the perturbations while h_{ij} represents the tensorial part.

We will adopt a generic prescription to define the matter perturbations in the stress-energy tensor in terms of its energy density ρ, pressure p, 3-d velocity of the fluid v_i, and its purely tensorial components, encoded in the anisotropic stress tensor Σ^i_j:

[1] Notice that ϕ now is one of the scalar metric perturbations and not the inflation field used in the previous Chapter.

$$\begin{aligned} T^0_0 &= -(\bar{\rho} + \delta\rho) \\ T^0_i &= (\bar{\rho} + \bar{p})v_i \\ T^i_0 &= -(\bar{\rho} + \bar{p})(v^i + B^i) \\ T^i_j &= (\bar{p} + \delta p) + \Sigma^i_j. \end{aligned} \tag{5.7}$$

Here again we find the different types of perturbations, namely the scalar, vector and tensor perturbations. Each one will be related with the metric perturbations via the Einstein equations (2.1). However, we will only focus on the scalar and tensor ones, as vector perturbations are not generated in Inflation and, in any case, they dilute with the expansion of the Universe.

Moreover, instead of writing down all scalar and tensor perturbation equations coming from the Einstein equations, in the following we will introduce some important quantities which are gauge invariant and derive the results for their power spectrum.

5.1.2 Gauge-Invariant Variables

Contrary to the case of the homogeneous and isotropic Universe, where the preferable coordinate system is fixed by the symmetry properties of the background, there are no obvious preferable coordinates for analyzing perturbations. The freedom in the coordinate choice, or gauge freedom, leads to the appearance of fictitious perturbation modes. These fictitious modes do not describe real inhomogeneities, but reflect only the properties of the coordinate system used. It is therefore mandatory to find gauge-invariant variables to safely describe the perturbations independently of the choice of coordinates made in any computation.

As an example, let us consider the transformation laws for the metric $g_{\mu\nu} \equiv \bar{g}_{\mu\nu} + \delta g_{\mu\nu}$ [2] for the following coordinate transformation:

$$x^\rho \to \tilde{x}^\rho = x^\rho + \xi^\rho, \tag{5.8}$$

where ξ^ρ are infinitesimally small functions of space and time. The metric tensor in the coordinates $\tilde{x}^\rho$ is related with the one in x^ρ by

$$\tilde{g}_{\mu\nu}(\tilde{x}^\rho) = \frac{\partial x^\alpha}{\partial \tilde{x}^\mu}\frac{\partial x^\beta}{\partial \tilde{x}^\nu} g_{\alpha\beta}(x^\rho) \approx \bar{g}_{\mu\nu}(x^\rho) + \delta g_{\mu\nu} - \bar{g}_{\mu\delta}\xi^\delta_{,\nu} - \bar{g}_{\delta\nu}\xi^\delta_{,\mu}, \tag{5.9}$$

keeping only terms linear in both δg and ξ. It is easy to show that the relationship among the metric perturbations in both coordinate systems is

$$\delta g_{\mu\nu} \to \delta\tilde{g}_{\mu\nu} = \delta g_{\mu\nu} - \bar{g}_{\mu\nu,\delta}\xi^\delta - \bar{g}_{\delta\nu}\xi^\delta_{,\mu} - \bar{g}_{\mu\delta}\xi^\delta_{,\nu}. \tag{5.10}$$

[2] $\bar{g}_{\mu\nu}$ represents the background value for the metric while $\delta g_{\mu\nu}$ are the metric perturbations.

Considering only scalar perturbations, the metric, Eq. (5.4), takes the form

$$ds^2 = -(1+2\phi)dt^2 + 2a\partial_i B dx^i dt + a^2[(1-2\psi)\delta_{ij} + \partial_i\partial_j]dx^i dx^j. \tag{5.11}$$

From Eq. (5.10) it is easy to infer how the scalar perturbations transform under (5.8):

$$\begin{aligned} \phi \to \tilde{\phi} = \phi + \dot{\xi}^0 \qquad & B \to \tilde{B} = B + \frac{1}{a}\left(-\xi^0 - \dot{\xi}_{||} + 2\frac{\dot{a}}{a}\xi_{||}\right) \\ \psi \to \tilde{\psi} = \psi - \frac{\dot{a}}{a}\xi^0 \qquad & E \to \tilde{E} = E - \frac{1}{a^2}\xi_{||}, \end{aligned} \tag{5.12}$$

where we have decomposed the spatial components of ξ^μ into a 3-vector with zero divergence $\xi^i_\perp$ and a scalar function $\xi_{||}$:

$$\xi^i = \xi^i_\perp + \xi^{,i}_{||}. \tag{5.13}$$

From the transformation laws in Eqs. (5.12) it is easy to see that only two scalar functions enter in the game: ξ^0 and $\xi_{||}$, and by choosing them appropriately, we can make 2 of the four functions ϕ, ψ, E and B vanish. As an example, the simplest gauge-invairant quantities are

$$\Phi \equiv \phi + \frac{d}{dt}\left[a^2\left(\frac{B}{a} - \dot{E}\right)\right] \qquad \Psi \equiv \psi - \dot{a}a\left(\frac{B}{a} - \dot{E}\right) \tag{5.14}$$

Vector perturbations are not produced in Inflation and, in any case, they are diluted by the expansion of the Universe. Hence, we will ignore them.

For tensor perturbations we have

$$ds^2 = -dt^2 + a^2(\delta_{ij} + h_{ij})dx^i dx^j, \tag{5.15}$$

and h_{ij} is already invariant under a coordinate transformation.

5.1.3 $\mathcal{R}$ and ζ

An important gauge-invariant quantity is the curvature perturbation on uniform density hypersurfaces [53, 54].

$$-\zeta \equiv \psi + \frac{H}{\dot{\bar{\rho}}}\delta\rho. \tag{5.16}$$

Another related scalar gauge invariant variable is the comoving curvature perturbation

$$\mathcal{R} \equiv \psi - \frac{H}{\bar{\rho} + \bar{p}} \delta q \tag{5.17}$$

where δq is the scalar part of the 3-momentum density $T_i^0 = \partial_i \delta q$. During Inflation $T_i^0 = -\dot{\bar{\phi}} \partial_i \delta\phi$, where $\delta\phi$ is the perturbation in the inflaton field, and hence

$$\mathcal{R} = \psi + \frac{H}{\dot{\bar{\phi}}} \delta\phi. \tag{5.18}$$

Geometrically, $\mathcal{R}$ measures the spatial curvature of comoving (or constant-ϕ) hypersurfaces. In slow-roll Inflation we have

$$\frac{\delta\rho}{\dot{\bar{\rho}}} \approx \frac{\delta\phi}{\dot{\bar{\phi}}}, \tag{5.19}$$

in agreement with the fact that actually, the inflaton field in the slow-roll regime is nothing but one simple way of parametrizing the energy scale of Inflation at any time. Comparing then Eq. (5.16) with Eq. (5.17) we find that during the slow-roll regime $\zeta = -\mathcal{R}$.

It can be shown [7] that the above relation also holds for superhorizon scales, $k \ll aH$, and both ζ and $\mathcal{R}$ are constant at these scales for adiabatic matter perturbations, *i.e.* perturbations that satisfy

$$\delta p - \frac{\dot{\bar{p}}}{\dot{\bar{\rho}}} \delta\rho = 0. \tag{5.20}$$

The conservation of ζ and $\mathcal{R}$ outside the horizon is extremely important since the statistical properties of these perturbations in superhorizon scales will remain invariable all the subsequent evolution of the Universe, until they re-enter again inside the horizon, either in radiation or in matter dominance. In the next Section we will come back to this property.

Tensor perturbations are already gauge invariant quantities and one of the modes remains constant after horizon crossing [11].

5.2 Scalar and Tensor power spectra of the perturbations

As already mentioned in Sec. 3.1, the quantities of greatest cosmological interest are *averages*. These averages can be used to constrain our cosmological model and its parameters in observations like the CMB or LSS. As we will see in this section, the 2-point correlation function or rather its Fourier transform, the *power spectrum*, carries most of the information of the physics behind the generation of perturbations during Inflation, and can be used to constrain inflationary models. In the last Section we will see how to relate these theoretical quantities with observations.

Let us define some crucial quantities which will be related later with observables in the CMB. The power spectrum of the gauge invariant scalar perturbation $\mathcal{R}$ (or equivalently of ζ), $P_{\mathcal{R}}(k)$ reads

$$\langle \mathcal{R}_{\mathbf{k}} \mathcal{R}_{\mathbf{k}'} \rangle = (2\pi)^3 \delta(\mathbf{k}+\mathbf{k}') P_{\mathcal{R}}(k), \qquad \Delta^2_{\mathcal{R}} = \frac{k^3}{2\pi^2} P_{\mathcal{R}}(k), \tag{5.21}$$

where $\langle \dots \rangle$ defines the ensemble average of the fluctuations and $\mathcal{R}_{\mathbf{k}}$ is the fourier transform of the scalar perturbation $\mathcal{R}$.

$$\mathcal{R}(\mathbf{x}, \mathbf{t}) = \int \mathrm{d}^{\mathbf{3}}\mathbf{k}\, \mathbf{e}^{\mathbf{i}\mathbf{k}\cdot\mathbf{x}} \mathcal{R}_{\mathbf{k}}(\mathbf{t}). \tag{5.22}$$

$\Delta^2_{\mathcal{R}}$ in Eq. (5.21) is the dimensionless power spectrum.

The scale dependence of the fluctuations can be also quantified. The *spectral index* n_s gives measure of it and it is defined as

$$n_s - 1 \equiv \frac{d \ln \Delta^2_{\mathcal{R}}}{d \ln k}. \tag{5.23}$$

Here, scale-invariance corresponds to $n_s = 1$. We may also define the *running of the spectral index* α_s that measures the scale-dependence of the spectral index

$$\alpha_s \equiv \frac{d\, n_s}{d \ln k}. \tag{5.24}$$

Parallel to the scalar perturbations, it is also possible to define the power spectrum and the spectral index for each one of the two polarizations of the tensor perturbations h_{ij}.

$$\langle h_{\mathbf{k}} h_{\mathbf{k}'} \rangle = (2\pi)^3 \delta(\mathbf{k}+\mathbf{k}') P_h(k), \qquad \Delta^2_h = \frac{k^3}{2\pi^2} P_h(k), \tag{5.25}$$

where h represents any of the two different polarizations of the tensor perturbations, h^+ or $h^\times$ [3].

[3] The Fourier transform of $h_{ij}(\mathbf{x}, t)$, $h_{ij}(\mathbf{p}, t)$ is defined as follows:

$$h_{ij}(\mathbf{x}, t) = \int \mathrm{d}^3 p e^{i\mathbf{p}\vec{\mathbf{x}}} h_{ij}(\mathbf{p}, t) \tag{5.26}$$

and it satisfies the following conditions:

$$h_{ij}(\mathbf{p}, t) = h_{ji}(\mathbf{p}, t), \quad h_{ii}(\mathbf{p}, t) = 0, \quad p_i h_{ij}(\mathbf{p}, t) = 0. \tag{5.27}$$

For a generic vector p in the 3 directions, the above conditions are satisfied for 3×3 matrices with $h_{11}(\mathbf{p}, t) = -h_{22}(\mathbf{p}, t) \equiv h^+(\mathbf{p}, t)$; $h_{12}(\mathbf{p}, t) = h_{21}(\mathbf{p}, t) \equiv h^\times(\mathbf{p}, t)$; $h_{i3}(\mathbf{p}, t) = h_{3i}(\mathbf{p}, t) = 0$. Only two scalar components, h^+ and $h^\times$, are needed to describe the tensor perturbations.

The dimensionless tensor power spectrum of tensor perturbations is defined as the sum for the two polarizations [4]:

$$\Delta_t^2 \equiv 2\Delta_h^2. \tag{5.28}$$

For historical reasons, its spectral index is defined analogously to Eq. (5.23) but without the -1

$$n_t \equiv \frac{d\ln\Delta_t^2}{d\ln k}. \tag{5.29}$$

We now compute the power spectrum and its spectral index of the scalar and tensor perturbations for a simple model such as the single field slow-roll model of Inflation. This will help us in Chapter 7 for more elaborated models. The aim is then to compute $\langle \mathcal{R}_{\mathbf{k}}\mathcal{R}_{\mathbf{k}'}\rangle$, $\langle h_{\mathbf{k}}h_{\mathbf{k}'}\rangle$ and their spectral index. For a complete derivation of the computation we refer to [55]. Here we will briefly summarize the procedure.

Let us consider the standard quantization in quantum mechanics. In this quantization, the classical variable x is promoted to a quantum operator $\hat{x}$. The operator $\hat{x}$ is then expanded in terms of creation and annihilation operators

$$\hat{x} = v(t)\hat{a} + v^*(t)\hat{a}^\dagger, \tag{5.30}$$

where the mode functions satisfy the classical equation of motion.

These creation and annihilation operators satisfy the canonical commutation relation

$$\left[\hat{a}, \hat{a}^\dagger\right] = 1. \tag{5.31}$$

coming from the commutation relation among the operator $\hat{x}$ and its momentum conjugate $\hat{p} \equiv \frac{d\mathcal{L}}{dx}$

$$[\hat{x}, \hat{p}] = i\hbar. \tag{5.32}$$

Defining the vacuum of the theory $|0\rangle$ as the state which is annihilated when applying the annihilation operator, $\hat{a}|0\rangle = 0$, it is easy to show that the mean square expectation value of the position operator $\hat{x}$ in the ground state $\langle|\hat{x}|^2\rangle$ is

$$\langle|\hat{x}|^2\rangle \equiv \langle 0|\hat{x}^\dagger\hat{x}|0\rangle = |v(t)|^2\,. \tag{5.33}$$

Hence, the square of the mode function of a perturbation in one field is all we need to compute the power spectrum of that perturbation. The last step is then the computation of the mode functions of both $\mathcal{R}$ and h.

[4] The two polarizations have the same equation of motion. Hence, the power spectrum of the sum is simply twice the power spectrum of one of them.

5.2.1 Scalar Perturbations

Following [56] we start from the action in Eq. (4.30), and fix the gauge to be

$$\delta\phi = 0, \qquad g_{ij} = a^2[(1-2\mathcal{R})\delta_{ij} + h_{ij}], \qquad \partial_i h_{ij} = 0, \quad h^i_i = 0. \tag{5.34}$$

It is possible to expand the action (Eq. (4.30)) to second order in $\mathcal{R}$:

$$S_2 = \frac{1}{2}\int \mathrm{d}^4x\, a^3 \frac{\dot{\phi}^2}{H^2}\left[\dot{\mathcal{R}}^2 - a^{-2}(\partial_i\mathcal{R})^2\right], \tag{5.35}$$

in units where $M_P^2 = 1/(8\pi G) = 1$. Defining the variable v

$$v \equiv z\mathcal{R}, \qquad \text{where} \qquad z^2 \equiv a^2\frac{\dot{\phi}^2}{H^2} = 2a^2\epsilon_H, \tag{5.36}$$

and going to Fourier space we find the following equation of motion for v_k

$$v_k'' + \left(k^2 - \frac{z''}{z}\right)v_k = 0, \tag{5.37}$$

where $' \equiv d/d\eta$ being η the conformal time defined as $\mathrm{d}t \equiv a\mathrm{d}\eta$ [5]. Due to the background dependence of z in Eq. (5.37), it is impossible to find a general solution for $v_k(\eta)$. However, for a quasi de-Sitter background ($H \approx$ const.),

$$\frac{z''}{z} \approx \frac{a''}{a} \approx \frac{2}{\tau^2}, \tag{5.38}$$

and Eq. (5.37) admits the following solution for the mode functions

$$v_k \approx \frac{e^{-ik\tau}}{\sqrt{2k}}\left(1 - \frac{i}{k\tau}\right). \tag{5.39}$$

To obtain Eq. (5.39) it is mandatory to define correctly the vacuum of the theory $\hat{a}_{\mathbf{k}}|0\rangle = 0$, which corresponds to specify a boundary condition for v_k. Our choice, which is the most common one, has been to select the Minkowsky vacuum for modes well inside the horizon, or rather in the infinite past $\eta \to -\infty$. In other words, the boundary condition reads

$$\lim_{\eta\to-\infty} v_k = \frac{e^{-ik\eta}}{\sqrt{2k}}. \tag{5.40}$$

That is the so-called Bunch-Davies Vacuum and Eq. (5.39) gives the Bunch-Davies mode functions.

[5] Notice that the parameter η here refers to the conformal time and not to any of the two slow-roll parameters η_H or η_V defined in the previous Chapter.

Once the mode functions have been obtained, the power spectrum of $\mathcal{R}$ can be easily computed:

$$\begin{aligned}\langle \mathcal{R}_{\mathbf{k}}(t)\mathcal{R}_{\mathbf{k}'}(t)\rangle &= (2\pi)^3\delta(\mathbf{k}+\mathbf{k}')\frac{H^2}{\dot\phi^2}\frac{|v_k(t)|^2}{a^2}\\ &\approx (2\pi)^3\delta(\mathbf{k}+\mathbf{k}')\frac{H^2}{2k^3}\frac{H^2}{\dot\phi^2}(1+k^2\tau^2)\\ &\approx (2\pi)^3\delta(\mathbf{k}+\mathbf{k}')\frac{H^2}{2k^3}\frac{H^2}{\dot\phi^2}\Big|_{k\tau\ll 1},\end{aligned} \tag{5.41}$$

where the last approximation holds well outside the horizon. The nearly time independence of $\mathcal{R}$ outside the horizon allows us to compute $\langle \mathcal{R}_{\mathbf{k}}(t)\mathcal{R}_{\mathbf{k}'}(t)\rangle$ at horizon crossing

$$\langle \mathcal{R}_{\mathbf{k}}(t)\mathcal{R}_{\mathbf{k}'}(t)\rangle \approx (2\pi)^3\delta(\mathbf{k}+\mathbf{k}')\frac{H_*^2}{2k^3}\frac{H_*^2}{\dot\phi_*^2}. \tag{5.42}$$

Here, $(\dots)_*$ indicates a quantity evaluated at horizon crossing, $a_*H_* = k$. The power spectrum can then be read from Eq. (5.21)

$$\Delta^2_{\mathcal{R}}(k) = \frac{H_*^2}{(2\pi)^2}\frac{H_*^2}{\dot\phi_*^2}. \tag{5.43}$$

Outside the horizon, $\mathcal{R}$ approaches a constant value. Therefore the power spectrum at horizon crossing gets frozen for super-horizon modes until those modes re-enter the horizon.

5.2.2 Tensor Perturbations

The calculation of the power spectrum for the tensor modes follows exactly the same steps as the scalar one. Therefore, here we will write down the starting point and the result. See [40] for a more detailed computation.

Expanding the Einstein-Hilbert action up to second order in h_{ij} we obtain

$$S_2 = \frac{M_P^2}{8}\int \mathrm{d}\eta\mathrm{d}^3x\, a^2[(h'_{ij})^2 - (\partial_l h_{ij})^2]. \tag{5.44}$$

Up to a normalization factor of $M_p^2/2$ this is the same action as the one for a massless scalar field in a FRW Universe.

Following the same procedure as in the scalar perturbations, it is straightforward to prove that the tensor power spectrum is

$$\Delta^2_t(k) = 2\Delta^2_h(k) = \frac{8}{M_P^2}\left(\frac{H_*}{2\pi}\right)^2. \tag{5.45}$$

Due to the slowly but not null variation in time of the background, different modes getting out of the horizon at different times will present a slightly different value for both the scalar and tensor power spectra. The spectral indexes n_s and n_t measure this variation. Here, we will only present the results in the slow-roll regime, since in this regime is straightforward to get them [56].

5.2.3 Results in the slow-roll regime

The results for the power spectra of the scalar and tensor perturbations generated during Inflation are

$$\Delta^2_{\mathcal{R}}(k) = \frac{1}{8\pi}\frac{H^2}{M_P^2}\frac{1}{\epsilon_H}\bigg|_{k=aH}, \qquad \Delta^2_t(k) = \frac{2}{\pi^2}\frac{H^2}{M_P^2}\bigg|_{k=aH}. \tag{5.46}$$

These results are exact. In the slow-roll approximation we can go further and use Eqs. (4.41) and (4.42) to give the two power spectra in terms of the potential of Inflation $V(\phi)$:

$$\Delta^2_{\mathcal{R}}(k) \approx \frac{1}{24\pi^2}\frac{V}{M_P^4}\frac{1}{\epsilon_V}\bigg|_{k=aH}, \qquad \Delta^2_t(k) \approx \frac{2}{3\pi^2}\frac{V}{M_P^4}\bigg|_{k=aH}. \tag{5.47}$$

For the spectral indexes we find,

$$n_s - 1 \approx 2\eta_{H*} - 4\epsilon_{H*} \approx 2\eta_{V*} - 6\epsilon_{V*} \qquad \text{and} \qquad n_t \approx -2\epsilon_{H*} \approx -2\epsilon_{V*}, \tag{5.48}$$

whereas for the running of the scalar spectral index we obtain

$$\alpha \equiv \frac{d\, n_s}{d\ln k} \approx -2\xi_{V*} + 16\epsilon_{V*}\eta_{V*} - 24\epsilon^2_{V*}, \tag{5.49}$$

where

$$\xi_V \equiv M_P^4 \frac{V_{,\phi}V_{,,,\phi}}{V^2}, \tag{5.50}$$

is the second order slow-roll parameter [6].

There is still a quantity worthy to be mentioned. That is the tensor to scalar ratio, r, defined as the ratio between the square of the amplitude of the tensor perturbations and the square of the amplitude of the scalar ones, or equivalently

[6] It is possible to define an infinite sequence of slow-roll parameters, $\beta^{(n)} \equiv M_P^{2n}\frac{(V_{,\phi})^{n-1}V^{(n+1)}}{V^n}$, $n \geq 1$, with $V^{(n+1)} \equiv d^{n+1}V/d\phi^{n+1}$. From this definition; $\eta_V = \beta^{(1)}$ and $\xi_V = \beta^{(2)}$. In the slow-roll regime, each one is slow-roll suppressed, compared with the previous one.

$$r \equiv \frac{\Delta_t^2}{\Delta_{\mathcal{R}}^2} = 16\epsilon_{H*}. \tag{5.51}$$

In the slow-roll regime we find a useful relationship among r and n_t

$$r \approx -8n_t. \tag{5.52}$$

In the slow-roll approximation measurements of the scalar and tensor power spectra are related directly to the shape of the potential $V(\phi)$. Observational measurements of these power spectra and their scale dependences can therefore give us valuable information about the potential driving the inflationary expansion.

5.3 Non-Gaussianity

Observations of the CMB [19] point towards a Universe where scalar perturbations are randomly distributed, following a gaussian statistics. This seems to be in agreement with the single scalar slow-roll scenario for Inflation, where non-gaussianities are expected to be very small [56], proportional to the slow-roll parameters. Nevertheless, there is still room for a non negligible deviation from Gaussianity. In the case that upcoming observations show a deviation from Gaussianity in the primordial power spectrum, it will be much larger than the one predicted by any single field slow-roll model, and hence it will favor some more complicated models like multi-field models [57, 58, 59] or single-field with non canonical kinetic terms [60, 61, 62].

For further discussions we introduce here how the deviation from Gaussianity is measured, and also how it is calculated in any particular model.

5.3.1 Bispectrum and non-Gaussianity

In the case of gaussian distributions, all the statistical information is encoded in the power spectrum. All higher order correlation functions are either products of two point correlation functions (in the case of an *even*-point correlation function) or vanish (for an *odd*-point correlation function). Departures from Gaussianity will appear for instance as non vanishing 3-point correlation function and also at higher orders.

Different models of Inflation, otherwise indistinguishable, may have their own non-Gaussian signal. Therefore, this fact may be used to favor some models and to rule out some others.

It is easy to introduce the notion of non-Gaussanity by defining the Fourier transform of the three point correlation function.

As Eq. (5.21) shows, the power spectrum is the Fourier transform of the two point function

$$\langle \mathcal{R}_{\mathbf{k}} \mathcal{R}_{\mathbf{k}'} \rangle = (2\pi)^3 \delta(\mathbf{k} + \mathbf{k}') P_{\mathcal{R}}(k). \tag{5.53}$$

Equivalently, the Fourier transform of the three point function is called the *bispectrum*

$$\langle \mathcal{R}_{\mathbf{k}_1} \mathcal{R}_{\mathbf{k}_2} \mathcal{R}_{\mathbf{k}_3} \rangle = (2\pi)^3 \delta(\mathbf{k}_1 + \mathbf{k}_2 + \mathbf{k}_3) F_{\mathcal{R}}(\mathbf{k}_1, \mathbf{k}_2, \mathbf{k}_3). \tag{5.54}$$

Translational invariance implies that any n-point correlation function must be proportional to the Dirac delta. This means that the power spectrum only depends on the modulus of the two momenta, which is the same. For the bispectrum this property does not longer hold. Therefore, in general, the bispectrum will also depend on the shape of the triangle formed by the three momentum vectors. That makes hard to evaluate the amount of non-Gaussianity generated by a model as it will be different for different shapes.

One of the first methods used to parametrize non-Gaussianity phenomenologically was via a non-linear correction to a gaussian perturbation $\mathcal{R}_g$ [63]

$$\mathcal{R}(\mathbf{x}) = \mathcal{R}_g(\mathbf{x}) + \frac{3}{5} f_{\mathrm{NL}}^{\mathrm{local}} [\mathcal{R}_g(\mathbf{x})^2 - \langle \mathcal{R}_g(\mathbf{x})^2 \rangle], \tag{5.55}$$

which in Fourier space corresponds to a bispectrum given by

$$F_{\mathcal{R}}(k_1, k_2, k_3) = \frac{6}{5} f_{\mathrm{NL}}^{\mathrm{local}} \times [P_{\mathcal{R}}(k_1) P_{\mathcal{R}}(k_2) + P_{\mathcal{R}}(k_2) P_{\mathcal{R}}(k_3) + P_{\mathcal{R}}(k_3) P_{\mathcal{R}}(k_1)]. \tag{5.56}$$

This definition is local in real space and hence it is called *local non-Gaussianity*. From this definition, it is straightforward to see that the bispectrum for local non-Gaussianity peaks in the *squeezed* limit, *i.e.* when one of the momenta is very small compared with the other two.

Another important shape for non-Gaussianity is the *equilateral* one. In this case, the bispectrum peaks when the three momenta are of the same order $k_1 \sim k_2 \sim k_3$, meaning that the triangle formed is equilateral.

Any given inflationary model leaves its largest non-Gaussianity signal for his own particular configuration of the triangle formed with the three momenta. For instance, multi-field models give an important amount of non-Gaussianity in the local form, whereas the equilateral type is present in single fields with non canonical kinetic terms for the inflaton. For this reason, for arbitrary shape functions we measure the magnitude of non-Gaussianity by defining the generalized f_{NL} parameter

$$f_{\mathrm{NL}} \equiv \frac{5}{18} \frac{F_{\mathcal{R}}(k, k, k)}{P_{\mathcal{R}}(k)^2}. \tag{5.57}$$

The current bounds of non-Gaussianity present in the CMB can be found in [19]. They also depend on the shape. For the two most common, namely the local and equilateral ones, these bounds are

$$-10 < f_{NL}^{\text{local}} < 74, \qquad \text{and} \qquad -214 < f_{NL}^{\text{equil}} < 266, \tag{5.58}$$

at 95% confidence level.

Given a theoretical model of Inflation, the calculation of the three point correlation function is done by means of the *in-in* formalism, firstly introduced by Maldacena in [56]

$$\langle \delta\phi^3(\eta_*)\rangle = \left\langle 0 \left| \bar{T} e^{i\int_{-\infty-i\epsilon}^{\eta_*} \mathcal{H}_{\text{int}}(\eta')\mathrm{d}\eta'} \delta\phi^3(\eta_*) T e^{-i\int_{-\infty+i\epsilon}^{\eta_*} \mathcal{H}_{\text{int}}(\eta')\mathrm{d}\eta'} \right| 0 \right\rangle, \tag{5.59}$$

where $|0\rangle$ is the Bunch-Davies vacuum, T ($\bar{T}$) indicates time (anti-time) ordering, η_* indicates the conformal time when Inflation ends, $\mathcal{H}_{\text{int}}$ is the interaction Hamiltonian and ϵ is an infinitesimal positive constant [7]. As it is shown in Eq. (5.59), primordial non-Gaussianity is entirely due to self-interactions in single field models. That is the reason why in slow-roll single field Inflation, non-Gaussianity is expected to be small, proportional to the slow-roll parameters [8] $f_{\text{NL}} \sim \mathcal{O}(0.01)$ [56].

The relation among $\delta\phi$ and $\mathcal{R}$ (Eq. (5.18)) is clearer in the spatially-flat gauge, where $\psi = 0$

$$\mathcal{R} = \frac{H}{\dot{\phi}}\delta\phi. \tag{5.60}$$

Hence, in this gauge

$$\langle \mathcal{R}^3(\eta_*)\rangle = \left(\frac{H}{\dot{\phi}}\right)^3 \langle \delta\phi^3(\eta_*)\rangle, \tag{5.61}$$

and computing Eq. (5.59) we can read directly $\langle \mathcal{R}^3(\eta_*)\rangle$ at horizon crossing, and therefore f_{NL}.

5.3.2 Higher order correlation functions

Obviously, the 3rd order point function is not the end of the story. Non-Gaussianity can appear at any order in the correlation functions. However given the observed, nearly gaussian perturbations, in order to fit with the observations, it is expected that the n-point correlation function is even more suppressed compared to the $(n-1)$-point one for any inflationary model. For completeness we define as well the n-point correlation function as the generalization of Eq. (5.59)

$$\langle \delta\phi^n(\eta_*)\rangle = \left\langle 0 \left| \bar{T} e^{i\int_{-\infty-i\epsilon}^{\eta_*} \mathcal{H}_{\text{int}}(\eta')\mathrm{d}\eta'} \delta\phi^n(\eta_*) T e^{-i\int_{-\infty+i\epsilon}^{\eta_*} \mathcal{H}_{\text{int}}(\eta')\mathrm{d}\eta'} \right| 0 \right\rangle. \tag{5.62}$$

[7] Notice that ϵ here has nothing to do with the slow-roll parameters, ϵ_H or ϵ_V.

[8] Recall that the required flatness of the potential imposes strict limits on the coupling constants in the interacting terms.

As it happened in the case of the three point correlation function, different models of Inflation can lead to different shapes of non-Gaussianity in the n-point correlation function, *e.g.* in the 4-point function. Unfortunately, in this case, there is more room for shaping the four momenta, implying a loss of predictive power for the models.

5.4 Connection with observations

Through all this Chapter we have computed all the statistical quantities at horizon crossing, relying on the conservation of these quantities outside the horizon. It is clear however that, for the main purpose, which is to extract as much information as possible from the observables such as the CMB or the LSS, it must be taken into account that these perturbations have re-entered the horizon at some moment in the subsequent evolution of the Universe. Once they come back inside the horizon, they start to evolve again. This causes for instance that the power spectrum computed in last Section, Eq. (5.43), does not correspond with the matter power spectrum observed in the CMB.

In this Section we will explain how to link the statistical information of the perturbations for a given inflationary model with the observations of the CMB. We will refer to [64] in order to link them with the LSS.

The link between one observable $\mathcal{Q}$ measured in an experiment and the curvature perturbation $\mathcal{R}$ is done by the so called *transfer function* $T_{\mathcal{Q}}$, defined as

$$\mathcal{Q}_{\mathbf{k}}(\eta) = T_{\mathcal{Q}}(k, \eta, \eta_*)\mathcal{R}_{\mathbf{k}}(\eta_*). \tag{5.63}$$

The quantity $\mathcal{Q}$ represents temperature fluctuations or polarization measured in the CMB. As already said, we will focus here on the CMB, giving only a brief review. More details can be found in Scott Dodelson cosmology book [65].

CMB fluctuations were introduced in Sec. 3.1. There it was defined the angular power spectrum C_l, Eq (3.6), which we will redefine as C_l^{TT} referring to the correlations among temperature fluctuations

$$C_l^{TT} = \frac{1}{4\pi}\int \mathrm{d}^2\hat{n}\mathrm{d}^2\hat{n}' P_l(\hat{n}\cdot\hat{n}')\langle\Delta T(\hat{n})\Delta T(\hat{n}')\rangle. \tag{5.64}$$

CMB temperature fluctuations are dominated by the scalar modes $\mathcal{R}$ produced in Inflation. For a given $\mathcal{R}$ we can compute the corresponding δT by means of the transfer function $\Delta_{Tl}(k)$ through the *k-space* integral [65]

$$a_{lm} = 4\pi(-i)^l \int \frac{\mathrm{d}^3k}{(2\pi)^3}\Delta_{Tl}(k)\mathcal{R}_{\mathbf{k}}Y_l^m(\hat{\mathbf{k}}), \tag{5.65}$$

and using the identity

$$\sum_{m=-l}^{l} Y_l^m(\hat{\mathbf{k}}) Y_l^m(\hat{\mathbf{k}}') = \frac{2l+1}{4\pi} P_l(\hat{\mathbf{k}} \cdot \hat{\mathbf{k}}'), \tag{5.66}$$

the angular power spectrum reads

$$C_l^{TT} = \frac{2}{\pi} \int k^2 \mathrm{d}k \, P_{\mathcal{R}}(k) \Delta_{Tl}(k) \Delta_{Tl}(k). \tag{5.67}$$

For simple cases, the transfer functions can be described analytically [65]. Nevertheless, in general they must be computed using Boltzmann-codes such as CMBFAST [66] or CAMB [67]. Such transfer functions depend on the cosmological background. Fixing the background, the angular power spectrum extracted from CMB temperature fluctuations gives information about the the physics of Inflation, encoded in the power spectrum $P_{\mathcal{R}}(k)$.

CMB polarization is also related to temperature fluctuations and can give us complementary information about primordial fluctuations. Here, we will only summarize the results. For a detailed treatment see [65, 15].

Polarization cannot be described by a scalar field but rather by a tensor (spin-2) field. The harmonic analysis therefore requires expansion on the sphere in terms of tensor spherical harmonics ${}_{\pm 2}Y_l^m(\hat{n})$ [68, 69].

Instead of the moments $a_{\pm 2,lm}$ related to ${}_{\pm 2}Y_l^m(\hat{n})$ it is convenient to introduce the linear combinations

$$a_{E,lm} \equiv -\frac{1}{2}(a_{2,lm} + a_{-2,lm}), \qquad a_{B,lm} \equiv -\frac{1}{2i}(a_{2,lm} - a_{-2,lm}). \tag{5.68}$$

These two linear combinations allow us to introduce two scalar quantities E and B as

$$E(\hat{n}) = \sum_{l,m} a_{E,lm} Y_l^m(\hat{n}), \qquad B(\hat{n}) = \sum_{l,m} a_{B,lm} Y_l^m(\hat{n}). \tag{5.69}$$

These scalar quantities characterize completely the linear polarization field. The cosmological significance of the E and B modes was realized by the authors of Refs. [68, 69], who proved the following facts:

- i) scalar (density) perturbations create only E-modes, but not B-modes.
- ii) vector (vorticity) perturbations create mainly B- modes [9].
- iii) tensor (gravitational wave) perturbations create both E-modes and B-modes.

[9] However, vector perturbations are not generated in Inflation and they decay quickly with the expansion. Hence we will ignore them.

Therefore, a hypothetical detection of B-modes would imply a very strong proof for Inflation since detectable primordial tensor modes can only be produced by a mechanism like Inflation.

The angular power spectrum for the E-modes and the cross-correlation among them and the temperature fluctuations are given approximately by

$$\begin{aligned} C_l^{EE} &\simeq (4\pi)^2 \int k^2 \mathrm{d}k \, P_{\mathcal{R}}(k) \Delta_{El}^2(k), \\ C_l^{TE} &\simeq (4\pi)^2 \int k^2 \mathrm{d}k \, P_{\mathcal{R}}(k) \Delta_{Tl}(k) \Delta_{El}(k). \end{aligned} \tag{5.70}$$

Again, both are dominated by scalar modes. However, as the transfer functions are different from the ones in C_l^{TT}, the signals are complementary.

For the case of the B-modes we have

$$C_l^{BB} = (4\pi)^2 \int k^2 \mathrm{d}k \, P_h(k) \Delta_{Bl}^2(k), \tag{5.71}$$

since they are only generated by tensor modes.

Finally, it is also possible to study non-gaussianities in the CMB temperature fluctuations. The bispectrum $B_{\mathcal{R}}(k_1, k_2, k_3)$, Eq. (5.54), gives the leading order for a non-Gaussian signal. The presence of a non-zero bispectrum leaves a signature in the angular bispectrum

$$B_{l_1 l_2 l_3}^{m_1 m_2 m_3} = \langle a_{l_1 m_1} a_{l_2 m_2} a_{l_3 m_3} \rangle. \tag{5.72}$$

Substituting Eq. (5.65) into Eq. (5.72) we may relate the primordial bispectrum to the observed CMB bispectrum [70].

In Chapters 4 and 5 we have described a qualitative analysis about most of the important properties about inflationary models, and their relation with observations. We will use some of these properties in Chapter 7 and in Chapter 8.

Chapter 6

Leptogenesis

6.1 Introduction

The Standard Model (SM) for particles and interactions is a successful theory based on the gauge symmetry $SU(2)_L \times U(1)_Y$ capable of describing a huge amount of experimental data, in principle uncorrelated, with an extremely high level of accuracy. However, there are still few open questions that are impossible to solve within the framework of the SM. Giving answer to one of these questions regarding the composition of the Universe, concretely why the observed Universe is mainly made of particles with nearly no presence of antiparticles, will be the goal of this Chapter. To be precise, we will focus on one of the possible answers to this problem, so called Leptogenesis.

6.1.1 Matter-antimatter asymmetry

There are many observational evidences [71, 72, 73, 74] that indicate that our Universe is filled mainly with matter (protons, electrons, neutrons...), with a small amount of antimatter, whose existency is consistent with secondary production in high energy collisions that occur in the atmosphere by incoming cosmic rays. The way to parametrize the matter-antimatter asymmetry is dividing the difference between the number density of baryons n_B and the one of antibaryons $n_{\bar{B}}$ by the photon number density n_γ (or equivalently to the entropy density s, if we compute both at the same moment in time). The current observational values are given in [75]:

$$\begin{aligned} \left(5.1 \leq \eta \equiv \tfrac{n_B - n_{\bar{B}}}{n_\gamma} \leq 6.5\right) \times 10^{-10} \ (95\,\%\,\mathrm{CL}), \\ \left(7.3 \leq Y_{\mathcal{B}} \equiv \tfrac{n_B - n_{\bar{B}}}{s} \leq 9.3\right) \times 10^{-11} \ (95\,\%\,\mathrm{CL}). \end{aligned} \tag{6.1}$$

These quantities can be extracted from two independent observations; Big Bang Nucleosyntesis (BBN) [75] (see [76] for an extensive review) and CMB [19]. The coincidence in the

results obtained from these two methods is a strong support for the Big Bang Cosmology.

Now the question is: *where does this asymmetry come from?* It seems quite natural to imagine a Universe which began completely symmetric but, due to the lack of a fundamental theory capable of describing the origin of the Universe, we cannot take this for granted. Therefore we could live in a Universe that has been always asymmetric. Nevertheless, as it has been explained in previous Chapters, even in the case of an original asymmetry, it would have been erased in the period of Inflation, and since there are good reasons to believe in Inflation, we conclude that this asymmetry must be generated dynamically after Inflation.

6.1.2 Sakharov conditions

In 1967 Sakharov [77] demonstrated that in order to generate an asymmetry in the number of baryons and antibaryons, starting from a symmetric Universe, the following 3 conditions must be satisfied:

- 1.- **Violation of baryon number**: The baryon number B of a system is the difference between the number of baryons and the number of antibarions. Hence, the interaction responsible for generating the asymmetry clearly must violate baryon number.
- 2.- **Violation of C and CP**: Even in the case of a baryon number violating interaction, if all the interactions preserve C and CP, processes involving antibaryons would generate a baryon asymmetry equal to the one generated by those involving baryons but with opposite sign. Both asymmetries would cancel one to each other leading to a baryon symmetric Universe.
- 3.- **Out of equilibrum conditions**: In thermal equilibrium, the distribution functions of particles depend only on their mass and their chemical potential. CPT symmetry implies that the mass of particles and their antiparticles coincide. Meanwhile, the chemical potential associated to a non-conserved quantity vanishes in equilibrium. Therefore, in thermal equilibrium the distribution function of particles and antiparticles so as their density number, coincide.

6.1.3 Can the SM fulfill the Sakharov conditions and generate the observed asymmetry of the Universe?

In the SM baryon (B) and lepton (L) numbers are violated at the quantum level, due to an anomaly related to the quiral character of the theory [78, 79], but with the combination $B-L$ being conserved [80]. This leads to a kind of non perturbative processes that violate baryon (and lepton) number, the so called *sphaleron processes* [81]. The probability of a process of this kind to occur below the electro-weak (EW) phase transition is proportional to the Boltzmann factor $\exp(-E_{\rm esf}(T)/T)$, being $E_{\rm esf}(T)$ the sphaleron energy [82]

$$E_{\text{esf}} = \frac{4\pi}{g_w} f(\lambda/g_w) \frac{v(T)}{\sqrt{2}}, \tag{6.2}$$

where g_w is the coupling constant of $SU(2)_L$, f varies between 1.6 and 2.7 depending on the value of the quartic coupling of the Higgs λ and $v(T) \equiv \langle 0|\Phi|0\rangle$ is the expectation value of the Higgs field Φ in vacuum at temperature T. At energies below the EW phase transition, giving the sphaleron energy $E_{\text{esf}} \approx 8 - 13$ TeV, leading to a extremely small Boltzmann factor. But above this phase transition $v(T) \to 0$ and the interactions reach the equilibrium and can occur at an observable rate. This equilibrium range goes from the EW phase transition till $T \sim 10^{12}$ GeV.

It is also well known that C and CP are violated in Nature. In the SM, C is violated maximally and the violation of CP has its origin in the phase δ_{KM} of the Cabibbo-Kobayashi-Maskawa mixing matrix (CKM).

Finally, out-of-equilibrium conditions can take place during the electroweak phase transition, if it is strongly first order.

Therefore, the SM contains all the ingredients for successful Baryogenesis. However it turns out that the amount of CP violation is too small and the phase transition is not strongly first order in the SM, and hence the departure from thermal equilibrium is too small to generate the right baryonic asymmetry. An extension of the SM is needed to explain the matter-antimatter asymmetry of the Universe.

6.1.4 Summary of Baryogenesis mechanisms

Here we present some mechanisms of Baryogenesis present in the literature. The information has been taken mainly from [83, 84, 85]

- **GUT Baryogenesis**: The baryon asymmetry is generated in the out of equilibrium decay of the heavy bosons present in Grand Unification Theories (GUT). These theories are no longer such attractive, as the non-observation of proton decay implies a very high mass for those bosons which in turn would yield to a reheating temperature too high, with the subsequent generation of "undesirable" particles in the following evolution of the Universe.

- **Electroweak Baryogenesis**: As already seen, a first-order electroweak phase transition could provide a sufficient out-of-equilibrium state to produce the observed asymmetry. In the SM, the electroweak transition is not first-order. Hence, there is no departure from thermal equilibrium and baryogenesis cannot take place. The picture changes in two-Higgs doublet models and in supersymmetric theories where it is possible to have such phase transition. Furthermore, these extensions of the SM contain new CP-violating terms which, together with the sphaleron processes make the three Sakharov conditions fulfilled.

- **Affleck-Dine Baryogenesis**: Usually the scalar potential of supersymmetric theories has many flat directions involving scalar fields which carry baryon or lepton number. These scalar fields are a combination of squark, Higgs and slepton fields. After Inflation they evolve from a large expectation value towards the minimum of their scalar potential. The decay of these condensates eventually converts the scalar charge densities that they carry to ordinary fermionic baryon and lepton number.

- **Leptogenesis**: The basis of this proposal is the seesaw mechanism, which explains the smallness of the light neutrino masses by mixings with heavy Majorana neutrinos. In this theories, the lightest of the heavy Majorana neutrinos, usually denoted by N_1, is the particle suited to generate the baryon asymmetry. The new Yukawa couplings provide the necessary source of CP violation. For a slow enough Yukawa interactions, the condition $\Gamma_{N_1} < H$ [1] is satisfied, providing the departure from thermal equilibrium. And as in the case of electroweak baryogenesis, the lepton asymmetry is partially converted to baryon asymmetry due to sphaleron processes.

In this Chapter we will focus on Leptogenesis

6.2 Basics of Leptogenesis

In this Section we will discuss the general aspects of the mechanism called Leptogenesis. Leptogenesis was firstly introducced by Fukugita and Yanagida in 1986 [86]. In this Section we will describe the basics of such theories, introducing them from their simplest lagrangian, studying how the 3 Sakharov conditions are achieved and finally, writing down the Boltzmann equations to compute the sought baryon asymmetry.

6.2.1 Seesaw lagrangian

Leptogenesis is based on the see-saw mechanism [2] [87, 88] that gives an explanation for the surprisingly low mass for the light neutrinos of the SM. This mechanism introduces new heavy Majorana neutrinos, N_i $(i = 1, 2, 3)$ to the SM lagrangian, singlets with respect to the SM gauge groups $SU(3) \times SU(2)_L \times U(1)_Y$, and only coupled to SM particles through Yukawa couplings. The lagrangian will be

$$\mathcal{L} = \mathcal{L}_{\rm SM} + i\overline{N_j}\partial\!\!\!/ N_j - \frac{1}{2}M_j\overline{N_j^c}N_j - h_{\alpha j}\tilde{H}^\dagger\overline{N_j}\ell_\alpha - h^*_{\alpha j}\overline{\ell_\alpha}N_j\tilde{H}. \tag{6.3}$$

[1] This condition means that the mean life time of the N_1 particles, $\tau_{\rm dec} \propto \Gamma^{-1}_{N_1}$, is bigger that the current age of the Universe $t \propto H^{-1}$.

[2] There are 3 types of see-saw models, and Leptogenesis can work for all of them. But since the general aspects that we need for our work are based on the Type-I, we will stick to it.

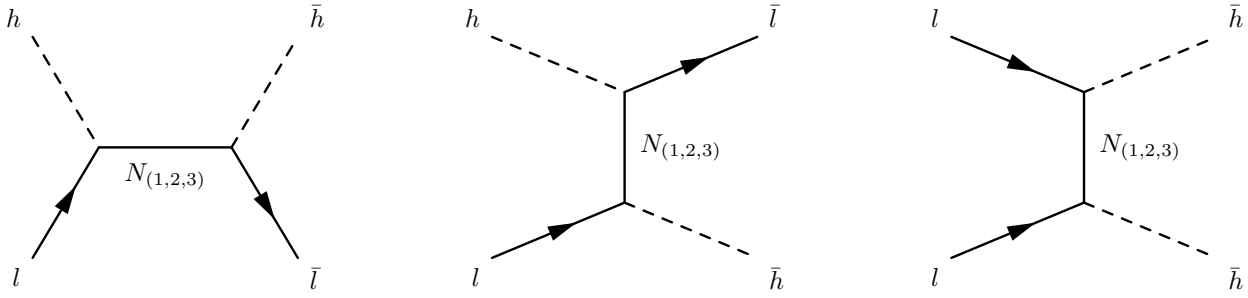

Figure 6.1: Scatterings with $\Delta L = 2$ involving the 3 heavy neutrinos $N_{(1,2,3)}$.

Here $\mathcal{L}_{\rm SM}$ is the SM lagrangian, the subindex α is the SM flavour index ($\alpha = e, \mu, \tau$), ℓ_i are the leptonic doublets of $SU(2)$ and H is the Higgs field, $H = (H^+, H^0)^T$ ($\tilde{H} \equiv i\tau_2 H^*$, with τ_2 the second Pauli matrix), M_α is the Majorana mass for N_α and finally $h_{i\alpha}$ are the Yukawa couplings among N_α and l_i. With the incorporation of the new heavy neutrinos, a mass matrix for the light neutrinos is generated when the Higgs field acquires a vacuum expectation value (vev), which, in the limit $hv \ll M$ takes the form

$$m_\nu = v^2 h M^{-1} h^T, \tag{6.4}$$

where M and h are the compact ways to parametrize the matrices M_j and $h_{\alpha j}$, and v is the vev of the Higgs field ($v = 174$ GeV). This mass matrix can be diagonalized using the Pontecorvo-Maki-Nakawa-Sakata (PMNS) matrix, U

$$D_\nu = U^T m_\nu U, \tag{6.5}$$

where $D_\nu = \text{diag}(m_1, m_2, m_3)$, and m_i ($i = 1, 2, 3$) are the light neutrino masses.

As realized by Fukugita and Yanagida, it turns out that the lagrangian (6.3) adds to the SM all the necessary pieces to fulfill the 3 Sakharov conditions and to obtain a right amount of baryon asymmetry for a wide range of the parameter space.

6.2.2 Sakharov conditions in Leptogenesis

- **Baryon number violation**: The baryon number is violated by the sphalerons. But since sphaleron processes violate $B + L$ leading the combination $B - L$ invariant, any theory of Baryogenesis that works above the electroweak phase transition (hence, when sphalerons are in equilibrium) must violate $B - L$. Otherwise, any baryon (and lepton) asymmetry will be erased by the sphaleron processes.

  In Leptogenesis, lepton number is violated by the simultaneous presence of the Yukawa couplings $h_{i\alpha}$ and the Majorana masses M_α, and once generated, this lepton asymmetry is partially converted into baryon asymmetry by the sphalerons.

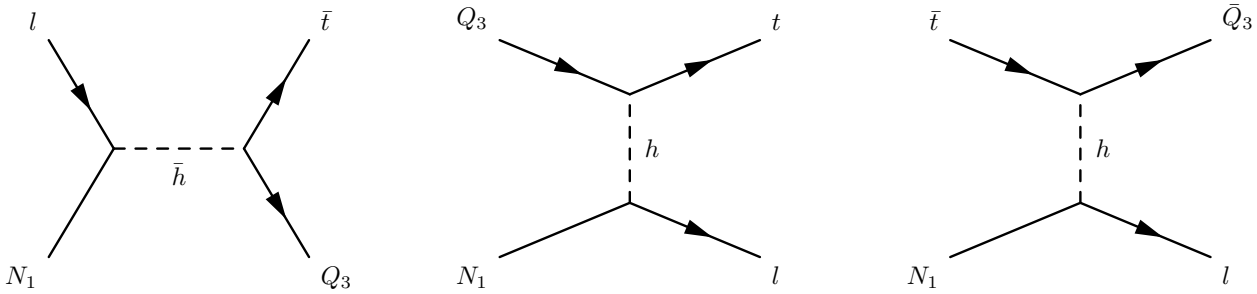

Figure 6.2: Scattering with $\Delta L = 1$ involving the higgs h.

- **C and CP violation**: $SU(2)_L \times U(1)_Y$ gauge symmetry is chiral and C (and also P) is violated maximally.

  Let us study more carefully the CP violation. The CP asymmetry in a process with initial state i and final state f is defined as:

$$\epsilon_f^i \equiv \frac{\gamma(i \to f) - \gamma(\overline{i} \to \overline{f})}{\gamma(i \to f) + \gamma(\overline{i} \to \overline{f})}, \tag{6.6}$$

  where $\gamma(i \to f)$ is the number of interactions per unit time and volume and it is called *density rate*. In Leptogenesis the CP asymmetry comes from the decay of the heavy Majorana neutrinos. The Feynmann diagrams that contribute to the CP asymmetry at leading order (1 loop) are show in Fig. 6.3. The leading contribution to the CP asymmetry in the flavour l_j comes from the interference among the tree diagram and the vertex and wave function diagrams (Fig. 6.3)

$$\epsilon_{\ell_\alpha}^{N_j} \equiv \frac{\gamma(N_j \to \ell_\alpha h) - \gamma(N_j \to \overline{\ell_\alpha}\bar{h})}{\sum_\alpha \gamma(N_j \to \ell_\alpha h) + \gamma(N_j \to \overline{\ell_\alpha}\bar{h})} = \epsilon_{\ell_\alpha}^{N_j}(\text{vertex}) + \epsilon_{\ell_\alpha}^{N_j}(\text{wave}). \tag{6.7}$$

  The vertex and wave CP asymmetries are respectively [89]

$$\begin{aligned} \epsilon_{\ell_\alpha}^{N_j}(\text{vertex}) &= \frac{1}{8\pi}\sum_k f(y_k)\frac{\text{Im}\left[h^*_{\alpha k}h_{\alpha j}(h^\dagger h)_{kj}\right]}{(h^\dagger h)_{jj}}, \\ \epsilon_{\ell_\alpha}^{N_j}(\text{wave}) &= -\frac{1}{8\pi}\sum_{k\neq j}\frac{M_j}{M_k^2 - M_j^2}\frac{\text{Im}\left[\{M_k(h^\dagger h)_{kj} + M_j(h^\dagger h)_{jk}\}h^*_{\alpha k}h_{\alpha j}\right]}{(h^\dagger h)_{jj}}. \end{aligned} \tag{6.8}$$

  Here, $y_k \equiv M_k^2/M_j^2$ and $f(x) = \sqrt{x}(1 - (1+x)\ln[(1+x)/x])$.

  In this work we will assume $M_1 < M_{2,3}$ and we will also ignore the hypothetic asymmetry generated during $N_{2,3}$ decays, that works pretty well for the simplest cases [90]

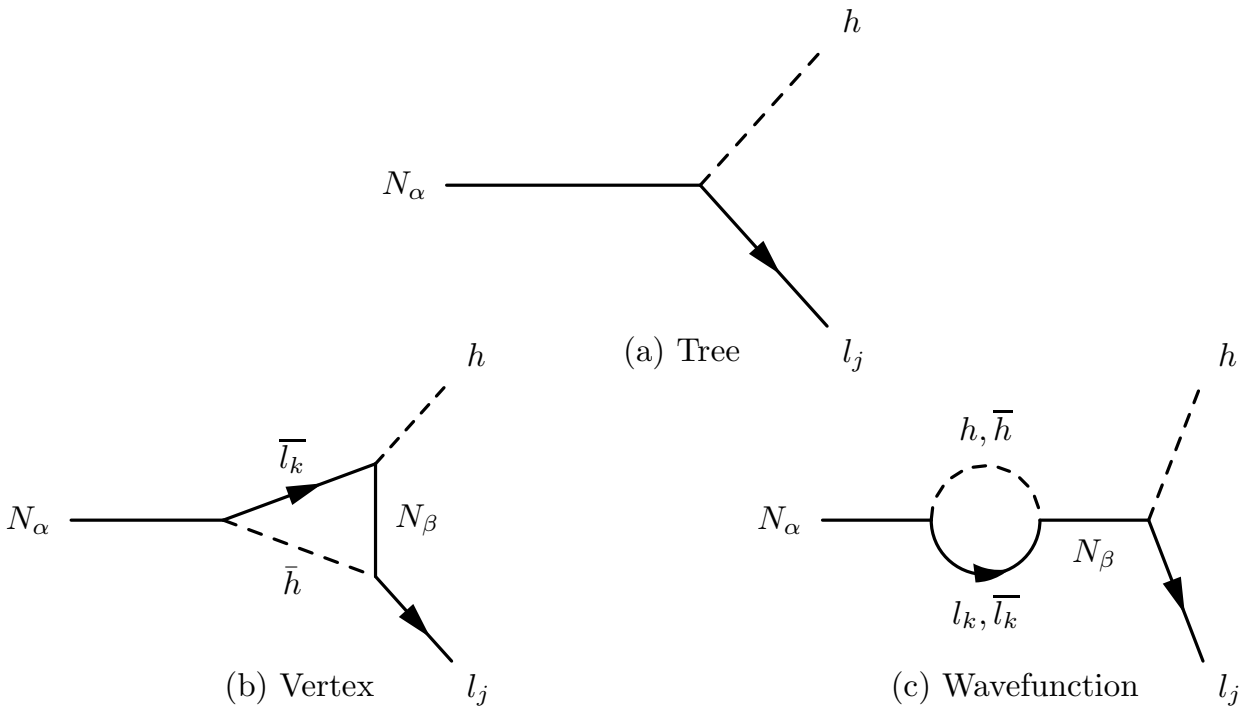

Figure 6.3: Diagrams that generate the CP asymmetry in the decay of the N_1. The lineal contribution to the CP asymmetry comes from the interference of the tree diagram (a) and the vertex and wave function diagrams (b and c).

- **Out-of-equilibrium condition**:

  The lepton asymmetry produced by the decays and inverse decays of the N_1 is generated approximately when $T \sim M_1$. In other words, M_1 determines the epoch when leptogenesis occurred and hence in which physical conditions it was produced.

  The realization of the out-of-equilibrium dynamics depends on the region of the parameter space under consideration. It is convenient to define the following quantities, which represent respectively the singlet neutrino decay rate Γ_{N_1} and the expansion rate of the Universe H at temperature $T = M_1$

$$\tilde{m} \equiv 8\pi \frac{v^2}{M_1^2}\Gamma_{N_1} = \frac{(\lambda^\dagger\lambda)_{11}}{M_1}v^2 \qquad\qquad m_* \equiv 8\pi \frac{v^2}{M_1^2}H\big|_{T=M_1}. \tag{6.9}$$

  The parameter $K \equiv \Gamma_{N_1}/H(T = M_1)$ can be used to define the type of washout regime. We first discuss the strong washout regime, where $K > 1$. In this case, at $T \sim M_1$ neutrino interactions are already in equilibrium, following the equilibrium abundances. Therefore the existing lepton asymmetry at that time is null. Then, the N_1 populating the plasma start to decay generating a lepton asymmetry. Inverse decays washout the produced asymmetry while they are fast enough. Once inverse decays are out-of-equilibrium ($\Gamma_{ID}(T) < H(T)$), this cancellation stops and an asymmetry survives.

  In the weak washout regime we have $K < 1$. In this case, at temperatures $T \sim M_1$, the N_1 have not reached their equilibrium densities. Hence the asymmetry produced during thermal production of N_1 does not vanish. As the temperature goes down, N_1 starts to decay producing an asymmetry opposite to the previous one. Thanks to the out-of-equilibrium inverse decays, an exact cancellation is avoided.

6.2.3 Boltzmann equations for Leptogenesis

In order to track the lepton asymmetry in each flavor along the history of the Universe, one should solve the set of Boltzmann equations that describe the out-of-equilibrium dynamics for the kinetic distributions of all particles involved [91]. The Boltzmann equation for a given species x is

$$\frac{\partial f_x}{\partial t} - Hp\frac{\partial f_x}{\partial p_x} = \frac{1}{2E_x}C[f_x], \tag{6.10}$$

where f_x is the momentum distribution of the particle x, p_x and E_x are the momentum and energy of the particle and $C[f_x]$ is the collision integral, which is given by

$$C[f_x] \equiv \sum_{xY\leftrightarrow Z}\int \mathrm{d}\pi_Y \mathrm{d}\pi_Z (2\pi)^4\delta^4(p_x+p_Y-p_Z)$$
$$\times\Big[f_x f_Y |A(xY\to Z)|^2\prod_{z\in Z}(1\pm f_z) \tag{6.11}$$
$$-f_Z|A(Z\to xY)|^2(1\pm f_x)\prod_{y\in Y}(1\pm f_y)\Big], \tag{6.12}$$

where

$$\begin{aligned} \mathrm{d}\pi_Y \equiv \textstyle\prod_{y\in Y}\mathrm{d}\pi_y, \quad \mathrm{d}\pi_y \equiv g_y\frac{\mathrm{d}^3p_y}{(2\pi)^3}\frac{1}{2E_y}, \\ p_Y \equiv \textstyle\sum_{y\in Y} p_y, \quad f_Y \equiv \prod_{y\in Y} f_y. \end{aligned} \tag{6.13}$$

Here, $|A|^2$ is the squared transition amplitude averaged over initial and final spins, and $(1\pm f)$ are the Bose enhancement and Pauli blocking factors.

If we integrate Eq. (6.10) over π_x we find an equation for the number density of the particle x (n_x)

$$\dot{n}_x + 3Hn_x = -\int \mathrm{d}\pi_x C[f_x], \tag{6.14}$$

with

$$n_x \equiv g_x\int\frac{\mathrm{d}^3p_x}{(2\pi)^3}f_x. \tag{6.15}$$

To move on, we will make use of two approximations: *kinetic equilibrium* and *Maxwell-Boltzmann statistics*. The first one allows us to write the distribution function with the same momentum dependence as if it were in equilibrium, that is

$$f_x(E) = \frac{n_x}{n_x^{eq}}f_x^{eq}(E_x). \tag{6.16}$$

This happens whenever the interactions among all particles are fast enough (compared to the expansion of the Universe) to change the kinetic energy. With Maxwell-Boltzmann statistics we have

$$f_x^{eq} = e^{-E/T}. \tag{6.17}$$

With all this, the Boltzmann equations are given by

$$\dot{n}_x + 3Hn_x = -\sum_{xY\leftrightarrow Z}[xY\leftrightarrow Z], \tag{6.18}$$

where

$$[xY \leftrightarrow Z] \equiv \frac{n_x}{n_x^{eq}} \prod_{y \in Y} \frac{n_y}{n_y^{eq}} \gamma^{eq}(xY \to Z) - \prod_{z \in Z} \frac{n_z}{n_z^{eq}} \gamma^{eq}(Z \to xY), \tag{6.19}$$

and γ^{eq} is the interaction density in equilibrium

$$\gamma^{eq}(xY \to Z) = \int \mathrm{d}\pi_x \mathrm{d}\pi_Y \mathrm{d}\pi_Z (2\pi)^4 \delta^4(p_x + p_Y - p_Z) f_x^{eq} f_Y^{eq} |A(xY \to Z)|^2. \tag{6.20}$$

We define the new variables $Y_x \equiv n_x/s$, being s the entropy density and $z \equiv m_{N_1}/T$. With these variables we write down the Boltzmann equations for both the lightest heavy neutrino, Y_{N_1}, and the Lepton asymmetry, $Y_L \equiv \sum_\alpha Y_{\ell_\alpha} - Y_{\bar{\ell}_\alpha}$, linearizing in this lepton asymmetry and in the total CP asymmetry, $\epsilon_\ell^{N_1} \equiv \sum_\alpha |\epsilon_{\ell_\alpha}^{N_1}$:

$$\begin{aligned} \frac{dY_{N_1}}{dz} &= -\frac{1}{zHs} \left(\frac{Y_{N_1}}{Y_{N_1}^{eq}} - 1 \right) \gamma_D, \\ \frac{dY_L}{dz} &= \frac{1}{zHs} \left\{ \epsilon_l^{N_1} \left(\frac{Y_{N_1}}{Y_{N_1}^{eq}} - 1 \right) \gamma_D - \frac{Y_L}{Y_L^{eq}} \left(\frac{\gamma_D}{2} + 2\gamma_{N_1 tu} + 2\gamma'_{N_1 s} \right) \right\}. \end{aligned} \tag{6.21}$$

All interaction densities are computed at tree level and correspond to N_1 decays and inverse decays, and $\Delta L = 2$ processes

$$\begin{aligned} \gamma_D &\equiv \gamma^{tree}(N_1 \to lh) + \gamma^{tree}(N \to \overline{lh}) = n_{N_1}^{eq} \frac{K_1(z)}{K_2(z)} \Gamma_{N_1}^{tree}, \\ \gamma_{N_1 tu} &= \gamma^{tree}(ll \to hh), \qquad \gamma'_{N_1 s} = \gamma'^{tree}(lh \to \overline{lh}). \end{aligned} \tag{6.22}$$

Here the prime in $\gamma'(lh \to \overline{lh})$ indicates that the on-shell contributions has to be subtracted since it has already been considered in the decays and inverse decays of the N_1. The exact definition is

$$\gamma'(lh \to \overline{lh}) \equiv \gamma(lh \to \overline{lh}) - \gamma(lh \to N_1) BR(N_1 \to \overline{lh}), \tag{6.23}$$

where $BR(x \to a, b, \dots)$ is the branching ratio, that is the fraction of decays of x in the channel $x \to a, b, \dots$ compared to the total one

$$BR(x \to a, b, \dots) \equiv \frac{\Gamma(x \to a, b, \dots)}{\Gamma_x^{tot}}, \tag{6.24}$$

with Γ_x^{tot} the total decay width.

Sphaleron processes finally convert part of the lepton asymmetry generated in Leptogenesis to a baryon asymmetry. It turns out that these processes convert 28/79 of the $B-L$ asymmetry into a baryon asymmetry in the SM [92]

$$Y_B^f = \frac{28}{79} Y_{B-L}^f \tag{6.25}$$

In computing Eq. (6.21) we have assumed that flavours are indisthinguisable and we have summed over all flavour contributions to compute the total asymmetry. In next Section we will introduce when and how flavor effects are important. This brief introduction will be useful in Chapter 9 where a more detailed study of flavor effects is made, particularizing to some specific models.

6.3 Flavor effects

At temperatures above $T \gtrsim 10^{12}$ GeV, no Yukawa interaction of the SM charged leptons is in equilibrium. N_1 decays and produces a lepton, l_1 in an specific direction in field space. This state, combination of the 3 SM charged leptons, remains coherent and it is the same state that enters in the washouts involving the N_1. Hence, only one Boltzmann equation is needed to compute the asymmetry. On the other hand, when those Yukawa interactions are fast enough, this lepton l_1 no longer remains coherent and in this case the asymmetries as well as the washouts terms all depend on the flavor states, and a full flavor computation is mandatory.

If $M_1 \gg 10^{12}$ GeV Leptogenesis takes place when all Yukawa interactions of the SM charged leptons are slower than the expansion of the Universe and, as already explained above, we can study it with only one Boltzmann equation. But when 10^9 GeV $< M_1 < 10^{12}$ GeV, τ interactions are faster than the expansion of the Universe and, if $M_1 < 10^9$ GeV also μ interactions are in equilibrium. Let us distinguish 3 different cases

- 1. Only τ interactions are faster than the expansion: If l_1 is a general combination of e, μ and τ, the generated leptons are projected either in the τ direction or in an specific direction in the $e-\mu$ plane in field space. The perpendicular direction in this plane does not play any role in Leptogenesis. We can therefore, approach the problem as if it was a two flavor problem.

- 2. Both τ and μ interactions are faster than the expansion: Here, a full 3 flavor treatment is needed since the perpendicular direction in field space to both μ and τ is precisely the e direction.

- 3. Alignment: If τ interactions (or τ and μ) are fast enough but, l_1 is parallel to one of the states with fast Yukawa interactions, or perpendicular to all of them, Leptogenesis reduces to a single flavor problem, similar to the case without flavor considerations.

6.3.1 Boltzmann equations

When flavour effects are important we shall include flavour changing processes that tend to re-equilibrate the asymmetries in the three different flavours ($\ell_j H \leftrightarrow \ell_k H$, $\ell_j \bar{H} \leftrightarrow \ell_k \bar{H}$ and $\ell_j \bar{\ell_k} \leftrightarrow \bar{H} H$). The Boltzmann equations now read

$$\begin{aligned}
\frac{\mathrm{d}Y_{N_1}}{\mathrm{d}z} &= \frac{-1}{sHz}\left(\frac{Y_{N_1}}{Y_{N_1}^{eq}} - 1\right)\gamma_{D_1}\ , \\
\frac{\mathrm{d}Y_{\ell_\alpha}}{\mathrm{d}z} &= \frac{1}{sHz}\left\{\left(\frac{Y_{N_1}}{Y_{N_1}^{eq}} - 1\right)\epsilon_{\ell_\alpha}^{N_1}\,\gamma_{D_1} - \sum_i \gamma_{\ell_\alpha h}^{N_i} y_{\ell_\alpha}\right. \\
&\qquad \left. - \sum_{\beta\neq\alpha}\left(\gamma_{\ell_\alpha h}^{\ell_\beta h\,'} + \gamma_{\ell_\alpha \bar{h}}^{\ell_\beta \bar{h}} + \gamma_{\ell_\alpha \bar{\ell_\beta}}^{h\bar{h}}\right)\left[y_{\ell_\alpha} - y_{\ell_\beta}\right]\right\}
\end{aligned} \tag{6.26}$$

As in the previous case, when we ignored flavor effects, here we also going to consider only the interactions mediated by the Yukawa couplings among the Higgs and the neutrinos, since for our purposes in Chapter 9 they are the most important interactions.

Part II

Scientific Research

Chapter 7

Khronon Inflation

Although the first goal of Inflation was to give an explanation of the homogeneity and isotropy of the observed Universe, together with the lack of relic particles such as monopoles and/or gravitinos, soon enough the most important achievement of inflationary theories was the fruitful explanation of the generation of perturbations that finally led to the formation of the structures in our Universe.

One of the most important properties of these perturbations is that they are nearly scale-invariant, at least for the observed scales. In Inflationary models this property is closely related with the approximate invariance of the theory by a shift in time of the form $t \to t+c$ with c constant. This in turn is a consequence of the small time variation of the energy scale (or the Hubble parameter $H(t)$) during Inflation, $\dot{H} \ll H^2$.

In this work [1] we study the possibility that the approximate time shift symmetry during Inflation is promoted to the full invariance under time reparametrization $t \to \tilde{t}(t)$, or equivalently under field redefinition of the inflaton $\phi \to \tilde{\phi}(\phi)$. The symmetry allows only two operators at leading order in derivatives, so that all n-point functions of scalar perturbations are fixed in terms of the power spectrum normalization and the speed of sound. During inflation the decaying mode only decays as $1/a$ and this opens up the possibility to violate some of the consistency relations in the squeezed limit, although this violation is suppressed by the (small) breaking of the field reparametrization symmetry. In particular one can get terms in the 3-point function that are only suppressed by $1/k_L$ in the squeezed limit $k_L \to 0$ compared to the local shape.

We will use an effective field approach through all the Chapter. Concretely, we will construct the most general lagrangian at low energy compatible with the symmetry $\phi \to \tilde{\phi}(\phi)$. To see how to build up effective theories in Inflation see [93].

7.1 Introduction

The approximate scale-invariance of correlation functions produced by Inflation is due to the dilation isometry of de Sitter space combined with the approximate symmetry of the inflaton dynamics under time translation [94]

$$t \to \tilde{t} = t + \text{const} \ . \tag{7.1}$$

In this work we want to explore the possibility that this symmetry is promoted to the full time reparametrization invariance

$$t \to \tilde{t}(t) \ . \tag{7.2}$$

Of course this symmetry can be a good approximation only during Inflation while it must be eventually broken, similarly to what happens with the standard symmetry (7.1), at the end of Inflation, when reheating takes place. This symmetry has recently been studied in the context of Hořava gravity and its healthy extensions [95, 96, 97]. In these references the scalar mode describing the preferred foliation has been dubbed 'khronon'. See [98, 99, 100, 101] for other possible connections between Hořava gravity and the creation of primordial curvature perturbations.

We will see that, once this symmetry is enforced, the inflationary dynamics becomes very constrained and unconventional. In particular three features are worth stressing.

1. All correlation functions of ζ are fixed, at the lowest order in derivatives, by only two coefficients, which can be written in terms of the normalization of the power spectrum and the speed of sound of perturbations. This is in contrast with the general case, where at any order in perturbations one can write new operators.

2. During Inflation the mode wavefunctions have the same form as in Minkowski. This apparently suggests the lack of a proper production of scalar perturbations. However, as we will argue below, this is not true if one considers the inevitable transition to a phase in which the time-reparametrization symmetry is broken.

3. The above feature leaves an interesting signature in the correlation functions of the model. Indeed, the "decaying" mode decays much slower than in the conventional case (as $1/a$ instead of $1/a^3$). This has remarkable consequences for the squeezed limits of correlation functions: the standard single-field theorems hold, but only at first order in the momentum of the long mode. One finds corrections at first order and, in particular, one has a $1/k_L^2$ behaviour of the 3-point function in the squeezed limit. Unfortunately, these effects are very suppressed and totally unobservable. Indeed, the field redefinition symmetry itself is such that a time-dependent background wave, which would violate the consistency relations, can be removed and set to zero. Therefore, these effects are not there in the limit of exact field redefinition symmetry and they will only appear once we consider the small breaking of the symmetry.

Section 7.2 describes the construction of the action compatible with the $t \to \tilde{t}(t)$ symmetry. The power spectrum is studied in Section 7.3, with some details left to the two Appendices. The 3- and 4- point functions are discussed respectively in Section 7.4 and 7.5, while conclusions are drawn in Section 7.6.

7.2 Derivation of the action

We want to write an inflaton action in which the usual (approximate) symmetry $\phi \to \phi + c$ is promoted to the full invariance under field redefinition $\phi \to \tilde{\phi}(\phi)$. We are going to assume an exact de Sitter metric and take the decoupling limit $M_P \to \infty$, in which the dynamics of the scalar perturbations can be studied without considering the mixing with gravity. We will check the validity of this approximation in Appendix A.1. The time dependent inflaton background defines a foliation and in the presence of ϕ reparameterization invariance, the only invariant object is the 4-vector perpendicular to the foliation [97]

$$u_\mu = \frac{\partial_\mu \phi}{\sqrt{-g^{\alpha\beta}\partial_\alpha\phi\partial_\beta\phi}} \,, \tag{7.3}$$

which is indeed invariant under $\phi \to \tilde{\phi}(\phi)$. At low energy the operators with the smallest number of derivatives will dominate. It is straightforward to realize that it is not possible to write an operator with a single derivative. With two derivatives we have

$$\left(\nabla_\mu u^\mu\right)^2 ; \quad \nabla_\mu u^\nu \nabla_\nu u^\mu ; \quad \nabla_\mu u^\nu \nabla^\mu u_\nu ; \quad u^\mu u^\nu \nabla_\mu u_\rho \nabla_\nu u^\rho . \tag{7.4}$$

The first two are the same by integration by parts (this is true in the de Sitter limit where the Riemann tensor is proportional to the metric). Another constraint comes from the fact that u^μ is hypersurface-orthogonal, so that the Frobenius theorem implies

$$\nabla_\mu u^\nu \nabla_\nu u^\mu = \nabla_\mu u^\nu \nabla^\mu u_\nu + u^\mu u^\nu \nabla_\mu u_\rho \nabla_\nu u^\rho \,. \tag{7.5}$$

We are thus left with two independent operators. The action to lowest order in derivative—and any order in u^μ—can thus be written as

$$S = \frac{1}{2}\int \mathrm{d}^4x\sqrt{-g}\left(M_{Pl}^2 R - 2\Lambda - M_\lambda^2\left(\nabla_\mu u^\mu - 3H\right)^2 + M_\alpha^2 u^\mu u^\nu \nabla_\mu u_\rho \nabla_\nu u^\rho\right), \tag{7.6}$$

where M_α and M_λ are the two parameters of our model, besides the vacuum energy Λ which is driving Inflation [1]. We subtracted $3H$ from the term proportional to M_λ^2 to reabsorb its contribution to the vacuum energy in Λ (notice that the cross term $\propto \nabla_\mu u^\mu$ is a total derivative). This action gives, at lowest order in derivatives, all the n-point functions and it will be the starting point for our calculations below.

[1] We will focus on perturbation theory. We will not enter on how to generate a real model that gives the action (7.6). Hence, we will suppose only a constant value of the energy density during Inflation given in terms of Λ.

Another equivalent way to describe the model is by following the general construction of [93]. Any Inflation model can be described in terms of the metric, in the gauge in which the inflaton perturbations are set to zero. One has to write operators invariant under time-dependent space diffeomorphisms and (approximately) invariant under time translations [93]

$$x_i \to \tilde{x}_i\left(\mathbf{x}, t\right); \quad t \to \tilde{t} = t + \text{const.} \tag{7.7}$$

Here we promote the symmetry of the inflationary action to [95, 97]

$$x_i \to \tilde{x}_i\left(\mathbf{x}, t\right); \quad t \to \tilde{t}(t)\ ; \tag{7.8}$$

the symmetry $\phi \to \tilde{\phi}(\phi)$ becomes invariance under time reparametrization, as in this gauge constant time surfaces coincide with the ones at constant inflaton. Notice that the time reparametrization symmetry forbids to write operators with g^{00}, which are otherwise allowed by the symmetries (7.7). The action (7.6) can be written geometrically as

$$S = \frac{M_P^2}{2}\int \mathrm{d}^3x\,\mathrm{d}t\sqrt{h}N\left(R^{(3)} + K_{ij}K^{ij} - \lambda(K-3H)^2 + \alpha a_i a^i\right), \tag{7.9}$$

in terms of the ADM variables

$$ds^2 = -N^2dt^2 + h_{ij}(dx^i + N^i dt)(dx^j + N^j dt)\ , \qquad K_{ij} = \frac{1}{2N}\left(\dot{h}_{ij} - \nabla_i N_j - \nabla_j N_i\right)\ , \tag{7.10}$$

and $a_i \equiv N^{-1}\partial_i N$. Indeed in this gauge one has $\left(u^\nu \nabla_\nu u^\mu\right)^2 = a_i a^i$ and $\left(\nabla_\mu u^\mu\right)^2 = K^2$, so that the equivalence of the two actions follows from the Gauss-Codazzi relation ($R^{(4)} = R^{(3)} + K_{ij}K^{ij} - K^2$ up to total covariant derivatives), with the identification $(\lambda - 1)M_P^2 = M_\lambda^2$ and $\alpha M_P^2 = M_\alpha^2$. Notice that in this language there are four invariant operators with two derivatives: $R^{(3)}$, $K_{ij}K^{ij}$, K^2 and $a_i a^i$. One can get rid of one with the Gauss-Codazzi relation, up to a redefinition of the Planck mass. We still have an additional operator compared to the previous description. Indeed $R^{(3)}$ does not play any role in the decoupling limit. Even more: as it is clear when one changes to spatially flat gauge, where $R^{(3)}$ only depends on tensor modes, this operator does not affect scalar perturbations even departing from the decoupling limit, or at non-linear order. This operator changes the speed of sound of gravitational waves as it affects their spatial kinetic term, but its effect is anyway negligible unless its coefficient is of the order M_P^2 ([2]).

The reader may be puzzled by the fact that the symmetry under field redefinition is incompatible with the fact that Inflation must end once a certain point in field space is reached. But the situation is not different from the case of the usual shift symmetry, which will be strongly broken at reheating. Also, here we only assume the field redefinition symmetry to be a good approximation while Inflation occurs and perturbations are generated. Notice that a strong breaking of the symmetry in a region of field space where reheating

[2]Notice also that one cannot induce sizeable graviton non-gaussianities cranking up the coefficient of this operator: indeed its coefficient cannot become parametrically large compared to M_P^2, as this would imply a superluminal propagation of tensor modes.

takes place will not spoil the symmetry somewhere else, as renormalization is local in field space. In other words, the symmetry is valid only in a limited range of field space and it is badly broken if one considers field redefinitions which are large enough to move the point out of the symmetric region

7.3 Power spectrum

To calculate the power spectrum we expand the action (7.6) at second order. Using the field redefinition symmetry we can assume to perturb around $\phi_0 = t$, i.e. $\phi(\mathbf{x}, t) = t + \pi(\mathbf{x}, t)$, in an unperturbed de Sitter space, which is a good approximation in the decoupling limit. Notice that the action does not contain any term linear in π, which implies that the unperturbed Universe we are expanding around is indeed a good solution. In conformal time we get [3]

$$S_2 = \int \mathrm{d}^3x\, \mathrm{d}\eta \left(\frac{M_\alpha^2}{2}(\partial\pi')^2 - \frac{M_\lambda^2}{2}(\partial^2\pi)^2 \right) . \tag{7.11}$$

This result is pretty unconventional. First of all, compared with the usual free-field action, each term has two additional spatial derivatives. This is not worrisome as additional spatial derivatives do not introduce extra pathological degrees of freedom. Second, the action does not contain any η dependence so that the field is not sensitive to the expansion of the Universe and behaves as in Minkowski space (though with a speed of sound which is, in general, different from the speed of light). Actually these two peculiarities in some sense cancel each other to give a scale-invariant spectrum. Indeed, we expect the mode functions to be of the Minkowski form, but with an additional factor of $1/k$ because of the presence of the additional spatial derivatives. It is easy to get the wavefunctions

$$\pi_k(\eta) = \frac{1}{\sqrt{2k^3}} \frac{1}{\sqrt{M_\alpha M_\lambda}} e^{\pm i \frac{M_\lambda}{M_\alpha} k\eta} , \tag{7.12}$$

which give a scale-invariant spectrum for π at late times $\eta \to 0$. The curvature perturbation ζ is given by $\zeta = -H\pi$ so that

$$\langle \zeta_{\vec{k}} \zeta_{\vec{k}'} \rangle = (2\pi)^3 \delta(\vec{k} + \vec{k}') \frac{1}{2k^3} \frac{H^2}{M_\alpha M_\lambda} . \tag{7.13}$$

Notice that the scale invariance of the power spectrum (and of higher-order correlation functions) can be justified by symmetry arguments [94], since we are in exact de Sitter and the action is shift symmetric. Of course, a small tilt is induced if the field redefinition symmetry is slightly broken.

[3] The π exchange may induce spatial non-locality when coupled to other fields, as discussed in [96]. This is not relevant for us as we are not interested in coupling with other particles in calculating primordial correlation functions. Spatial non-locality may be relevant in discussing the horizon and flatness problem.

The result is encouraging, but the reader may be suspicious of this derivation. After all, how is it possible that perturbations are created if the field behaves as in Minkowski space? To understand what happens, let us follow the classical dynamics of a given Fourier mode. Although it is not sensitive to the Hubble friction, its wavelength is stretched and it eventually becomes much longer than the Hubble radius. In this regime the frequency of the mode, which keeps on oscillating as in Minkowski, becomes much slower than the rate of the expansion of the Universe. This means that, on a Hubble timescale, the time-dependence of the mode can be neglected and, similarly, its space-dependence becomes very small in a Hubble patch. We conclude that the solution we are describing is an attractor since the effect of perturbations becomes smaller and smaller as time evolves.

This also sheds light on the quantum mechanical behaviour. Although each Fourier mode effectively remains in Minkowski, hindering a classical interpretation, the fact that its frequency becomes much smaller than the rate of expansion means that one is sensitive only to π and not to $\dot{\pi}$. It is like probing in a laboratory a harmonic oscillator with an experiment which is very short compared to the period of oscillation: it will only be sensitive to the probability distribution of the position, but not to the momentum. The difference with the standard situation in Inflation is quantitative, but not qualitative. Usually the time dependence of the mode decays, compared with the Hubble rate, as a^{-3} and it can safely be neglected. Here it decays as a^{-1}.

The same logic also implies another important result: the conservation of ζ on super-Hubble scales during the reheating stage and later. Independently of the details of reheating, we can assume that it will be insensitive to $\dot{\pi}$ which is exponentially small compared to π. This means that locally we are following the same unperturbed solution, with ζ describing the relative difference in expansion between different points. In Appendix A.2 we verify these intuitive arguments in an explicit toy example. We will see, in the following Sections, that this slow decay of the decaying mode leaves some signature in the higher-order correlation functions, which is a quite distinctive feature of this model.

Due to the field redefinition symmetry one can choose the background solution to be $\phi_0 = -\eta$ and perturb now around this background $\phi = -\eta + \chi$. It is straightforward to express at linear order these perturbations in terms of the perturbations around cosmic time as $\chi = \pi/a$, and write the second order action in terms of χ from Eq. (7.11)

$$S_2(\chi) = \int \mathrm{d}^3x\, \mathrm{d}\eta\, a^2 \left(\frac{M_\alpha^2}{2} (\partial\chi')^2 - \frac{M_\lambda^2}{2} (\partial^2\chi)^2 - M_\alpha^2 \mathcal{H}^2 (\partial\chi)^2 \right) . \tag{7.14}$$

This is compatible with the results of [102], where it was noted that the effective mass is that of a conformally coupled field; this is consistent with the fact that the equations of motion for the field are like in Minkowski. Moreover, note that this action gives a power spectrum for χ which is still scale invariant (since χ and π are related simply by a function of time) but with an amplitude that decreases exponentially during Inflation. Different choices for the background solution seem to give different answers for the power spectrum in spite of the field redefinition symmetry. The issue is settled by the fact that what is

more closely related to observations is the curvature perturbation conserved outside of the horizon ζ which is equal to π up to a constant factor as computed in Appendix A.1.

7.4 The 3-point function

As we saw in the previous Section, the power spectrum for the fluctuations is scale invariant and indistinguishable from the predictions of more conventional inflationary scenarios. Let us now study the 3-point correlation function which carries additional information. It is conventional to define

$$\langle \zeta_{\vec{k}_1} \zeta_{\vec{k}_2} \zeta_{\vec{k}_3} \rangle \equiv (2\pi)^3 \delta(\vec{k}_1 + \vec{k}_2 + \vec{k}_3) F_\zeta(k_1, k_2, k_3) \,, \tag{7.15}$$

where translational invariance implies that the 3-point function must be proportional to the Dirac delta, and rotational invariance implies that the function F_ζ, called the bispectrum of ζ, is a function only of the magnitude of the momenta. As discussed in the previous Section, the dilation isometry of de Sitter, together with the time shift symmetry implies that the bispectrum is a homogeneous function of degree -6.

The 3-point function of the field perturbation π can be computed using the in-in formalism. It is given by (see Eq. (5.59))

$$\langle \pi^3(\eta_*) \rangle = \left\langle 0 \left| \bar{T} e^{i \int_{-\infty - i\epsilon}^{\eta_*} H_{int}(\eta') \mathrm{d}\eta'} \pi^3(\eta_*) T e^{-i \int_{-\infty + i\epsilon}^{\eta_*} H_{int}(\eta') \mathrm{d}\eta'} \right| 0 \right\rangle , \tag{7.16}$$

where, as already explained, $|0\rangle$ is the Bunch-Davies vacuum, T (and $\bar{T}$) indicates time ordering (and anti time ordering), η_* indicates the time at which inflation ends, $\mathcal{H}_{\rm int}$ is the interaction Hamiltonian and ϵ is an infinitesimal positive constant. At leading order only the cubic part of the interaction Hamiltonian contributes, and one can show that $\mathcal{H}_{\rm int} = -\mathcal{L}_{\rm int}$. Therefore one can use the third order piece of the Lagrangian to compute the three-point function using

$$\langle \pi^3(\eta_*) \rangle = i \int_{-\infty}^{\eta_*} \mathrm{d}\eta \left\langle \left[\pi^3(\eta_*), \int \mathrm{d}^3x \, \mathcal{L}_{\rm int}(t, \vec{x}) \right] \right\rangle . \tag{7.17}$$

The interaction Lagrangian can be computed by expanding the action, Eq. (7.6), to third order. We get, after several integrations by parts [4],

$$S_3 = \int \mathrm{d}^3x \, \mathrm{d}\eta \, \frac{1}{a} \Big[M_\lambda^2 \big(2\partial_i \pi' \partial_i \pi \partial^2 \pi + \pi' \partial_i \partial_j \pi \partial_i \partial_j \pi \big) + M_\alpha^2 \big(\pi' \partial_i \pi'' \partial_i \pi - \partial_i \pi' \partial_j \pi \partial_i \partial_j \pi \big) \Big] \,. \tag{7.20}$$

[4] The reader might be worried about the appearance of an interacting term in the action that contains explicitly a second time derivative acting on π that cannot be removed by a partial integration. This would not be a problem for us as we are treating these higher derivative terms as small corrections to the free action. However, it was noted in [97] that this term can actually be reabsorbed by performing a field redefinition of the form

$$\pi = \bar{\pi} + \bar{\pi}\bar{\pi}' , \tag{7.18}$$

leading to the following action

$$S_3 = \int \mathrm{d}^3x \, \mathrm{d}\eta \, \frac{1}{a} \Big[- M_\lambda^2 \Big(\bar{\pi} \partial^2 \bar{\pi} \partial^2 \bar{\pi}' - \frac{\mathcal{H}}{2} (\partial \bar{\pi})^2 \partial^2 \bar{\pi} \Big) + M_\alpha^2 \Big(\frac{1}{2} \bar{\pi} (\partial \bar{\pi}')^2 - \frac{\mathcal{H}}{2} \bar{\pi} (\partial \bar{\pi}')^2 - \partial_i \bar{\pi}' \partial_j \bar{\pi} \partial_i \partial_j \bar{\pi} \Big) \Big] \,. \tag{7.19}$$

This cubic action coincides with Eq. (5.10) of [97] in the Minkowski limit. In order to compute the 3-point function for ζ we use the relation $\zeta = -H\pi$, additional non-linear terms in this relation either involve higher derivatives, which vanish outside of the horizon, or are suppressed by slow-roll factors, see [56, 103]. We thus obtain the following expression for the bispectrum:

$$F_\zeta(k_1,k_2,k_3) = \frac{1}{\prod k_i^3} P_\zeta^2 \left[-\frac{k_1}{k_t^2}(k_3^2 \vec{k}_1\cdot\vec{k}_2 + k_2^2 \vec{k}_1\cdot\vec{k}_3) - \frac{k_1^2}{k_t}\vec{k}_2\cdot\vec{k}_3 - \frac{M_\alpha^2}{M_\lambda^2}\frac{k_1^3}{k_t^2}\vec{k}_2\cdot\vec{k}_3 \right] + \text{cyclic perms.}\,, \tag{7.21}$$

where $k_t \equiv k_1+k_2+k_3$ and $P_\zeta = H^2/(2M_\alpha M_\lambda)$ is the ζ power spectrum, Eq. (7.13). All the contributions but the last cannot be large and give an $f_{\rm NL}\sim 1$. The contribution from the last term on the other hand is proportional to $M_\alpha^2/M_\lambda^2 \equiv 1/c_s^2$. Actually it is easy to estimate the effect of each operator of the cubic action (7.20) comparing them with the quadratic action when modes freeze ($\partial_t \sim H$, $\partial_i \sim H/c_s$). The only operator that can give a parametrically large 3-point function is the last in Eq. (7.21).

We find an interesting feature of the model: it gives a single potentially large shape with an amplitude controlled by a single parameter, namely c_s^2. We plot the shape of this contribution in Fig. 7.1.

In order to understand the phenomenological implications of this result, let us first introduce a quantitative way of comparing bispectra. One defines the scalar product between two shapes as [104]

$$F_1 \cdot F_2 = \sum_{\text{triangles}} \frac{F_1(k_1,k_2,k_3)F_2(k_1,k_2,k_3)}{P(k_1)P(k_2)P(k_3)}\,, \tag{7.22}$$

where the sum is over values of the momenta that form a closed triangle. One can then define the "cosine" of two shapes in the following way

$$\cos(F_1,F_2) = \frac{F_1\cdot F_2}{(F_1\cdot F_1\, F_2\cdot F_2)^{1/2}}\,. \tag{7.23}$$

If the cosine between two shapes is close to one, one expects the data to be unable to distinguish between the two; conversely, if the cosine between two shapes is very small, constraints on the amplitude of one of the shapes do not constrain the amplitude of the other[5].

In CMB data analysis, a crucial numerical boost is gained when looking for shapes which are factorizable, *i.e.* which can be written as monomials of k_1, k_2, and k_3. The

This action produces the same three-point function, Eq. (7.17), since the field redefinition, Eq. (7.18), vanishes outside of the horizon. One expects this to be true at every order in perturbations since in the unitary gauge, Eq. (7.9), the number of degrees of freedom is fixed [97].

[5]For CMB applications, this statement can be made more precise by defining a "two-dimensional" cosine, which takes into account the geometry and the effect of the linear transfer functions, to get closer to what it is actually observed [104].

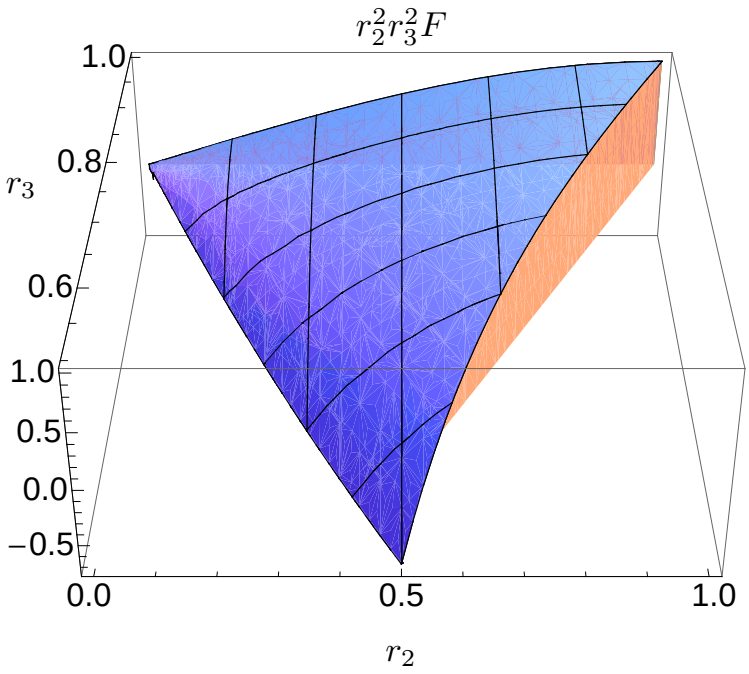

Figure 7.1: We plot the shape of the part proportional to $1/c_s^2$ of the 3-point function, Eq. (7.21), as a function of the ratios between momenta $r_2 \equiv k_2/k_1$ and $r_3 \equiv k_3/k_1$, multiplied by $r_2^2 r_3^2$. The shape is normalized such that its amplitude is one at the equilateral point $r_2 = r_3 = 1$.

standard procedure when comparing a theoretical 3-point function with constraints from CMB data is then to look for a factorizable shape which has a large cosine with the shape generated by a given inflationary model. Such shapes are often termed templates, which can be expressed as linear combinations of the so-called local, equilateral and orthogonal templates (see refs. [104, 105]). The cosines of the shape depicted in figure 7.1 with these three standard templates are

$$\cos(F_\zeta, F_{\rm local}) = 0.17\,, \tag{7.24}$$

$$\cos(F_\zeta, F_{\rm equilateral}) = 0.93\,, \tag{7.25}$$

$$\cos(F_\zeta, F_{\rm orthogonal}) = 0.49\,. \tag{7.26}$$

It is therefore a good approximation to take the shape as equilateral. Its amplitude can be read from the expression (7.21) above

$$f_{\rm NL}^{\rm eq} = \frac{5}{108}\frac{1}{c_s^2}\,. \tag{7.27}$$

The limits on the equilateral shape obtained from WMAP 7 data given in ref. [19] can be used to put bounds on c_s: $c_s \gtrsim 0.013$ at the 95% confidence level. Notice that (the potentially large contribution to) the 3-point function has a fixed positive sign in this model [6]. This is

[6] We are using the WMAP sign convention for $f_{\rm NL}$.

the opposite of what happens in more conventional models with reduced speed of sound (K-inflation), where the operator which reduces the speed of sound gives $f_{\rm NL}^{\rm eq} \propto -1/c_s^2$. However in those models one has another operator which contributes to the 3-point function and can flip the sign of $f_{\rm NL}^{\rm eq}$; in our case we have no freedom. It is worth stressing that, although the shape given in Eq. (7.21) has a large overlap with the equilateral one, the result has no free parameter and thus represents a potential smoking gun of the model.

If one calculates the contribution to the 3-point function of the second and third operator in the action (7.20), each of them, when taking the squeezed limit $k_1 \ll k_2, k_3$, diverges like $1/k_1^2$ (while the leading term discussed above goes as $1/k_1$). This seems to contradict the results of references [106, 107] where it is shown that, ignoring small deviations from scale invariance, in single field inflationary models the squeezed limit of the 3-point function diverges like $1/k_1$ in that squeezed limit. This is due to the fact that the proof given there relies on $\zeta_k'(\eta)$ vanishing at least like k^2/H^2 outside of the horizon, while Eq. (7.12) shows that in the model we are studying here $\zeta_k'(\eta)$ vanishes only like k/H. However, this $1/k_1^2$ divergence cancels between the two operators as it is evident in Eq. (5.59) ([7]). This is not an accident, but a consequence of the field redefinition symmetry. Indeed, a homogeneous time-dependent background mode, which would lead to the violation of the consistency relations, can be redefined away using the symmetry. Our theory is invariant under

$$t + \pi \to F(t+\pi) \simeq t + \pi + \epsilon(t+\pi) + \ldots = t + \pi + \epsilon(t) + \dot\epsilon(t)\pi + \frac{1}{2}\ddot\epsilon(t)\pi^2 + \ldots \qquad (7.28)$$

This means that a time-dependent background $\epsilon(t)$ can be removed, provided we also redefine the field π as above. This redefinition, however, is irrelevant at late times as $\dot\epsilon \to 0$, so we can conclude that the background wave has no effect and thus we do not violate any consistency relation. We checked explicitly that terms obtained from the cubic action with $\pi \to \pi + \epsilon(t)$ cancel with terms in the quadratic action (7.11) that appear after $\pi \to \pi + \dot\epsilon(t)\pi$.

Notice, however, that the slow decay of the modes still opens up the possibility to violate the consistency relations: it is enough to consider terms which violate the original field redefinition symmetry. Of course, we expect these terms to be suppressed but to be there anyway, as indicated by the small observed deviation from a scale invariant spectrum. For example, we can add to the action (7.9) the cubic operator in unitary gauge

$$S \supset \int {\rm d}^3x\, {\rm d}t \sqrt{h} N\, (g^{00} - 1)(K - 3H)^2\,, \qquad (7.29)$$

which is *not* invariant under the field redefinition symmetry. This operator starts at cubic order, so that it does not modify the mode evolution, and it gives a cubic term $\pi'(\partial^2\pi)^2$ which will violate the consistency relations. One might hope that such a non-standard behavior leaves an observational signature for example in the scale-dependence of the halo bias [108, 109, 110]. However, even under the optimistic assumption that the effect is suppressed by a single power of slow-roll compared to the leading $1/c_s^2$ term, the analysis of references [111, 112] (though performed for a different model) indicates that the observation of this effect with such a small amplitude seems unfeasible with planned surveys.

[7] We are indebted to Austin Joyce for pointing out an error in the first version of the paper.

7.5 The 4-point function

Given that all the correlation functions to leading order in derivatives are completely fixed by two coefficients, it is of some interest to look at the 4-point function. In this section we compute the 4-point function focusing only on the leading contribution proportional to c_s^{-4}. This part of the 4-point function is important since observationally it gives the most relevant contribution in the case of small c_s.

In order to compute the 4-point function we need the interaction Hamiltonian to fourth order, for which it is no longer true that $\mathcal{H}_{int} = -\mathcal{L}_{int}$. Let us start by expanding the action (7.6) to fourth order focusing on the term proportional to M_α^2, which gives the largest contribution

$$\begin{aligned} S_\alpha^{(4)} = M_\alpha^2 \int \mathrm{d}^3x\, \mathrm{d}\eta \Bigg(& \frac{H^2}{2}\pi'\pi'(\partial\pi)^2 - \frac{H}{a}\left((\partial\pi)^2\partial_i\pi\partial_i\pi' + \pi'\pi''(\partial\pi)^2 + \pi'\partial_i\pi\partial_j\pi\partial_i\partial_j\pi\right) \\ & - \frac{3H}{a}\pi'\pi'\partial_i\pi\partial_i\pi' + \frac{1}{2a^2}\left(\pi''\pi''(\partial\pi)^2 + 6\pi'\pi''\partial_i\pi\partial_i\pi' + 3\pi'\pi'\partial_i\pi'\partial_i\pi' + 3\partial_i\pi\partial_j\pi\partial_i\pi'\partial_j\pi'\right) \\ & + \frac{1}{a^2}\pi''\partial_i\pi\partial_j\pi\partial_i\partial_j\pi + \frac{3}{a^2}\pi'\partial_i\pi\partial_j\pi'\partial_i\partial_j\pi + \frac{1}{a^2}(\partial\pi)^2(\partial\pi')^2 + \frac{1}{2a^2}\partial_i\pi\partial_j\pi\partial_i\partial_l\pi\partial_j\partial_l\pi \Bigg) \,. \end{aligned} \tag{7.30}$$

The second and third order pieces of the action are given by Eqs. (7.11) and (7.20) respectively. Throughout this section we will only keep those terms that give the largest contributions to the 4-point function in the small c_s^2 case. As before, it is easy to estimate the amplitude of the 4-point funcion by comparing each term in the quartic action (7.30) with the kinetic terms, Eq. (7.11), once the modes freeze ($\partial_t \sim H$ and $\partial_i \sim H/c_s$). The amplitude of the largest piece of the 4-point function can thus be estimated to be proportional to c_s^{-4}, generated by those terms in the non-linear action which are proportional to M_α^2 and containing the highest number of spatial derivatives. Thus, we will keep only the last terms in Eqs. (7.20) and (7.30).

As stressed above, in order to obtain the correct expression for the 4-point function one must explicitly compute the Hamiltonian [8] $\mathcal{H}(P,\pi) = P\pi' - \mathcal{L}(P,\pi)$, where the generalized momentum (keeping only the most relevant pieces in the small c_s^2 case) is given by

$$P = \frac{\partial\mathcal{L}}{\partial\pi'} = -M_\alpha^2\partial^2\pi' + \frac{M_\alpha^2}{2a}\partial^2(\partial_i\pi)^2 \,. \tag{7.31}$$

A straightforward computation of the terms in the fourth order interaction Hamiltonian which could potentially generate a 4-point function proportional to c_s^{-4} using Eqs. (7.30)

[8] Notice that the canonical variables satisfying the commutation relations after quantization are the field π and the generalized momentum P, and the Hamiltonian is a function of these variables. Wherever we write π' in the explicit expression for the Hamiltonian, it should be understood as shorthand for the appropriate expression in terms of π and P.

and (7.31) shows that it vanishes [9].

In principle, two types of diagrams can contribute to the 4-point function: exchange diagrams and contact diagrams. However, since the fourth order interaction Hamiltonian vanishes, there is no contact diagram and the vacuum expectation value for the four-point equal-time correlation function in momentum space is given only by the exchange diagrams. In the in-in formalism the 4-point function can then be computed as

$$\langle 0|\zeta_{\vec{k}_1}\zeta_{\vec{k}_2}\zeta_{\vec{k}_3}\zeta_{\vec{k}_4}(\eta)|0\rangle = \int_{-\infty}^{\eta} \mathrm{d}\eta' \int_{-\infty}^{\eta} \mathrm{d}\eta'' \langle 0|\mathcal{H}^{(3)}_{int}(\eta')\zeta_{\vec{k}_1}\zeta_{\vec{k}_2}\zeta_{\vec{k}_3}\zeta_{\vec{k}_4}(\eta)\mathcal{H}^{(3)}_{int}(\eta'')|0\rangle$$
$$- 2\,\mathrm{Re}\left(\int_{-\infty}^{\eta} \mathrm{d}\eta' \int_{-\infty}^{\eta'} \mathrm{d}\eta'' \langle 0|\zeta_{\vec{k}_1}\zeta_{\vec{k}_2}\zeta_{\vec{k}_3}\zeta_{\vec{k}_4}(\eta)\mathcal{H}^{(3)}_{int}(\eta')\mathcal{H}^{(3)}_{int}(\eta'')|0\rangle\right) , \quad (7.32)$$

The third order interaction Hamiltonian can be read from Eq. (7.20). We are interested in the piece that can give a contribution to the 4-point function proportional to $1/c_s^4$ which, after an integration by parts, we write as

$$\mathcal{H}^{(3)}_{int} = -\frac{M_\alpha^2}{2a}\partial^2\pi'(\partial\pi)^2 \, . \quad (7.33)$$

The time integrations appearing in Eq. (7.32) can be performed using

$$\int_{-\infty}^{0} \frac{\mathrm{d}\tau'}{a(\tau')} e^{-i\frac{M_\lambda}{M_\alpha}(p+k_1+k_2)\tau'} \int_{-\infty}^{0} \frac{\mathrm{d}\tau''}{a(\tau'')} e^{i\frac{M_\lambda}{M_\alpha}(p+k_3+k_4)\tau''} = H^2\frac{M_\alpha^4}{M_\lambda^4}\frac{1}{2p^3}\frac{1}{(p+k_1+k_2)^2}\frac{1}{(p+k_3+k_4)^2} \, , \quad (7.34)$$

and

$$\int_{-\infty}^{0} \frac{\mathrm{d}\tau'}{a(\tau')} e^{i\frac{M_\lambda}{M_\alpha}(k_1+k_2-p)\tau'} \int_{-\infty}^{\tau'} \frac{\mathrm{d}\tau''}{a(\tau'')} e^{i\frac{M_\lambda}{M_\alpha}(p+k_3+k_4)\tau''} =$$
$$H^2\frac{M_\alpha^4}{M_\lambda^4}\frac{1}{2p^3}\frac{1}{(p+k_3+k_4)^2}\left(\frac{1}{k_t^2} + 2\frac{p+k_3+k_4}{k_t^3}\right) . \quad (7.35)$$

[9] It is important to note that in the full fourth order action, Eq. (7.30), there are terms containing two time derivatives acting on the field π'' in such a way that they cannot be eliminated by an integration by parts. Similarly to what we did in the case of the 3-point function, we could have removed these terms from the action by a suitable field redefinition

$$\pi = \bar{\pi} + \bar{\pi}\bar{\pi}' + \partial^{-2}\partial_i\left(\frac{1}{a}\bar{\pi}'\partial_i\bar{\pi}\right) ,$$

which vanishes outside the horizon and does not change the result for the correlation functions.

The 4-point function can then be computed using Eqs. (7.32) to (7.35)

$$\langle\zeta_{\vec{k}_1}\zeta_{\vec{k}_2}\zeta_{\vec{k}_3}\zeta_{\vec{k}_4}\rangle_c = (2\pi)^3\delta(\sum\vec{k}_a)P_\zeta^3\frac{M_\alpha^4}{M_\lambda^4}\frac{1}{\prod_a k_a^3}\frac{1}{4p^3(p+k_1+k_2)^2}$$
$$\times\left\{\left(p^6(\vec{k}_1\cdot\vec{k}_2)(\vec{k}_3\cdot\vec{k}_4)-2p^3k_1^3(\vec{p}\cdot\vec{k}_2)(\vec{k}_3\cdot\vec{k}_4)\right)\left[\frac{1}{4(p+k_3+k_4)^2}-\frac{1}{2k_t^3}\big(k_t+2(p+k_1+k_2)\big)\right]\right.$$
$$\left.+\left(2p^3k_3^3(\vec{k}_1\cdot\vec{k}_2)(\vec{p}\cdot\vec{k}_4)-4k_1^3k_3^3(\vec{p}\cdot\vec{k}_2)(\vec{p}\cdot\vec{k}_4)\right)\left[\frac{1}{4(p+k_3+k_4)^2}+\frac{1}{2k_t^3}\big(k_t+2(p+k_1+k_2)\big)\right]\right\}$$
$$+\,23\text{ perms.}\,, \quad (7.36)$$

where $\vec{p}=\vec{k}_1+\vec{k}_2$.

Equation (7.36) is suppressed in the squeezed limit and does not contribute to the consistency relation [107]

$$\langle\zeta_{\vec{q}}\zeta_{\vec{k}_1}\zeta_{\vec{k}_2}\zeta_{\vec{k}_3}\rangle'_{\vec{q}\to 0}\sim\frac{1}{c_s^4}\mathcal{O}\left(\frac{q^2}{k^2}\right)P(q)P(k)^2\,. \quad (7.37)$$

This is easy to understand since it receives contributions only from exchange diagrams: when $\partial^2\pi'$ corresponds to the external leg going to zero it will be trivially suppressed by q^3, when $\partial_i\pi$ corresponds to the external leg going to zero it will be contracted with both the other external leg which has some momentum $\vec{k}$ and the internal leg with momentum $-\vec{k}-\vec{q}$, which cancel at leading order in q.

We checked also at the quartic level that the symmetry, Eq. (7.28), holds [10] and this will prevent any violation of the consistency relations. Violations are possible, like in the cubic case, if one considers quartic terms which do not respect the field redefinition symmetry.

7.6 Conclusions and outlook

Given the simplicity of single-field Inflation, it is certainly worthwhile exploring all the possible symmetries that can be imposed on its dynamics and their phenomenological consequences. Here we have studied the implications of imposing an approximate field redefinition symmetry $\phi\to\tilde{\phi}(\phi)$ on the inflaton. The predictions are very sharp since—after fixing the normalization of the spectrum—all correlation functions depend only on the speed of sound c_s and are somewhat unusual, as a consequence of the slow decay of the decaying mode during Inflation.

What we have studied represents another de Sitter limit of Inflation, as Inflation can (but need not) take place with the metric being exactly de Sitter. This parallels the case

[10] For this check it is crucial to keep also the quadratic action and vary it with the last term of Eq. (7.28): this term cannot be neglected, because in going to conformal time it also gives an $H\epsilon'$ contribution.

of ghost Inflation [61], while another example has been studied in [93]. Like in the case of ghost Inflation, the dynamics that may be responsible for modification of gravity in the late Universe, can be applied to Inflation. This is not surprising, as models of modification of gravity often involve a scalar which defines a preferred foliation of space-time. And this is exactly what we need for inflation.

It is useful to think about this model as another corner of the EFT of Inflation [93]. Starting from a general situation, the limit $\dot{H} \to 0$ kills the unitary gauge operator g^{00}, and therefore the standard spatial kinetic term of the inflaton. This is the limit of ghost Inflation [61], when the spatial kinetic term is given by higher order spatial derivatives (K^2 and $K_{\mu\nu}K^{\mu\nu}$), while a standard time kinetic term $\dot{\pi}^2$ comes from the unitary gauge operator $(g^{00}+1)^2$. The symmetry that we discussed forbids any operator of the form $(g^{00}+1)^n$, so that also the time kinetic term is now given by the higher derivative operator $N^{-2}(\partial_i N)^2$. Of course these are only limiting cases: intermediate regimes in which various operators are relevant may have interesting features. We leave this to future investigations.

It is important to stress a relevant drawback of our model, *i.e.*, its spatial non-locality: the Green function of π shows instantaneous propagation of the signal as discussed in [114]. Most likely, this implies that our EFT cannot be embedded in a standard Lorentz invariant UV completion [11]. This is similar to what happens in models of k-inflation with superluminal speed of sound $c_s > 1$.

[11] We thank D. Baumann for useful correspondence about this point.

Chapter 8

Impact of general reionization scenarios on extraction of inflationary parameters

We revisit constraints on inflationary models using more general reionization scenarios. While the bounds on the tensor-to-scalar ratio are largely unmodified, when different reionization schemes are addressed, hybrid models are back into the inflationary game.

8.1 Introduction

As already explained in Section 4, the simplest inflationary model makes use of a single scalar field ϕ (the inflaton), which slowly evolves in a very shallow, nearly constant, potential $V(\phi)$. The dynamics of slow roll gives rise to a quasi-de Sitter phase of exponential expansion which, in turn implies a nearly scale invariant power spectrum of both scalar and tensor perturbations. We can parametrize the deviation of scale invariance of the power spectra by introducing the spectral indexes (see Eqs. (5.23) (5.29))

$$P_{\mathcal{R}}(k) \propto k^{n_s-1}, \quad P_T(k) \propto k^{n_t}. \tag{8.1}$$

In other words, inflation predicts $n_s \simeq 1$, but usually $n_s \neq 1$.

A scale-invariant scalar power spectrum corresponding to the value $n_s = 1$ is the model proposed by Harrison, Zel'dovich, and Peebles [115].

The most recent analysis by the Wilkinson Microwave Anisotropy Probe (WMAP) team of their seven-year data [19] rule out the Harrison-Zel'dovich (H–Z) primordial power spectrum at more than 3σ when ignoring tensor modes: $n_s = 0.963 \pm 0.012$. But this, as well as most other previously derived constraints from CMB data on cosmological parameters have assumed a "sudden" and complete reionization at a single redshift z_r. The reionization

redshift, z_r, is taken to be in the range $4 < z_r < 32$, and the cosmological constraints are obtained after marginalization over z_r. The electron ionization fraction $x_e(z)$ is such that for $z \ll z_r$ $x_e(z) = 1$ ($x_e(z) = 1.08$ for $z < 3$ taking into account Helium recombination) and $x_e(z) = 2 \times 10^{-4}$ for $z > z_r$, *i.e.,* joining the value after primordial recombination with a smooth interpolation.

The process of structure formation that led to gravitational collapse of objects in which the first stars formed are still subject to theoretical and observational uncertainties. As these first sources began to illuminate their local neighborhoods, the HI present in the IGM was "reionized." The end of the Dark Ages (the period between the end of CMB recombination and the appearance of the first stars) remains to be explored and understood.

There are two main effects on the CMB anisotropies produced by the free electrons of the ionized gas: the first one washes out the primary anisotropies of the temperature autocorrelation (TT) spectrum. The damping of the TT signal is quantified by the optical depth parameter τ, proportional to the column density of ionized hydrogen. Earlier reionization leads to a larger suppression of the TT acoustic peaks. The second effect produces a damping and an additional peak in the polarization autocorrelation spectrum (EE) [117]. The position of this new peak in the polarization signal is proportional to the square root of the redshift at which the reionization occurs, and its amplitude is proportional to the optical depth. Since the precise details of reionization processes are currently unknown, it is mandatory to explore the imprints of general reionization histories on the CMB spectra. In the standard, sudden reionization scenario, the EE spectrum depends exclusively on the value of Thomson optical depth τ. In turn, in extended reionization schemes, the precise history of how the Universe became ionized affects the large-scale EE power spectrum in a crucial way [118], and the power is transferred from larger to smaller scales when considering that reionization processes could take place in a non-negligible redshift (time) interval.

The major goal of this work is to study how current constraints on the scalar spectral index n and the tensor-to-scalar ratio r are modified if the standard ("sudden") reionization assumption is relaxed. In a precursor study it was demonstrated that in a general reionization scenario the Harrison-Zel'dovich spectrum ($n = 1$) is perfectly consistent with observations [119]. In this study we shall also include information from tensors modes, showing that inflationary models that are ruled out in the sudden reionization scheme are allowed in more general reionization scenarios. We also reconstruct both the shape and the amplitude of the inflationary potential $V(\phi)$ allowed by current data in both sudden and general reionization schemes.

The Chapter is organized as follows. Section 8.2 introduces the formalism we will use. A possible classification of different models of inflation is presented in Sec. 8.3. The analysis method used here to derive the cosmological constraints is described in Sec. 8.4. Section 8.5 gives the resulting constraints on cosmological parameters and their implications for inflationary models. We conclude in Sec. 8.6.

8.2 The Hamilton-Jacobi formalism

A very powerful way of describing the inflationary dynamics is given by the Hamilton-Jacobi formulation of inflation. The basic idea is to consider the scalar field ϕ itself to be the time variable; this can be done as long as it varies monotonically with time. Then, expressing the Hubble parameter as a function of the field, $H = H(\phi)$, the equations of motion become

$$\dot{\phi} = -\frac{M_{Pl}^2}{4\pi} H'(\phi), \tag{8.2}$$

$$[H'(\phi)]^2 - \frac{12\pi}{M_{Pl}^2} H^2(\phi) = -\frac{32\pi^2}{M_{Pl}^4} V(\phi). \tag{8.3}$$

The second of these equations is called the Hamilton-Jacobi equation. Inflation takes place while the field is slowly rolling towards a minimum of the potential, and the field energy density is dominated by its potential energy. More quantitatively, the slow-roll approximation holds in the limit in which $\ddot{\phi} \ll 3H\dot{\phi}$ and $\dot{\phi}^2 \ll V$, so that Eqs. (4.36) become

$$\begin{aligned} \dot{\phi} &\simeq -\frac{V'(\phi)}{3H}, \\ H^2 &\simeq \frac{8\pi}{3M_{Pl}^2} V(\phi). \end{aligned} \tag{8.4}$$

From Eq. (8.4), we can see that this gives rise to a (quasi-) de Sitter phase with H almost constant. The amplitude of the potential must be sufficiently large to dominate the energy density of the Universe at that epoch. Using the definition of ϵ_V in Eq. (4.41), the Hamilton-Jacobi equation can be rewritten in the useful form

$$H^2(\phi) \left[1 - \frac{1}{3}\epsilon_V(\phi)\right] = \frac{8\pi}{3M_{Pl}^2} V(\phi) \ . \tag{8.5}$$

Inflation also provides a natural mechanism to generate the inhomogeneities presently observed in the Universe. During Inflation, quantum fluctuations, inevitably present at small scales, are quickly redshifted to scales much larger than the horizon size and then frozen in as perturbations to the background metric. The perturbations created during Inflation can be of two types: scalar (or curvature) perturbations, which couple to the matter stress-energy tensor, and tensor perturbations (gravitational waves), which do not couple to matter. The power spectrum of scalar perturbations (quantified as perturbations in the Ricci scalar $\mathcal{R}$) is described by

$$\Delta_{\mathcal{R}}^{1/2}(k) = \left(\frac{H^2}{2\pi|\dot{\phi}|}\right)_{k=aH} = \left[\frac{H}{\sqrt{\pi} M_{Pl}} \frac{1}{\sqrt{\epsilon_V}}\right] \ , \tag{8.6}$$

and its spectral index n_s reads

$$n_s - 1 \equiv \frac{d\ln \Delta_{\mathcal{R}}}{d\ln k} \ . \tag{8.7}$$

The power spectrum of tensor fluctuation modes is given by

$$\Delta_t^{1/2}(k) = \left(\frac{4}{\sqrt{\pi}}\frac{H}{M_{Pl}}\right)_{k=aH} , \tag{8.8}$$

again evaluated when the mode k crosses the horizon.

The ratio of the tensor-to-scalar perturbation is defined as

$$\frac{\Delta_t}{\Delta_{\mathcal{R}}} \equiv r , \tag{8.9}$$

and, as in the scalar power spectrum case, one can write $P_t \propto k^{n_t}$. The two spectral indices expressed in terms of the slow-roll parameters are

$$n_s \simeq 1 - 4\epsilon_V + 2\eta_V , \tag{8.10}$$

$$n_t \simeq -2\epsilon_V , \tag{8.11}$$

where η_V is the other slow-roll parameter defined in Eq. (4.42) and the tensor-to-scalar ratio r is

$$r \equiv 16\epsilon_V . \tag{8.12}$$

The relations above are valid at first-order approximation in the slow-roll parameters. Therefore, if primordial perturbations originated from the dynamics of a slow-rolling scalar field, the spectrum should not be exactly scale invariant. In fact, since the slow-roll parameters ϵ_V and η_V are small, but not vanishing (in other words, since the potential is very close to flat but not *exactly* flat), we expect that $n_s \simeq 1$ but nevertheless $n_s \neq 1$. A scale-invariant power spectrum corresponds to the value $n = 1$ is the aforementioned model proposed by Harrison, Zel'dovich, and Peebles [115]. Given the fact that $\Delta_{\mathcal{R}} \propto k^{n_s-1}$, the spectral index can be thought as a measure of the departure of the spectrum of the scalar perturbations from an exactly scale-invariant power spectrum.

8.3 Zoology of inflationary models

In Section 4.6 we introduce a useful classification for slow-roll single-field inflationary models. Here we use this classification focusing on two parameters, the scalar spectral index n_s and the tensor-to-scalar ratio r, following Kinney *et al.* [120]. At lowest order in the slow-roll approximation the relevant parameters to distinguish among inflationary models are n_s and r [121]. The different classes of models are characterized by the relation between these two parameters, or equivalently, by the relation between ϵ_V and η_V. At lowest order in the slow-roll approximation we can divide the inflationary models into three general types (see Section 4.6): *large-field*, *small-field* and *hybrid*. The boundary between large-field and small-field models is represented by the so called *linear* models.

- Large-field models are characterized by $-\epsilon_V < \eta_V \leq \epsilon_V$. Popular examples of large-field models are $V(\phi) = \Lambda^4(\phi/\mu)^p$ and exponential potentials, $V(\phi) = \Lambda^4 \exp(\phi/\mu)$.

- Small-field models are characterized by $\eta_V < -\epsilon_V$. They result from a generic potential of the form $V(\phi) = \Lambda^4[1-(\phi/\mu)^p]$, which can be understood as the lowest-order Taylor expansion of an arbitrary potential about the origin.
- Hybrid models are characterized by $0 < \epsilon_V < \eta_V$. A generic hybrid potential is of the form $V(\phi) = \Lambda^4[1 + (\phi/\mu)^p]$.
- Linear models are on the boundary between large-field and small-field, and they are characterized for this reason by $\eta_v = -\epsilon_V$. The generic linear potential is of the form: $V(\phi) \propto \phi$.

With the above classification we can cover the entire n-r plane and derive constraints on the inflationary models directly from the constraints on the n_s-r plane that arise from cosmological observations; see Sec. 8.5.

8.4 Analysis method

We adopt two different methods for parametrization of the reionization history. The first method, developed in Ref. [118], is based on principal components that provide a complete basis for describing the effects of reionization on large-scale E-mode polarization. Following Ref. [118], one can parametrize the reionization history as a free function of redshift by decomposing $x_e(z)$ into its principal components:

$$x_e(z) = x_e^f(z) + \sum_\mu m_\mu S_\mu(z), \tag{8.13}$$

where the principal components, $S_\mu(z)$, are the eigenfunctions of the Fisher matrix that describes the dependence of the polarization spectra on the electron ionization fraction $x_e(z)$, m_μ are the amplitudes of the principal components for a particular reionization history, and $x_e^f(z)$ is the WMAP fiducial model at which the Fisher matrix is computed and from which the principal components are obtained. In what follows we use the publicly available $S_\mu(z)$ functions and vary the amplitudes m_μ for $\mu = 1, ..., 5$ for the first five eigenfunctions. Hereafter we refer to this method as the MH (Mortonson-Hu) case.

In a second approach to a general reionization prescription we employ a different parametrization, sampling the evolution of the ionization fraction x_e as a function of redshift z at seven points ($z = 9, 12, 15, 18, 21, 24,$ and 27), and interpolating the value of $x_e(z)$ between them with a cubic spline. For $30 < z$ we fix $x_e = 2 \times 10^{-4}$ as the value of x_e expected before reionization (and after primordial recombination), while $x_e = 1$ for $3 < z < 6$ and $x_e = 1.08$ for $z < 3$ in order to be in agreement with both Helium ionization and Gunn-Peterson test observations. This approach is very similar to the one used in Ref. [122], and we will refer to it as the LWB (Lewis-Weller-Battye) case.

We then modified the Boltzmann CAMB code [67], incorporating the two generalized reionization scenarios and extracted cosmological parameters from current data using a

Monte Carlo Markov Chain (MCMC) analysis based on the publicly available MCMC package `cosmomc` [123].

We consider here a flat ΛCDM universe described by a set of cosmological parameters

$$\{\omega_b, \omega_c, \Theta_s, n_s, \log[10^{10} A_s], r, \alpha_s\}, \tag{8.14}$$

where $\omega_b \equiv \Omega_b h^2$ and $\omega_c \equiv \Omega_c h^2$ are the physical baryon and cold dark matter densities relative to the critical density, Θ_s is the ratio between the sound horizon and the angular diameter distance at decoupling, A_s is the amplitude of the primordial spectrum, n_s is the scalar spectral index, r is the tensor-to-scalar ratio, and $\alpha_s \equiv dn_s/d\ln k$ is the running of the scalar spectral index:

$$\Delta^2_{\mathcal{R}}(k) = \Delta^2_{\mathcal{R}}(k_0) \left(\frac{k}{k_0}\right)^{n(k_0)-1+\frac{1}{2}\ln(k/k_0)\alpha_s} . \tag{8.15}$$

Here, $k_0 = 0.002$ Mpc^{-1} is the pivot scale.

The extra parameters needed to describe reionization are the five amplitudes of the eigenfunctions for the MH case, or the seven amplitudes in the seven bins for the LWB case, and one single common parameter, the optical depth, τ, for the sudden reionization case.

Our basic data set is the seven–year WMAP data [19] (temperature, polarization, and tensor modes) with the routine for computing the likelihood supplied by the WMAP team. We also augment the WMAP7 data with the CMB data sets from BOOMERanG [124], QUAD [125], ACBAR [126], and BICEP [127]. For all these experiments we marginalize over a possible contamination from the Sunyaev-Zel'dovich component, rescaling the WMAP template at the corresponding experimental frequencies. We therefore consider two cases: we first analyze the WMAP data alone, referring to it as to the "WMAP7" case, and we then include the remaining CMB experiments ("CMB-ALL").

8.5 Results

Table 8.1 summarizes the main results of the analysis for different cosmological data sets, showing the constraints on n_s and r for the MH, LWB, and sudden reionization schemes. When the sudden reionization assumption is relaxed, the mean values of n_s and r tend to shift to higher values. The shift in n_s was already noted in the previous paper [119]. The importance of this shift is that in a general reionization scheme the H–Z spectrum is perfectly consistent. Notice, however, that the presence of tensors and/or a running spectral index in the analysis allows for a H–Z spectrum even in the sudden reionization scheme (at a confidence level (c.l.) corresponding to 2σ). Nevertheless, in the case of the MH reionization scenario, without running of the index, the best fit for the scalar spectral index is already higher than one at 68% c.l. In a general reionization scenario the allowed values of r also shift to higher values. When additional data from other CMB probes are added to the WMAP7 data, the constraints on n_s and r are shifted back toward lower values. In summary, in the

	WMAP7			CMB-ALL			Planck
	Sudden	MH	LWB	Sudden	MH	LWB	Sudden
			no running of scalar spectral index				
n_s (68% c.l.)	0.987 ± 0.020	1.001 ± 0.027	0.992 ± 0.021	0.974 ± 0.016	0.985 ± 0.020	0.977 ± 0.017	0.960 ± 0.004
n_s (95% c.l.)	$n_s \leq 1.031$	$n_s \leq 1.067$	$n_s \leq 1.039$	$n_s \leq 1.007$	$n_s \leq 1.026$	$n_s \leq 1.012$	$n_s \leq 0.968$
r (68% c.l.)	0.142 ± 0.116	0.141 ± 0.119	0.149 ± 0.115	0.095 ± 0.079	0.101 ± 0.085	0.103 ± 0.087	0.053 ± 0.022
r (95% c.l.)	$r \leq 0.373$	$r \leq 0.376$	$r \leq 0.371$	$r \leq 0.251$	$r \leq 0.266$	$r \leq 0.275$	$r \leq 0.093$
			running of scalar spectral index				
n_s (68% c.l.)	1.067 ± 0.062	1.080 ± 0.065	—	1.094 ± 0.052	1.106 ± 0.054	—	—
n_s (95% c.l.)	$n_s \leq 1.192$	$n_s \leq 1.207$	—	$n_s \leq 1.197$	$n_s \leq 1.222$	—	—
r (68% c.l.)	0.191 ± 0.154	0.200 ± 0.158	—	0.181 ± 0.141	0.185 ± 0.140	—	—
r (95% c.l.)	$r \leq 0.497$	$r \leq 0.515$	—	$r \leq 0.451$	$r \leq 0.445$	—	—
α_s (68% c.l.)	-0.040 ± 0.029	-0.036 ± 0.031	—	-0.056 ± 0.021	-0.058 ± 0.022	—	—

Table 8.1: Constraints for different data sets on n_s, r, and α_s in different reionization scenarios with and without the running of the scalar spectral index n_s.

MH reionization case ignoring running of the spectral index, using WMAP7 data the H–Z spectrum ($n_s = 1$) is very close to the best fit value, and inside the 68% c.l. for the case CMB-ALL.

The values for the tensor-to-scalar ratio r and the running of the spectral index α_s at 95% c.l. are slightly higher considering a general reionization scenario. However, their 68% c.l. constraints barely change when the reionization history is modified, as expected, due to the large uncertainties on r and α_s.

The shift induced on allowed values of inflationary parameters n_s and r by different assumptions for the reionization history is important for the subsequent constraints on inflationary models. To study this, we have reconstructed the relation between n_s and r in the different classes of models described in the previous section, and we have plotted these relations in the n_s-r plane, together with the cosmological constraints.

Figure 8.1 depicts the 68% and 95% c.l. allowed contours by the WMAP7 data and the CMB-ALL data sets without running of the scalar spectral index for different assumptions of the reionization history. The indicated contours denote the allowed regions when tensor modes are included in the analysis, and when the reionization is assumed to be sudden and when using the MH procedure (see the figure caption for details).

Figure 8.2 is the same as Fig. 8.1 but now allowing for a running of the scalar spectral index.

Following Ref. [120] we can easily develop the different expressions concerning the n_s-r parameter space. For instance, for large-field models, with a polynomial potential $V \propto \phi^p$, the relation among these parameters is

$$n_s = 1 - \frac{r}{8}\left(1 + \frac{2}{p}\right) \ . \tag{8.16}$$

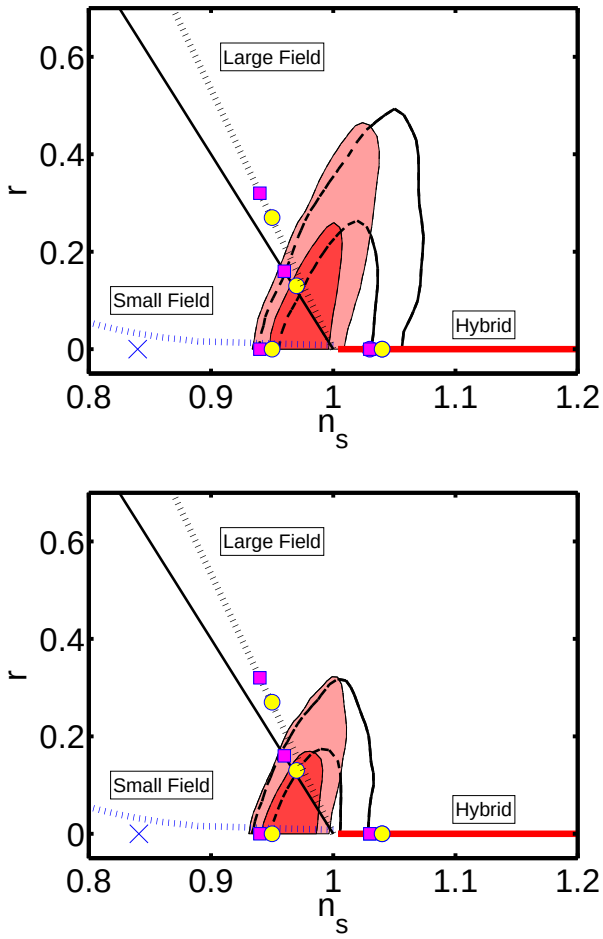

Figure 8.1: Two-dimensional contour plots at the 68% and 95% confidence levels without running of the scalar spectral index for the WMAP7 data (upper figure) and the CMB-ALL data set (lower figure). Shaded contours correspond to the sudden reionization approximation, while open contours model reionization as MH. The dark solid (dashed) lines refer to large-field models with $p = 2$ ($p = 4$). The lighter cross (dashed) curves depict small-field models with $p = 2$ ($p = 4$). The solid horizontal line that basically coincides with the x axis depicts hybrid models with $p = 2$ (the $p = 4$ case basically overlaps the $p = 2$ case). The filled circles (squares) denote the points in the parameter space for which the number of e-folds N is equal to 60 (50).

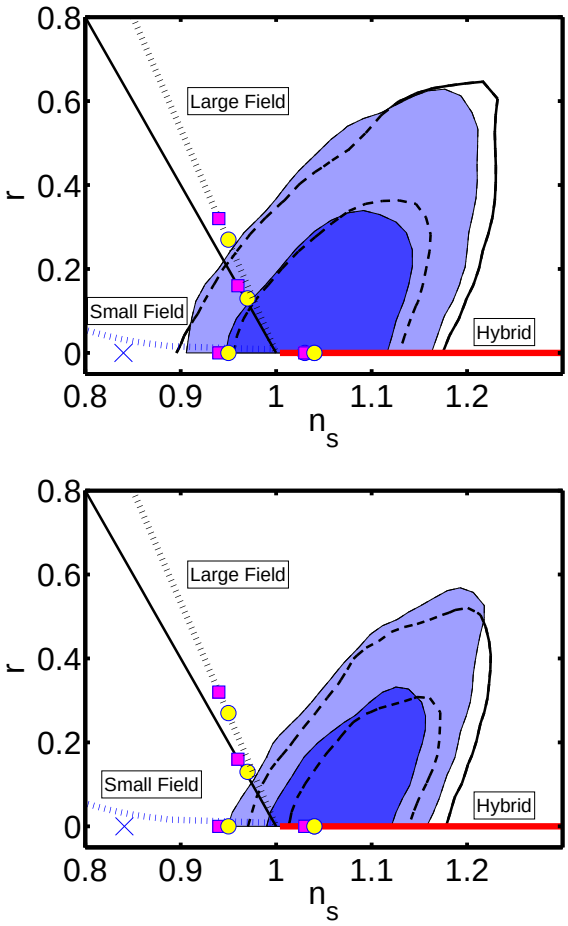

Figure 8.2: Two-dimensional contour plots at the 68% and 95% confidence levels with running of the scalar spectral index for the WMAP7 data (left figure) and the CMB-ALL data set (lower figure). The key for the figures is the same as in Fig. 8.1.

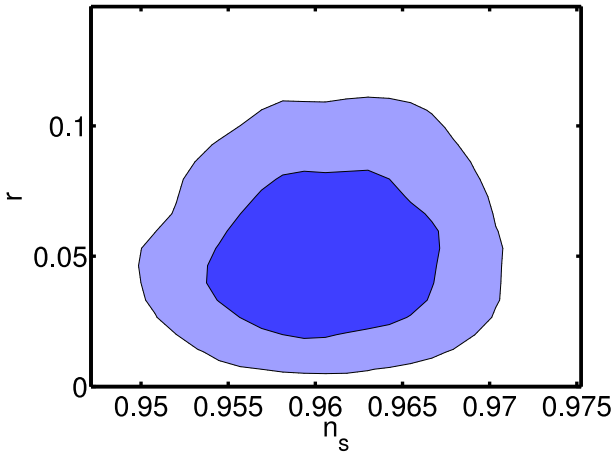

Figure 8.3: The 68% and 95% c.l. constraints forecast on the n_s vs. r plane from Planck mock data for $n_s = 0.96$ and $r = 0.05$ and sudden reionization (dark contour), and (wrongly) fitted assuming MH reionization (light contour).

The dark lines in Figs. 8.1 and 8.2 refer to this relation for quadratic ($p = 2$) and quartic ($p = 4$) potentials. It is straightforward to relate r with N (the number of e-foldings before the end of inflation):

$$r = 4p/N \ , \tag{8.17}$$

which allows us to draw points with $N = 50$ (squares) and $N = 60$ (circles) in Figs. 8.1 and 8.2.

Similarly, we can relate n_s to r, and both of them in terms of N for both small-field and hybrid models. For small-field models, the generic potential we are using is of the form $V(\phi) = \Lambda^4[1-(\phi/\mu)^p]$. Typically in these models the slow-roll parameter ϵ_V (and hence, r) is close to zero. The spectral index can be written as

$$n_s \simeq 1 - \frac{p(p-1)}{4\pi}\frac{M_{Pl}^2}{\mu^p}\left[\frac{\pi\mu^{2p}}{M_{Pl}^2 p^2}\, r\right]^{(p-2)/(2p-2)} \ . \tag{8.18}$$

It is straightforward to see that for $p = 2$

$$n_s \simeq 1 - \left(\frac{1}{2\pi}\right)\left(\frac{M_{Pl}}{\mu}\right)^2 \ , \tag{8.19}$$

while for $p = 4$ we have

$$n_s \simeq 1 - \frac{3}{\pi}\left(\frac{\pi M_{Pl}^4 r}{16\mu^4}\right)^{1/3} \approx 1 - \frac{3}{N} \ . \tag{8.20}$$

Figs. 8.1 and 8.2 also contain the small-field model case, depicted by cross for $p = 2$ and by the indicated dashed curve for $p = 4$ (assuming $\mu \approx M_{Pl}$).

For hybrid models, the potential chosen is $V(\phi) = \Lambda^4[1-\alpha(m_{Pl}/\phi)^p]$, based on potentials generated in dynamical SUSY breaking models [51]. As in small-field models, the tensor-to-scalar ratio r is negligible. The expression for n_s is given by

$$n_s \approx 1 + 2\frac{(p+1)}{(p+2)(N_{\rm tot} - N)} \ , \tag{8.21}$$

where $N_{\rm tot}$ is the *total* number of e-foldings (chosen to be 100 in this example). Notice that Eq. (8.21) indicates that the power spectrum in these sort of models is blue ($n_s > 1$). Indeed, in the sudden reionization scenario with negligible running of the spectral index these hybrid models are highly disfavored; in more general reionization schemes such models are allowed by WMAP7 data; see Fig. 8.1. When more CMB data sets are included in the analysis, hybrid Inflation models with a blue tilt are again disfavored at 95% c.l., even in the more general reionization scenarios considered here; see the CMB-ALL part of Fig. 8.1. When a running scalar spectral index is allowed, hybrid models are perfectly compatible with data, regardless of the assumptions about the reionization processes; see Fig. 8.2.

The LWB reionization scheme leads to very similar constraints to those of MH parametrization on the $n_s - r$ plane (albeit slightly closer to the sudden reionization case). Indeed, n_s is constrained to be red at the 68% c.l. in the CMB-ALL case, but the H–Z model is still consistent with data within two standard deviations.

We also forecast future constraints from the Planck experiment with the specifications of Ref. [128], assuming that $n_s = 0.96$ and $r = 0.05$ and sudden reionization. If the data is (wrongly) fitted assuming a more general reionization scenario (MH reionization, for instance), the constraints that one would obtain on the $n_s - r$ plane are shown in Fig. 8.3. Notice that Planck will be able to tell $n_s \neq 1$ at a very high confidence level even if the precise details of the reionization processes are unknown. Planck data will also be sensitive to the tensor-to-scalar ratio at the 95% c.l. for $r \geq 0.05$.

8.6 Conclusions

Details of the reionization processes in the late universe are not very well known. In the absence of a precise, full-redshift evolution description of the ionization fraction during the reionization period, a simple parametrization with a single parameter z_r has become the standard reionization scheme in numerical analyses. More general reionization schemes have been shown to allow values of the scalar spectral index consistent with a scale-invariant power spectrum. In this paper we deduce information about tensor modes, and explore how the Inflation constraints are modified when the standard reionization assumption is relaxed. The tensor-to-scalar ratio bounds are largely unmodified under more general reionization scenarios. Therefore, present (future) primordial gravitational wave searches are (will be) unaffected by the precise details of reionization processes. In the absence of a running spectral index, hybrid models, ruled out in the standard reionization scheme, are still allowed

at the 95% c.l. by WMAP7 data. The constraints on other inflationary models, such as large-field or small-field models, do not change. Future Planck data will be able to measure the scalar spectral index n_s with unprecedented precision and be sensitive to tensor modes if $r > 0.05$ at the 95% c.l.

Chapter 9

Leptogenesis with small violation of $B - L$

We analyze leptogenesis in the context of seesaw models with almost conserved lepton number, focusing on the L-conserving contribution to the flavoured CP asymmetries. We find that, contrary to previous claims, successful leptogenesis is feasible for masses of the lightest heavy neutrino as low as $M_1 \sim 10^6$ GeV, without relying on the resonant enhancement of the CP asymmetry for strongly degenerate heavy neutrinos. This lower limit renders thermal leptogenesis compatible with the gravitino bound in supersymmetric scenarios.

9.1 Introduction

Two of the main evidences of physics beyond the Standard Model (SM), namely the observed (tiny) neutrino masses and the baryon asymmetry of the universe (BAU), are naturally explained in the context of the seesaw mechanism [87, 129, 130, 131]. In type I seesaw models, the SM is extended with at least two singlet Majorana neutrinos which can produce the observed BAU via leptogenesis [85, 86]: a lepton asymmetry is dynamically generated in the out of equilibrium decay of the heavy Majorana neutrinos, and then partially converted into a baryon asymmetry due to $(B + L)$-violating non-perturbative sphaleron interactions [82].

For a very hierarchical spectrum of heavy singlet neutrinos $M_1 \ll M_2 \ll M_3$ [1], the L-violating CP asymmetry generated in the decay of the lightest singlet has an upper bound proportional to M_1, the so-called Davidson-Ibarra (DI) bound [132]. This implies a lower bound $\sim 10^9$ GeV for the mass of the sterile neutrinos in order for N_1-dominated leptogenesis to be successful. Careful numerical studies show that the DI bound can be evaded for moderate hierarchies, e.g. the lower bound on M_1 is relaxed by more than one order of

[1] It seems quite natural to extend the SM with 3 heavy neutrinos, as 3 are the number of families in the SM both in the quark and in the lepton sectors.

magnitude with respect to the hierarchical limit one for $M_3/M_2 \sim M_2/M_1 \sim 10$ [133]. However to reach these low values of M_1 some unlikely cancellations are needed, which are not motivated by any underlying symmetry. Flavour effects [134, 135, 136, 137, 138, 139] do not substantially change this result. The authors of [140] make an analysis of the parameter space for successful leptogenesis relaxing also the condition of hierarchical neutrinos and including the L-conserving part of the flavoured CP asymmetries, finding a lower bound $M_1 \gtrsim 10^8$ GeV.

Such lower bound on M_1 in turn yields a lower bound for the reheating temperature, T_{reh}, of the same order, since to thermally produce the neutrinos $M_1 \lesssim 5\, T_{reh}$ [141, 142, 143]. On the other hand, in supersymmetric scenarios gravitinos are copiously produced in the high temperature plasma, and their late decay can jeopardize successful nucleosynthesis (BBN), leading to an upper bound on T_{reh}, which depends on the gravitino mass [35, 144]. If the gravitino is unstable, for gravitino masses, $m_{3/2}$, in the natural range from 100 GeV to 1 TeV, and within the minimal supergravity framework, T_{reh} should be smaller than $10^5 - 10^7$ GeV, while for $m_{3/2} \gtrsim 10$ TeV, T_{reh} can be of order $10^9 - 10^{10}$ GeV [145]. As a consequence, in supersymmetric thermal leptogenesis there is some conflict between the gravitino bound on the reheat temperature and the thermal production of heavy neutrinos. There are several possible ways out of this conflict: for instance, if the gravitino is stable, the nucleosynthesis bound depends on the next-to-lightest supersymmetric particle, but $T_{reh} \gtrsim 10^9$ GeV can be obtained for $m_{3/2} \gtrsim 10$ GeV [145]. Also, one can avoid the DI bound resorting to resonant leptogenesis, i.e., a resonant enhancement of the CP asymmetry which occurs when there are at least two strongly degenerated heavy neutrinos, such that $M_2 - M_1 \sim \Gamma_N$, being Γ_N their decay width [146, 147]. In this scenario, leptogenesis is feasible at much lower temperatures, $T \sim \mathcal{O}(1\text{ TeV})$ [148, 149, 150], solving the gravitino problem.

Although such quasi-degeneracy of the heavy neutrinos might seem unnatural, there are well motivated seesaw models which yield a heavy neutrino quasi-degenerate spectrum, namely those with an approximately conserved $B-L$ [151, 152]. In this scenario, the tiny neutrino masses are proportional to small lepton number-breaking parameters, which are technically natural since a larger symmetry is realized when they vanish [153]. Moreover, the heavy neutrinos can be much lighter than in the generic seesaw, within the energy reach of LHC, and there can be a large active-sterile neutrino mixing. Also, lepton flavour violation rare decays as well as non-unitarity of the leptonic mixing matrix are present even in the limit of conserved $B-L$, and therefore unsuppressed by the light neutrino masses [152, 154, 155]. As a consequence, much attention has been devoted recently to this class of low scale seesaw models, since they have a rich phenomenology both at LHC [156, 157, 158] and at low energy charged lepton rare decay experiments, such as $\mu \to e\gamma$, and also lead to successful resonant leptogenesis [159, 160].

In order to see more clearly the structure of seesaw models with small violation of $B-L$, it is useful to expand the low energy effective Lagrangian as

$$\mathcal{L} = \mathcal{L}_{\rm SM} + \frac{c^{d=5}}{\Lambda_{LN}}\mathcal{O}^{d=5} + \sum_i \frac{c_i^{d=6}}{\Lambda_{FL}^2}\mathcal{O}_i^{d=6} + \dots \,, \tag{9.1}$$

where the dimensionless couplings $c^{d=5}, c_i^{d=6}$ are assumed to be of $\mathcal{O}(1)$.

The only operator of $d = 5$ is Weinberg's operator, responsible for neutrino masses, which is suppressed by the lepton number violating scale Λ_{LN}, while flavour changing but lepton number conserving $d = 6$ operators $\mathcal{O}_i^{d=6}$ are suppressed by a different scale Λ_{FL}. In models with approximately conserved lepton number, there is a separation of scales: $\Lambda_{FL} \sim \mathcal{O}(\text{TeV})$ can be related to the heavy neutrinos mass scale, but $\Lambda_{LN} \gg \Lambda_{FL}$, since light neutrino masses only appear when small L-violating perturbations in the Yukawa couplings and/or the singlet neutrino mass matrix are introduced; in this scenario, Λ_{LN} does not correspond to any particle mass.

It has been noticed that even if the heavy neutrino that generates the BAU is not quasi-Dirac, or the mass splitting is outside the resonant regime, in seesaw models with almost conserved L the scale of leptogenesis can be lower than in the standard seesaw [140, 161], provided flavour effects are at work. This is so because in these models leptogenesis can be driven by the $d = 6$ operators, that contribute only to the L-conserving part of the flavoured CP-asymmetries which escape the DI bound, even if the heavy neutrinos are hierarchical, because these operators are not linked to neutrino masses. The drawback is that the same $d = 6$ operators induce large lepton flavour violating (but lepton number conserving) washout processes, which tend to equilibrate the flavoured asymmetries diminishing the total lepton asymmetry [162, 163], and were not taken into account in [140].

In this work we reanalyze the possibility of having successful leptogenesis driven by the purely flavoured L-conserving contribution to the CP asymmetries, in the context of seesaw models with small violation of $B-L$. In the numerical analysis of [140] such contribution was included, however they did not consider in detail models with almost conserved $B-L$, which can lead to larger CP asymmetries. A study of the lower bound on M_1 for approximately $B - L$-conserving models was carried out in [161], but their cross sections are different from ours and the analysis of the parameter space seems to be non-exhaustive. We have computed the cross sections for the crucial lepton flavour changing processes which lead to flavour equilibration, and we have found important differences with respect to previous results [149]. We have also taken into account decays and inverse decays of the next-to-lightest neutrinos, neglected in [161], and thoroughly scanned the parameter space to find the lowest M_1 able to generate the BAU within this framework. Moreover, we have included a detailed discussion about leptogenesis in models with almost conserved $B - L$, which depends on the heavy neutrino spectrum.

The Chapter is divided as follows. In Section 9.2 we discuss the main features of leptogenesis within the framework of seesaw models with approximately conserved $B - L$. In Section 9.3 we write the set of Boltzmann equations (BE) relevant for leptogenesis in this scenario and compute the cross sections for the lepton flavour violating (but total lepton number conserving) washout processes, which play a crucial role in models with null (or negligible) total CP asymmetry. In Section 9.4 we perform a detailed analysis of the parameter space which leads to successful leptogenesis with only L-conserving CP asymmetries, and we conclude in Section 9.5.

9.2 Leptogenesis in models with small violation of $B-L$

In this section we want to determine what can be distinct, regarding leptogenesis, among different models with small violation of $B-L$. Let us call N_1 the Standard Model (SM) fermion singlet that is mainly responsible for the generation of the lepton asymmetry. Additionally we call N_2 the SM fermion singlet that makes the most important virtual contribution to the CP asymmetry in the N_1 decays. They have Yukawa interactions with the lepton doublets of the SM ℓ_α ($\alpha = e, \mu, \tau$) described by the Lagrangian

$$\mathcal{L}_Y = -\lambda_{\alpha i}\, \widetilde{h}^\dagger\, \overline{P_R N_i}\ell_\alpha - \lambda^*_{\alpha i}\overline{\ell}_\alpha P_R N_i \widetilde{h}\ . \tag{9.2}$$

If $B-L$ is only slightly violated, then for each N_i the conditions (i) or (ii) described below must be satisfied:

(i) N_i is a Majorana neutrino with two degrees of freedom, whose Yukawa interactions violate lepton number and therefore the couplings $\lambda_{\alpha i}$ must be small. This is analogous to the standard seesaw, so the N_i contribution to the $d=5$ Weinberg operator is given by

$$(c_M^{d=5})_{\alpha\beta} = \lambda_{\alpha i}\lambda_{\beta i}\ . \tag{9.3}$$

(ii) The N_i is a Dirac or quasi Dirac neutrino with four degrees of freedom; this means that there are two Majorana neutrinos N_{ih} and N_{il} with masses $M_i+\mu_i$ and $M_i-\mu_i$ respectively. The parameter $\mu_i \ll M_i$ measures the amount of $B-L$ violation, so that if $B-L$ is conserved, $\mu_i = 0$ and $N_i = (N_{ih}+iN_{il})/\sqrt{2}$ is a Dirac fermion. The Yukawa interactions can be expressed as

$$\mathcal{L}_{Y_{Ni}} = -\lambda_{\alpha i}\, \widetilde{h}^\dagger\, \overline{P_R \frac{N_{ih}+iN_{il}}{\sqrt{2}}}\ell_\alpha - \lambda'_{\alpha i}\, \widetilde{h}^\dagger\, \overline{P_R \frac{N_{ih}-iN_{il}}{\sqrt{2}}}\ell_\alpha + h.c., \tag{9.4}$$

where $\lambda'_{\alpha i} \ll 1$. The terms proportional to $\lambda'_{\alpha i}$ induce lepton number violation even when $\mu_i \to 0$ and hence they are similar in nature to the ones described in (i). Neglecting these terms, the Yukawa couplings of N_{ih} and N_{il} are equal to $\lambda_{\alpha\, ih} = \frac{\lambda_{\alpha i}}{\sqrt{2}}$ and $\lambda_{\alpha\, il} = i\frac{\lambda_{\alpha i}}{\sqrt{2}}$, respectively. These $\lambda_{\alpha i}$ can be large, because they do not vanish in the $B-L$ conserved limit: in the absence of μ_i and $\lambda'_{\alpha i}$, a perturbatively conserved lepton number can be defined, by assigning $L_N = 1$ to N_i, and $L_{\ell_\alpha} = 1$ to the SM leptons.

At leading order in the small $B-L$ breaking parameters $(\lambda'_{\alpha i}, \mu_i/M_i)$, the contribution of a quasi Dirac heavy neutrino to the Weinberg operator is

$$\frac{(c_{QD}^{d=5})_{\alpha\beta}}{\Lambda_{LN}} = (\lambda'_{\alpha i} - \frac{\mu_i}{M_i}\lambda_{\alpha i})\frac{1}{M_i}\lambda_{\beta i} + \lambda_{\alpha i}\frac{1}{M_i}(\lambda'_{\beta i} - \frac{\mu_i}{M_i}\lambda_{\beta i}) + \ldots \tag{9.5}$$

so the scale Λ_{LN} in this case is not identified with the neutrino mass M_i but with $M_i^2/\mu_i, M_i/\lambda'_{\alpha i} \gg M_i$. As a result, one can reproduce the tiny light neutrino masses

with large Yukawa couplings and heavy neutrino masses M_i as low as the TeV scale. Moreover, the admixture among singlet and doublet $SU(2)$ neutral leptons (and the corresponding violation of unitarity in the light neutrino sector) is of order $\lambda_{\alpha i} v/M_i$ and can be large.

In this work we will consider the cases

- (iia) $\mu_i \ll \Gamma_{N_{ih}}, \Gamma_{N_{il}}$ (Dirac limit), and
- (iib) $\Gamma_{N_{ih}}, \Gamma_{N_{il}} \ll \mu_i \ll M_i$ (Majorana limit),

where the decay widths Γ_s are given by

$$\Gamma_{N_{ih}} = \frac{M_i + \mu_i}{8\pi} \frac{\left(\lambda^\dagger \lambda\right)_{ii}}{2} \approx \frac{M_i - \mu_i}{8\pi} \frac{\left(\lambda^\dagger \lambda\right)_{ii}}{2} = \Gamma_{N_{il}} \,. \tag{9.6}$$

Instead we leave the study of $\mu_i \sim \Gamma_{N_{ih,il}}$ for future research because it is not clear that this case can be described with the simple BE used here [164, 165].

Then, the study of leptogenesis for a large class of models with small violation of $B-L$ can be covered by considering the different combinations of options for both N_1 and N_2. Next we comment on some key points for the different possibilities, while the complete quantitative analysis is made in Sec. 9.4. We assume that N_1 is lighter than N_2, leaving some remarks of the opposite case $M_2 < M_1$ for Sec. 9.4.

I. N_1 and N_2 satisfy (i): This case is not very interesting since the CP asymmetries $\epsilon_{\alpha 1}$, being proportional to the square of the Yukawa couplings of N_2, are very small, so it is not different from the standard seesaw.

II. N_1 satisfies (i) and N_2 (ii): The L-violating part of the CP asymmetry, $\epsilon^{\not L}_{\alpha 1}$, is suppressed by μ_2 while the L-conserving part, $\epsilon^{L}_{\alpha 1}$, is not. To see this, let us write $\epsilon_{\alpha 1} = \epsilon^{\not L}_{\alpha 1} + \epsilon^{L}_{\alpha 1}$ as [89, 166]

$$\epsilon_{\alpha 1} = \sum_{j=2h,2l} f(a_j) \mathrm{Im}\left[\lambda^*_{\alpha j} \lambda_{\alpha 1} (\lambda^\dagger \lambda)_{j1}\right] + \sum_{j=2h,2l} g(a_j) \mathrm{Im}\left[\lambda^*_{\alpha j} \lambda_{\alpha 1} (\lambda^\dagger \lambda)_{1j}\right] \,, \tag{9.7}$$

where $f(a_j)$ and $g(a_j)$ are functions of $a_j \equiv M_j^2/M_1^2$ and contain the factor $1/(\lambda^\dagger\lambda)_{11}$. The terms proportional to $f(a_j)$ and $g(a_j)$ come from the L-violating and L-conserving contributions, respectively. To lowest order in μ_2, $f(a_{2h}) = f(a_{2l})$ and $g(a_{2h}) = g(a_{2l})$. Taking into account the alignment between the Yukawa couplings of N_{2l} and N_{2h}, $\lambda_{\alpha\, 2l} = a \lambda_{\alpha\, 2h}$ with $a = i$, it is clear that

$$\begin{aligned} \epsilon_{\alpha 1} \xrightarrow[\mu_2 \to 0]{} & f(a_{2h}) \mathrm{Im}\left[\lambda^*_{\alpha\, 2h} \lambda_{\alpha 1} (\lambda^\dagger \lambda)_{2h\, 1}\right] (1 + a^{*2}) + \\ & g(a_{2h}) \mathrm{Im}\left[\lambda^*_{\alpha\, 2h} \lambda_{\alpha 1} (\lambda^\dagger \lambda)_{1\, 2h}\right] (1 + |a|^2) \\ & = 0 + 2 g(a_{2h}) \mathrm{Im}\left[\lambda^*_{\alpha\, 2h} \lambda_{\alpha 1} (\lambda^\dagger \lambda)_{1\, 2h}\right] \,. \end{aligned} \tag{9.8}$$

Hence we see that the contributions from N_{2h} and N_{2l} add up in the L-conserving part and cancel in the L-violating one.

While the total CP asymmetry $\epsilon_1 \equiv \sum_\alpha \epsilon_{\alpha 1}$ is proportional to μ_2 because $\sum_\alpha \epsilon^L_{\alpha 1} = 0$, the amount of matter-antimatter asymmetry produced during leptogenesis generally is not suppressed by μ_2 due to flavour effects (it is possible to have successful leptogenesis even with $\epsilon_1 = 0$ [137]). Nevertheless, this asymmetry does vanishes or becomes proportional to μ_2 when the L-violating parameter $(\lambda^\dagger\lambda)_{11} \to 0$, independently of whether the density of N_1 at the onset of leptogenesis is null or thermal. This is because for an initial null density of heavy neutrinos and small values of $(\lambda^\dagger\lambda)_{11}$ the final baryon asymmetry is proportional to $(\lambda^\dagger\lambda)^2_{11}$ [143], while for an initial thermal N_1 density the washouts become negligible and so do the flavour effects, in which case the total asymmetry generated is proportional to $\epsilon_1 \propto \mu_2$.

III. N_1 satisfies (ii) and N_2 (i): Since the Yukawa couplings of N_2 are small, the virtual contribution of N_2 to the CP asymmetries $\epsilon_{\alpha\, 1l}$ and $\epsilon_{\alpha\, 1h}$ in the decays of N_{1l} and N_{1h}, respectively, is small. More interesting is the virtual contribution of N_{1l} to $\epsilon_{\alpha\, 1h}$ and of N_{1h} to $\epsilon_{\alpha\, 1l}$, due to the resonant enhancement of the CP asymmetry for degenerate neutrinos. However these contributions are suppressed by $\frac{\lambda'_{\alpha 1}}{\sqrt{(\lambda^\dagger\lambda)_{11}}}$ because of the alignment of the Yukawa couplings of N_{1l} and N_{1h} for $\lambda'_{\alpha 1} = 0$, therefore the CP asymmetry cannot reach the maximum value $1/2$ of more generic resonant leptogenesis models. A detailed study of this case was made in [159], in the limit $\mu_1 \gg \Gamma_{N_{1l},N_{1h}}$: they found that it is possible to lower the scale of leptogenesis provided that the parameter which controls lepton number violation in the Yukawa couplings $\epsilon = \lambda'/\lambda$ is much larger than the one describing the mass splitting between the quasi-Dirac heavy neutrinos, $\epsilon_M = \Delta M/M$. For instance, in order to obtain successful leptogenesis with $M = 10^6$ GeV (1 TeV), one needs $\epsilon \sim 10^{-3}$ and $\epsilon_M \sim 10^{-8}$ (10^{-11}). The case $\mu_1 \lesssim \Gamma_{N_{1l},N_{1h}}$ has been considered in [167], however it has been shown that in this maximal resonant regime the Boltzmann picture breaks down and the Schwinger-Keldysh/Kadanoff-Baym formalism is required [164].

IV. N_1 and N_2 satisfy (ii): Besides the resonant contributions which are the same as in III, now also the virtual contribution of N_2 to the CP asymmetries $\epsilon_{\alpha\, 1l}$ and $\epsilon_{\alpha\, 1h}$ can be large, so we focus on these terms. Neglecting the $\lambda'_{\alpha i} \ll \lambda_{\alpha i}$ couplings, the CP asymmetries in the decays of N_{1l} and N_{1h} become equal. Here it is very important to distinguish between the cases $\mu_1 \gg \Gamma_{N_{1l},N_{1h}}$ and $\mu_1 \ll \Gamma_{N_{1l},N_{1h}}$. In the first one, N_{1l} and N_{1h} behave as two independent Majorana neutrinos regarding the generation of the lepton asymmetry, which can hence be roughly double with respect to II. However in the second case N_1 is (or effectively behaves as) a Dirac neutrino, i.e. lepton number is conserved in its decay, and therefore the only possibilities to end up with a non zero baryon asymmetry is to have important washouts from the two Majorana components of N_2 (if $\mu_2 \gg \Gamma_{N_{2l},N_{2h}}$) or let the sphalerons freeze out during leptogenesis [168].

Summarizing, in models with small violation of $B-L$ the CP asymmetries in the decay of N_1 can be enhanced in cases II, III and IV. Since the resonant contribution to the L-violating CP asymmetry has been widely studied, we develop in Sec. 9.4 a quantitative analysis which covers all the non-resonant interesting cases, i.e., II and IV with $\mu_1 \gg \Gamma_{N_{1l},N_{1h}}$. With respect to N_2, we consider two possibilities, $\mu_2 \gg \Gamma_{N_{2l},N_{2h}}$ and $\mu_2 \ll \Gamma_{N_{2l},N_{2h}}$ (see [168] for leptogenesis with both N_1 and N_2 satisfying $\mu_i \ll \Gamma_{N_{il},N_{ih}}$).

9.3 Boltzmann equations

Motivated by the above discussion we consider a scenario for leptogenesis involving three fermion singlets N_1, N_{2l}, N_{2h} (each of them having two degrees of freedom), with respective masses $M_1, M_2-\mu_2, M_2+\mu_2$ and Yukawa couplings given by the Lagrangian

$$\mathcal{L}_Y = \lambda_{\alpha 1}\,\widetilde{h}^\dagger\,\overline{P_R N_1}\ell_\alpha - \lambda_{\alpha 2}\,\widetilde{h}^\dagger\,\overline{P_R\frac{N_{2h}+iN_{2l}}{\sqrt{2}}}\ell_\alpha + h.c.\,. \tag{9.9}$$

Recall that the parameters $\lambda_{\alpha 1}$ violate lepton number and hence $\lambda_{\alpha 1} \ll \lambda_{\alpha 2}$. In turn this implies that the CP asymmetry in N_1 decays is the dominant one. As a first approximation, in the Eq. (9.9) we have neglected the L-violating couplings $\lambda'_{\alpha 2} \ll \lambda_{\alpha 2}$, because we expect that their contribution to the CP asymmetries and washouts is negligible. We have checked indeed that this is the case in the parameter space region relevant for leptogenesis that can also accommodate the observed light neutrino masses (see Sec. 9.4). As we will explain below, it is convenient to take $M_1 < M_2$ in order to obtain the lowest energy scale for leptogenesis within this framework.

The amount of leptons and antileptons can be described by density matrices in flavour space. The evolution equations of these density matrices take the simplest form in the basis that diagonalize them, which are determined by the fastest interactions in flavour space (if there is a hierarchy among the different interactions). Let us suppose that the fastest interactions during N_1-leptogenesis are the N_2-Yukawa interactions [2]. In this case the BE would be diagonal in a basis $(\ell_2, \ell_{2\perp}, \ell'_{2\perp})$, with $\ell_{2\perp}$ and $\ell'_{2\perp}$ two orthogonal lepton flavour states perpendicular to the N_2-decay eigenstate ℓ_2. But $\epsilon(N_1 \to \ell_{2\perp}h, \ell'_{2\perp}h) = 0$, and since the total CP asymmetry is null, then also $\epsilon(N_1 \to \ell_2 h) = 0$, with the result that no lepton asymmetry would be produced. Moreover, no asymmetry is generated when the N_1-Yukawa interactions are the fastest ones, because in this case the BE would be diagonal in the basis $(\ell_1, \ell_{1\perp}, \ell'_{1\perp})$, and since the CP asymmetry in the N_1-decay eigenstate $\epsilon(N_1 \to \ell_1 h)$ coincides with the total CP asymmetry, it also vanishes. So we demand that the couplings of N_1 and N_2 be small enough, such that the Yukawa interactions of the τ are the dominant ones. This implies that the BE are diagonal in the orthogonal basis $(\ell_\tau, \ell_{\tau\perp}, \ell'_{\tau\perp})$, with $\ell_{\tau\perp}$ and

[2] When the effects of N_{2l} and N_{2h} simply add up we will refer to these states generically as N_2. In the models considered here the only situation which requires a differentiated treatment of the degrees of freedom associated to N_2 is when $\mu_2 \ll \Gamma_{N_{2l,2h}}$, because a density asymmetry can develop between the states produced by ℓh and $\overline{\ell h}$ (see below).

$\ell'_{\tau\perp}$ being determined by the fastest interaction acting in the plane perpendicular to ℓ_τ. For simplicity we take the N_1 and N_2 decay eigenstates to be perpendicular to ℓ_e, in which case the aforementioned basis is $\ell_\tau, \ell_\mu, \ell_e$. Since no asymmetry is generated in the ℓ_e flavour, two BE will be enough to determine the evolution of the lepton asymmetry and consequently the flavour indices α and β run over the species μ and τ. Later we will comment on the more general case with three non null flavour asymmetries.

Besides the charged leptons Yukawa interactions, the most relevant processes are the decays and inverse decays of the different heavy neutrinos, and the L-conserving but L_α-violating scatterings $\gamma^{\ell_\beta h\,'}_{\ell_\alpha h}$, $\gamma^{\ell_\beta \bar{h}}_{\ell_\alpha \bar{h}}$, and $\gamma^{h\bar{h}}_{\ell_\alpha \bar{\ell}_\beta}$, hereafter called generically flavour changing interactions (FCI). We will not consider finite temperature corrections to the particle masses and couplings [142], moreover we also neglect spectator processes and the asymmetry developed among the degrees of freedom of the Higgs [169, 170], as well as $\Delta L = 1$ scatterings [171, 172] [3]. The relevant set of BE for the case $\mu_2 \gg \Gamma_{N_{2l,2h}}$ is

$$\frac{\mathrm{d}Y_{N_1}}{\mathrm{d}z} = \frac{-1}{sHz}\left(\frac{Y_{N_1}}{Y^{eq}_{N_1}} - 1\right)\gamma_{D_1}\,, \tag{9.10}$$

$$\frac{\mathrm{d}Y_{\Delta_\alpha}}{\mathrm{d}z} = \frac{-1}{sHz}\left\{\left(\frac{Y_{N_1}}{Y^{eq}_{N_1}} - 1\right)\epsilon_{\alpha 1}\,\gamma_{D_1} - \sum_i \gamma^{N_i}_{\ell_\alpha h} y_{\ell_\alpha} - \sum_{\beta\neq\alpha}\left(\gamma^{\ell_\beta h\,'}_{\ell_\alpha h} + \gamma^{\ell_\beta \bar{h}}_{\ell_\alpha \bar{h}} + \gamma^{h\bar{h}}_{\ell_\alpha \bar{\ell}_\beta}\right)\left[y_{\ell_\alpha} - y_{\ell_\beta}\right]\right\}\,, \tag{9.11}$$

where $Y_X \equiv n_X/s$ is the number density of a single degree of freedom of the particle species X normalized to the entropy density, $y_X \equiv (Y_X - Y_{\bar{X}})/Y^{eq}_X$ (to be used below) is the asymmetry density normalized to the equilibrium density Y^{eq}_X, and $Y_{\Delta_\alpha} \equiv Y_B/3 - Y_{L_\alpha}$, with Y_B the baryon asymmetry and Y_{L_α} the lepton asymmetry in the flavour α. Since we are neglecting spectator processes, the asymmetry in the lepton doublets ℓ_α can be expressed in terms of Y_{Δ_α} using the simple relation $Y_{\Delta_\alpha} = -Y_{L_\alpha} = -2y_{\ell_\alpha}Y^{eq}_{\ell_\alpha}$ [170]. We have also introduced the notation $\gamma^{a,b,\ldots}_{c,d,\ldots} \equiv \gamma(a,b,\ldots \to c,d,\ldots)$ for the reaction density of the process $a,b,\ldots \to c,d,\ldots$, the prime in $\gamma^{\ell_\beta h\,'}_{\ell_\alpha h}$ indicating that the on-shell contribution has to be subtracted since it has already been considered in the decays and inverse decays of the heavy neutrinos, and $\gamma_{D_i} \equiv \sum_\alpha \gamma^{N_i}_{\ell_\alpha h} + \gamma^{N_i}_{\bar{\ell}_\alpha \bar{h}}$. Finally notice that the lepton asymmetry generated by N_2 decays has not been taken into account, given that $\epsilon_{\alpha 2} \ll \epsilon_{\alpha 1}$.

Instead, if $\mu_2 \ll \Gamma_{N_{2l,2h}}$ then N_{2l} and N_{2h} combine to form a Dirac neutrino $N_2 \equiv (N_{2h} + iN_{2l})/\sqrt{2}$, and therefore there is an asymmetry generated among the degrees of freedom of N_2 which has to be taken into account [168]. An appropriate set of BE for this

[3] We have checked that the inclusion of spectator processes and $\Delta L = 1$ scatterings modifies the results by at most a few tens of percent.

case is

$$\frac{\mathrm{d}Y_{N_1}}{\mathrm{d}z} = \frac{-1}{sHz}\left(\frac{Y_{N_1}}{Y_{N_1}^{eq}}-1\right)\gamma_{D_1}\,, \tag{9.12}$$

$$\frac{\mathrm{d}Y_{N_2-\bar{N}_2}}{\mathrm{d}z} = \frac{-1}{sHz}\sum_{\alpha}\gamma_{\ell_\alpha h}^{N_2}\left[y_{N_2}-y_{\ell_\alpha}\right]\,, \tag{9.13}$$

$$\begin{aligned}\frac{\mathrm{d}Y_{\Delta_\alpha}}{\mathrm{d}z} = \frac{-1}{sHz}\Bigg\{&\left(\frac{Y_{N_1}}{Y_{N_1}^{eq}}-1\right)\epsilon_{\alpha 1}\,\gamma_{D_1}-\gamma_{\ell_\alpha h}^{N_1}y_{\ell_\alpha}+\gamma_{\ell_\alpha h}^{N_2}\left[y_{N_2}-y_{\ell_\alpha}\right]\\ &-\sum_{\beta\neq\alpha}\left(\gamma_{\ell_\alpha h}^{\ell_\beta h\,\prime}+\gamma_{\ell_\alpha\bar{h}}^{\ell_\beta\bar{h}}+\gamma_{\ell_\alpha\bar{\ell}_\beta}^{h\bar{h}}\right)\left[y_{\ell_\alpha}-y_{\ell_\beta}\right]\Bigg\}\,.\end{aligned} \tag{9.14}$$

The reaction densities for the FCI are obtained integrating the corresponding cross section $\sigma_{\rm FCI}$, $\gamma_{\rm FCI}=\dfrac{T}{64\pi^4}\displaystyle\int_0^\infty \mathrm{d}s\, s^{1/2}\hat{\sigma}_{\rm FCI}K_1\left(\frac{\sqrt{s}}{T}\right)$, with the reduced cross sections $\hat{\sigma}_{\rm FCI}\equiv 2s\sigma_{\rm FCI}$. To avoid confusion with our notation for the Yukawa couplings of the model being considered, in the expressions for the cross sections given below we take the FCI to be mediated by any number of Dirac or Majorana neutrinos N_i $(i=1,2,\dots)$ with masses M_i, whose Yukawa couplings with the lepton doublets ℓ_α are called $h_{\alpha i}$. We find [4]:

$$\begin{aligned}\hat{\sigma}(\ell_\beta h\to\ell_\alpha h) &= \frac{1}{4\pi}\sum_{i,j}h_{\alpha i}^*h_{\beta i}h_{\alpha j}h_{\beta j}^*\frac{s^2\left(s-M_i^2-iM_i\Gamma_i\right)\left(s-M_j^2-iM_j\Gamma_j\right)}{\left[\left(s-M_i^2\right)^2+M_i^2\Gamma_i^2\right]\left[\left(s-M_j^2\right)^2+M_j^2\Gamma_j^2\right]}\,,\\
\hat{\sigma}(\ell_\beta\bar{h}\to\ell_\alpha\bar{h}) &= \frac{1}{2\pi}\sum_{\substack{i,j\\ i\neq j}}h_{\alpha i}^*h_{\beta i}h_{\alpha j}h_{\beta j}^*\frac{1}{M_i^2-M_j^2}\left\{M_i^2\ln\frac{s+M_i^2}{M_i^2}-M_j^2\ln\frac{s+M_j^2}{M_j^2}\right\}\\
&\quad+\frac{1}{2\pi}\sum_{\substack{i,j\\ i=j}}h_{\alpha i}^*h_{\beta i}h_{\alpha j}h_{\beta j}^*\left\{\ln\frac{s+M_i^2}{M_i^2}-\frac{s}{s+M_i^2}\right\}\,,\\
\hat{\sigma}(h\bar{h}\to\ell_\alpha\bar{\ell}_\beta) &= \frac{1}{2\pi}\sum_{\substack{i,j\\ i\neq j}}h_{\alpha i}^*h_{\beta i}h_{\alpha j}h_{\beta j}^*\left\{-1+\frac{M_i^2(s+M_i^2)}{s(M_i^2-M_j^2)}\ln\frac{s+M_i^2}{M_i^2}+\right.\\
&\qquad\left.\frac{M_j^2(s+M_j^2)}{s(M_j^2-M_i^2)}\ln\frac{s+M_j^2}{M_j^2}\right\}+\\
&\quad\frac{1}{2\pi}\sum_{\substack{i,j\\ i=j}}h_{\alpha i}^*h_{\beta i}h_{\alpha j}h_{\beta j}^*\left\{-2+\frac{s+2M_i^2}{s}\ln\frac{s+M_i^2}{M_i^2}\right\}\,.\end{aligned} \tag{9.15}$$

Moreover, the subtracted reaction density is given by

$$\gamma_{\ell_\alpha h}^{\ell_\beta h\,\prime}=\gamma_{\ell_\alpha h}^{\ell_\beta h}-\sum_i\gamma_{N_i}^{\ell_\beta h}\mathrm{Br}(N_i\to\ell_\alpha h)\,, \tag{9.16}$$

[4] Our expressions for these cross sections differ from the ones used in [161], which were taken from [149].

with $\mathrm{Br}(N_i \to \ell_\alpha h)$ the branching ratio of the process $N_i \to \ell_\alpha h$.

For the models we are considering the dominant contribution to the FCI comes from the interchange of a neutrino with mass M_2 and Yukawa couplings $h_{\alpha 2} = \lambda_{\alpha 2}$.

9.4 Results

We will find the lower bound for M_1 under the requirement that leptogenesis be successful in these scenarios. The relevant parameters for leptogenesis are M_1, M_2/M_1, $(\lambda^\dagger\lambda)_{11}$, $(\lambda^\dagger\lambda)_{22}$, the projectors $K_{\alpha i} \equiv \lambda_{\alpha i}\lambda^*_{\alpha i}/(\lambda^\dagger\lambda)_{ii}$ ($\alpha = \mu, \tau; i = 1, 2$), and μ_2. Next we comment on the role of these parameters.

- M_1: For a fix value of the Yukawa couplings (and in particular of the CP asymmetry when M_2/M_1 is kept fixed) the lower is M_1, the stronger the washouts become (because the expansion rate becomes slower with decreasing T). This is why M_1 cannot be very low.

- M_2/M_1: The hierarchy among the masses appears in the CP asymmetry, with $\epsilon_{\alpha 1} \propto (M_2/M_1)^{-2}$ for $M_2 \gg M_1$, and in the FCI when these are mediated mainly by N_2 (as always happens in the interesting cases for this work), $\gamma_{\rm FCI}(T) \propto (M_2/M_1)^{-4}$ for $T \sim M_1 \ll M_2$. Also note that if $M_2/M_1 \lesssim 20$ the inverse decays of N_2 could erase part of the asymmetry generated during N_1 leptogenesis and therefore they should be included in the BE.

- $(\lambda^\dagger\lambda)_{11}$: The intensity of the washouts due to processes involving N_1 is determined by the effective mass $\tilde{m}_1 \equiv (\lambda^\dagger\lambda)_{11}v^2/M_1$. In order to make full use of the -mandatory- flavour effects we take $\tilde{m}_1 \gtrsim m_* \simeq 10^{-3}$ eV. However, since $(\lambda^\dagger\lambda)_{11}$ violates lepton number it cannot be very large in the scenarios we are considering.

- $(\lambda^\dagger\lambda)_{22}$: The CP asymmetry $\epsilon_{\alpha 1}$ is directly proportional to $(\lambda^\dagger\lambda)_{22}$, hence this parameter should be taken as large as possible. There are two reasons that prevent it from being very large. One is that the washouts due to processes involving N_2 increase with $(\lambda^\dagger\lambda)_{22}$. The other is that, as explained at the beginning of Sec. 9.3, the Yukawa interactions of N_2 must be slower than those of the τ. Below we explain in more detail how this constrain has been dealt with.

- $K_{\alpha i}$: The flavoured CP asymmetries depend on the square root of the projectors while the washouts in the flavour "α" depend linearly on $K_{\alpha i}$, hence the washouts decrease faster than the CP asymmetries with decreasing projectors. This fact must be taken into account in order to maximize the production of lepton asymmetry. Note that since $\sum_\alpha K_{\alpha i} = 1$ and we are taking $K_{ei} = 0$, there are only two independent projectors, which can be chosen as $K_{\mu 1}$ and $K_{\mu 2}$.

- μ_2: Since we are not considering the case $\mu_2 \sim \Gamma_{N_{2l,2h}}$, μ_2 only enters as a discrete parameter, the baryon asymmetry taking one μ_2-independent value when $\mu_2 \gg \Gamma_{N_{2l,2h}}$ and another when $\mu_2 \ll \Gamma_{N_{2l,2h}}$.

Given that the hierarchy M_2/M_1 is an interesting and crucial parameter, we have determined the minimum value of M_1 compatible with successful leptogenesis as a function of M_2/M_1, maximizing the final baryon asymmetry over the remaining parameters, i.e. over the relevant combinations of Yukawa couplings: $(\lambda^\dagger\lambda)_{11}, (\lambda^\dagger\lambda)_{22}, K_{\mu 1}$, and $K_{\mu 2}$. To obtain the baryon asymmetry we have solved numerically the appropriate set of BE, and to get successful leptogenesis we have required $Y_B = 8.75$ [19]. The result is represented with the thick continuous curves in Fig. 9.1, the red line corresponding to the case $\mu_2 \gg \Gamma_{N_{2l,2h}}$ and the green one to $\mu_2 \ll \Gamma_{N_{2l,2h}}$.

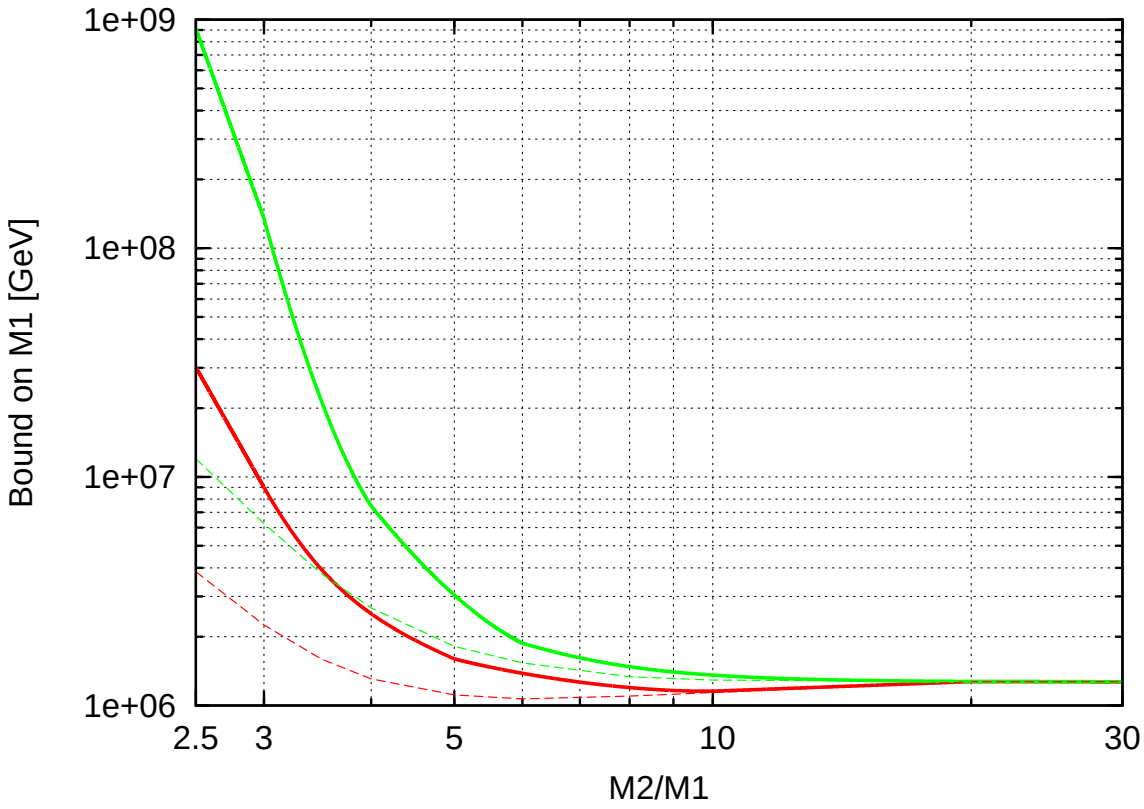

Figure 9.1: Lowest value of M_1 yielding successful leptogenesis as a function of M_2/M_1. The red curves are for the case $\mu_2 \gg \Gamma_{N_{2l,2h}}$ and the green ones for $\mu_2 \ll \Gamma_{N_{2l,2h}}$. The thick continuous curves give the physically correct bound, while the thin dashed ones show the result that would be obtained if the Yukawa couplings of N_2 were allowed to take values as large as 1 for all values of M_2/M_1.

As can be seen it is possible to have neutrino masses as low as $M_1 \sim 10^6$ GeV, i.e. around three orders of magnitude below the lower bound for the standard case of type I

seesaw with hierarchical heavy neutrinos. In particular this value can be compatible with the upper bound on the reheating temperature required to avoid the gravitino problem in SUGRA models. Moreover, M_1 values around 10^6 GeV can be achieved for a wide range of N_2 masses and also for different values of the Yukawa couplings. In particular, the maximum value of the baryon asymmetry is obtained for $\tilde{m}_1 \sim 10^{-2}$ eV and $K_{\mu 1}$ (or $K_{\tau 1}$) ~ 0.1, but it does not change much if $\tilde{m}_1$ is varied within the range 5×10^{-3} eV $\lesssim \tilde{m}_1 \lesssim 10^{-1}$ eV as long as the projectors are adjusted in order to have strong washouts in one flavour and weak washouts in the other, e.g. $K_{\mu 1}\tilde{m}_1 \lesssim m_*$ and $K_{\tau 1}\tilde{m}_1 \gtrsim (5-10)m_*$. Regarding the Yukawa couplings of N_2, $(\lambda^\dagger\lambda)_{22}$ lies approximately between [5] 0.01 and 1, while for intermediate to large M_2 masses, $M_2 \gtrsim 5M_1$, the smallest projector can take values as large as 0.1 to 0.5, without changing the bound shown in Fig. 9.1 by more than a factor 2. Instead, for $M_2 \lesssim 5M_1$, some hierarchy among the Yukawa couplings of N_2 is required, namely $\lambda_{\mu 2}/\lambda_{\tau 2}$ (or $\lambda_{\tau 2}/\lambda_{\mu 2}$) $\sim (1-3)\times 10^{-2}$ to achieve the values shown in Fig. 9.1.

An important issue for obtaining the bound on M_1 is to determine how large the Yukawa couplings of N_2 can be without violating the condition that the rates of processes involving N_2 be slower than the rates of the τ-Yukawa interactions [6]. For reference purposes we plot in Fig. 9.2 the ratio between the rates of these interactions, distinguishing between processes with a real or virtual N_2, for $M_2 = 10^7$ GeV and $\sqrt{(\lambda^\dagger\lambda)_{22}} = 0.01 \sim h_\tau$ (the rates of the τ-Yukawa interactions have been taken from [173, 174]). On one hand, note that the τ-Yukawa interactions tend to become dominant over the N_2 ones as the temperature decreases. On the other hand, for each set of parameters there exists a temperature T_{in} such that the final baryon asymmetry (Y_B^f) does not depend on what happens at $T > T_{in}$ (because there are strong washouts for all the interesting regions of the parameter space). Then the largest possible value for $(\lambda^\dagger\lambda)_{22}$ has been set by requiring that the τ-Yukawa interactions be faster than the N_2 ones for all temperatures *below* T_{in}. In practice we have determined T_{in} finding the lowest value of T such that Y_B^f does not change by more than 10% when the initial conditions at T, namely $Y_{N_i}(T)$ and $Y_{\Delta_\alpha}(T)$, are varied. The value of T_{in} as a function of M_2/M_1 is shown in Fig. 9.3, reinterpreted as an approximate lower bound for the reheating temperature. Also note that the independence from the initial conditions is an interesting feature by itself, since the models become more predictive.

For comparison we have also plotted in Fig. 9.1 the -wrong- bound that would be obtained if $(\lambda^\dagger\lambda)_{22}$ were allowed to be as large as 1, ignoring the above discussion. It is clear that as M_2 approaches M_1 the requirement of an upper bound for $(\lambda^\dagger\lambda)_{22}$ becomes very relevant. This requirement is also the reason why it is convenient to take $M_2 > M_1$, because in the opposite case (when the lepton asymmetry is produced by the decay of the next-to-lightest singlet neutrino, usually called "N_2 leptogenesis") the bound on $(\lambda^\dagger\lambda)_{22}$ would not allow for large values of the CP asymmetry.

[5] In the analysis presented here we have restricted $|\lambda_{\alpha 2}| \leq 1$, but we have checked that the results do not change significantly when allowing these Yukawa couplings to take somewhat larger values (but below the perturbative bound).

[6] There are not relevant experimental bounds on the Yukawa couplings of N_2 for the masses of heavy neutrinos we are considering.

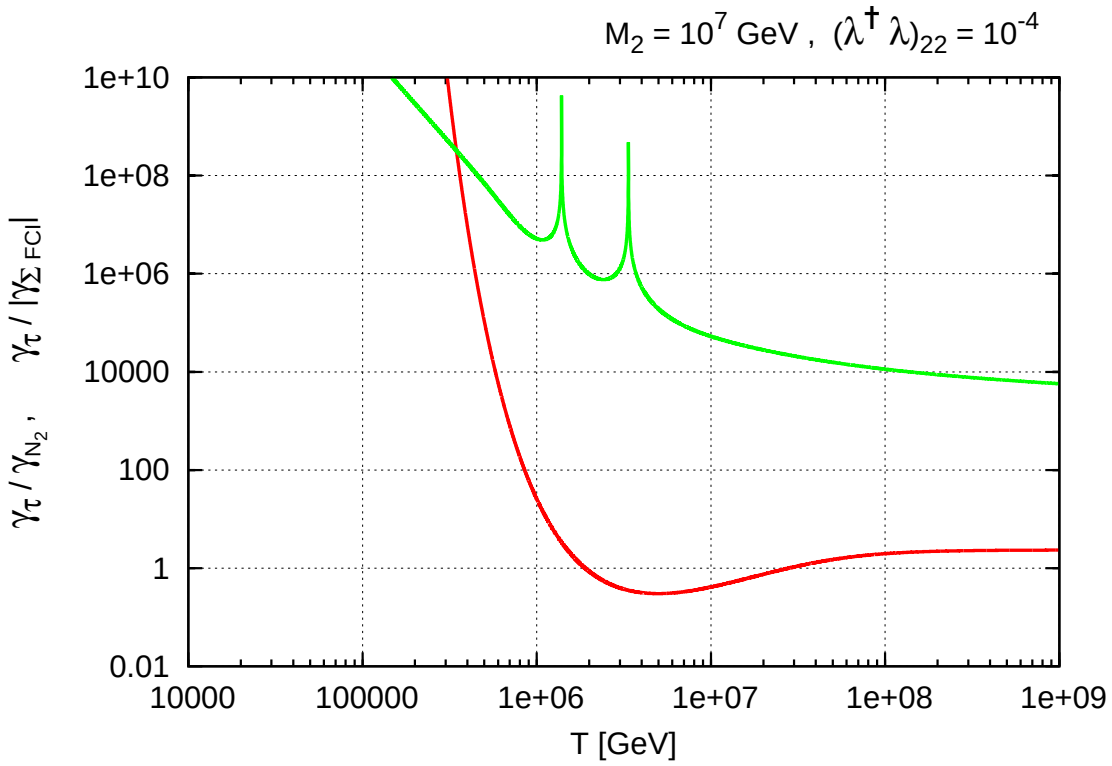

Figure 9.2: Comparison between the rates of the Yukawa interactions of N_2 and τ as a function of the temperature. The red line gives γ_τ/γ_{N_2} and the green one $\gamma_\tau/\left|\gamma_{\Sigma\,\mathrm{FCI}}\right|$, where γ_τ is the rate of the Yukawa interactions of the τ, γ_{N_2} is the sum of the rates of processes involving a real N_2 (here we have included the decay and scatterings with the top quark summing over all lepton flavours), and $\gamma_{\Sigma\,\mathrm{FCI}}$ is basically the sum of the rates of the FCI mediated by an off-shell N_2, $\gamma_{\Sigma\,\mathrm{FCI}} \equiv \left(\gamma_{\ell_\mu h}^{\ell_\tau h\,\prime} + \gamma_{\ell_\mu \bar{h}}^{\ell_\tau \bar{h}} + \gamma_{h\bar{h}}^{\ell_\tau \bar{\ell}_\mu}\right)/(K_{\mu 2}K_{\tau 2})$. We have taken $M_2 = 10^7$ GeV and $(\lambda^\dagger\lambda)_{22} = 10^{-4} \simeq h_\tau^2$ (with h_τ the Yukawa coupling of the τ). Note that the interactions involving a real N_2 scale as $(\lambda^\dagger\lambda)_{22}$, while the FCI are proportional to $(\lambda^\dagger\lambda)_{22}^2$. The corresponding curves for other values of M_2 can be obtained simply by making the appropriate translation along the T-axis. The spiky shape of the green curve for $0.1M_2 \lesssim T \lesssim M_2$ is due to the substraction of the on-shell contribution to the process $\ell_\tau h \to \ell_\mu h$.

Another feature apparent in Fig. 9.1 is the constant behaviour of the bound on M_1 for large values of M_2/M_1. This can be understood quite easily as follows. The asymmetry Y_B^f is proportional to the CP asymmetry in N_1 decays, $\epsilon_{\mu 1} = -\epsilon_{\tau 1}$, which in turn satisfies $\epsilon_{\mu 1} \propto (M_1/M_2)^2(\lambda_{\mu 2}\lambda_{\tau 2})$. For $M_2 \gg M_1$, Y_B^f increases with $(\lambda_{\mu 2}\lambda_{\tau 2})$ up to a certain value $(\lambda_{\mu 2}\lambda_{\tau 2})_{\max}$ for which the FCI become important, equilibrating the asymmetries generated in the two flavours with the consequent decrease of the baryon asymmetry [162, 163]. At the temperatures relevant for leptogenesis, $T \sim M_1 \ll M_2$, the rates of the FCI scale as $\gamma_{\mathrm{FCI}} \propto (M_1/M_2)^4(\lambda_{\mu 2}\lambda_{\tau 2})^2$. Hence we see that if (M_1/M_2) is decreased by a factor a, $(\lambda_{\mu 2}\lambda_{\tau 2})_{\max}$ can be increased by a factor a^2 keeping constant the rates of the FCI. Therefore $(\lambda_{\mu 2}\lambda_{\tau 2})_{\max} \propto (M_1/M_2)^{-2}$ and hence the maximum value of Y_B^f, being proportional to

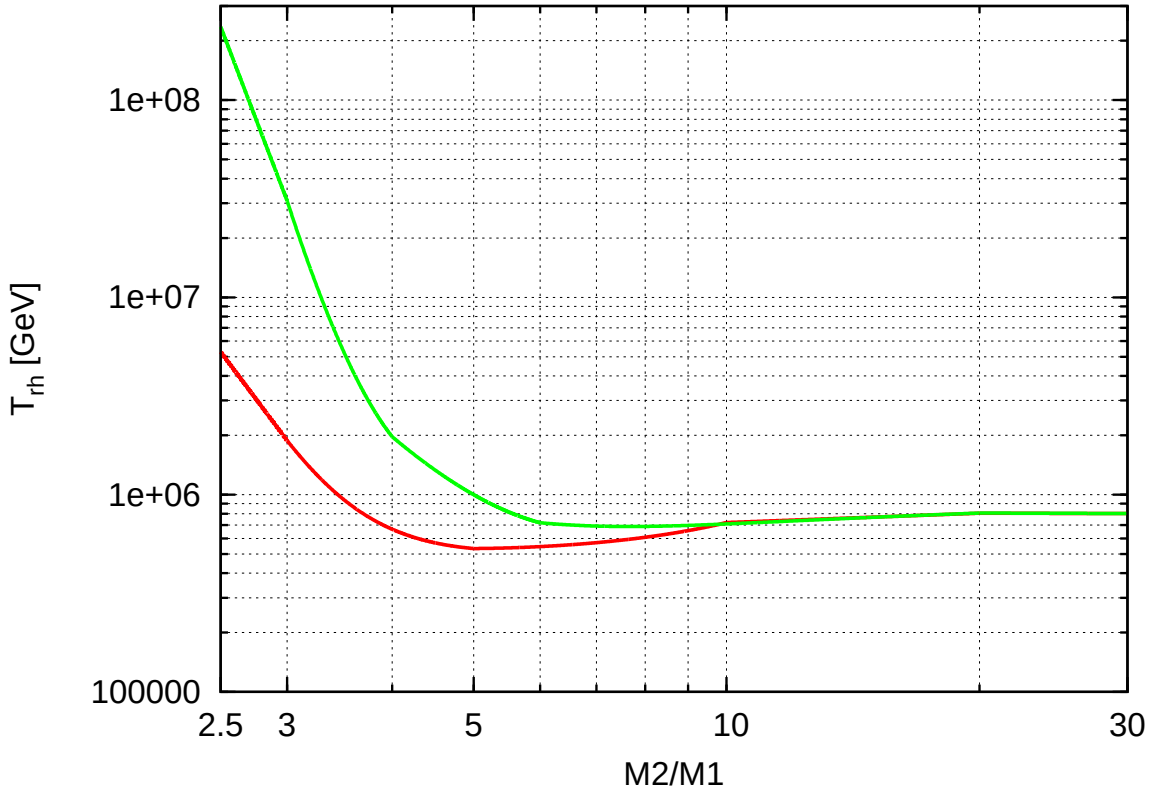

Figure 9.3: The lower bound on the reheating temperature as a function of M_2/M_1. The red curve is for the case $\mu_2 \gg \Gamma_{N_{2l,2h}}$ and the green one for $\mu_2 \ll \Gamma_{N_{2l,2h}}$.

$(M_1/M_2)^2\,(\lambda_{\mu 2}\lambda_{\tau 2})_{\rm max}$, becomes independent of M_2/M_1.

As mentioned in Sec. 9.3, for simplicity we have taken ℓ_e to be perpendicular to N_1 and N_2, so that only two flavour asymmetries are generated. We have checked that in the more general three flavour case it is possible to lower the bound on M_1 by a factor up to almost 4 with respect to the two flavour case. This is due to the combination of two effects. On one hand, Y_B^f can be almost twice as large compared to the two flavour case (this happens when $K_{\alpha 1}\tilde{m}_1 \lesssim m_*$ for two different flavours). On the other hand, it can be shown that for a given value of M_2/M_1, the maximum value of Y_B^f is proportional to $\sim \sqrt{M_1}$ in the relevant region of the parameter space. Hence an increase in Y_B^f by a factor 2 leads to a decrease in the lower bound of M_1 by a factor 4.

Finally let us comment on the relation between the parameters defined above and the light neutrino masses. To lowest order in the L-violating parameters, the light neutrino masses m_ν are given by

$$(m_\nu)_{\alpha\beta} \sim \lambda_{\alpha 1}\frac{v^2}{M_1}\lambda_{\beta 1} + (\lambda'_{\alpha 2} - \frac{\mu_2}{M_2}\lambda_{\alpha 2})\frac{v^2}{M_2}\lambda_{\beta 2} + \lambda_{\alpha 2}\frac{v^2}{M_2}(\lambda'_{\beta 2} - \frac{\mu_2}{M_2}\lambda_{\beta 2}) \tag{9.17}$$

where $v = \langle h \rangle = 174$ GeV is the vev of the Higgs field.

We have seen that M_1 is minimized for values of $\tilde{m}_1 \equiv (\lambda^\dagger\lambda)_{11}v^2/M_1$ in the range 10^{-2} eV $\lesssim \tilde{m}_1 \lesssim 10^{-1}$ eV, therefore the contribution of N_1 to light neutrino masses is expected to be of the same order, barring cancellations due to phases. Imposing that such contributions are of order $m_{atm} \sim 0.05$ eV, we get $\lambda_{\alpha 1} \sim 10^{-5} - 10^{-4}$.

To reproduce the observed solar and atmospheric mass scales, at least one of the contributions from N_2 in Eq.(9.17) should be also of order 10^{-2} eV; for the parameters that minimize M_1, this requirement leads to $\mu_2/M_2 \sim 10^{-8} - 10^{-6}$, independently of the ratio M_2/M_1. Moreover, $\Gamma_{N_{2l,2h}}/M_2 \sim 5 \times (10^{-4} - 10^{-2})$, therefore typically $\mu_2 \ll \Gamma_{N_{2l,2h}}$. However, for $M_1 \gtrsim 5 \times 10^6$ GeV, and still not considering large fine tunings related to phase cancellations, smaller values of $\lambda_{\alpha 2}$ can lead to successful leptogenesis, and in this region it is possible to have $\mu_2 \gtrsim \Gamma_{N_{2l,2h}}$.

With respect to the L-violating parameters $\lambda'_{\alpha 2}$, their contribution to the masses of the light neutrinos is $m_\nu \sim m_{atm}$ typically for $\lambda'_{\alpha 2} \sim 10^{-8} - 10^{-7}$. We have checked for consistency that these small values give a negligible contribution to leptogenesis (more specifically to the CP asymmetries and washouts).

9.5 Conclusions

We have studied leptogenesis in the framework of the seesaw mechanism with small violation of $B-L$. If $B-L$ is only slightly broken, then either the heavy neutrinos which generate the baryon asymmetry are almost degenerate and combine to form a quasi-Dirac fermion, which can have large lepton number conserving Yukawa couplings or it is a Majorana fermion with small lepton number violating Yukawa couplings.

In both cases there are interesting consequences for leptogenesis: in the first one, the strong degeneracy of the heavy neutrinos leads to a resonant enhancement of the CP asymmetry, avoiding the DI bound on M_1 which applies to hierarchical SM singlets. In the second case, the L-conserving part of the flavoured CP asymmetries in N_1 decays can be much larger than the L-violating one, since the former is not linked to light neutrino masses and also escapes the DI bound, even if the heavy neutrinos are hierarchical. As a consequence, in models with almost conserved $B - L$ successful leptogenesis may be possible at lower temperatures than in the standard seesaw, alleviating the gravitino problem in supersymmetric scenarios.

In this paper we have focused on the second possibility, i.e., without resorting to the resonant enhancement of the CP asymmetry. We have found that the largest baryon asymmetry is generated by the lightest SM singlet, and it rapidly decreases if $|M_2 - M_1| \lesssim 2M_1$ but far from the resonance region, $|M_2 - M_1| \sim \Gamma_2$. Thus we have restricted the heavy neutrino masses to the region $M_2 \gtrsim 2M_1$, being N_2 the next-to-lightest heavy neutrino. The L-conserving part of the flavoured CP asymmetries in N_1 decays is not suppressed by light neutrino masses, and can easily dominate over the L-violating piece if $B - L$ is almost conserved. Such contributions cancel in the total CP asymmetry, $\epsilon_1 = \sum_\alpha \epsilon_{1\alpha}$, so it is

mandatory that flavour effects are at work for this terms to have an impact in leptogenesis.

We have exhaustively scanned the parameter space of seesaw models with almost conserved $B - L$, in which this L-conserving piece of the flavoured CP asymmetry dominates (purely flavoured leptogenesis). The relevant parameters are M_1, M_2/M_1, $(\lambda^\dagger\lambda)_{11}$, $(\lambda^\dagger\lambda)_{22}$ and the flavour projectors $K_{\alpha i} \equiv \lambda_{\alpha i}\lambda^*_{\alpha i}/(\lambda^\dagger\lambda)_{ii}$. The same N_2-Yukawa couplings which enhance the L-conserving CP asymmetries induce large FCI mediated by N_2, which tend to equilibrate the asymmetries in the different lepton flavours, especially if both N_1 and N_2 have similar masses and are simultaneously present in the thermal bath. Therefore, for each value of M_2/M_1 we have determined the minimum M_1 compatible with successful leptogenesis, maximizing the final baryon asymmetry over the remaining parameters. We have solved numerically the relevant set of BE, including decays and inverse decays of the two singlet neutrino species, as well as the FCI. We have considered two possibilities: N_2 is a pseudo-Dirac fermion (i.e., two Majorana neutrinos with masses $M_2 \pm \mu_2$, $\mu_2 \ll M_2$) and N_2 is approximately Dirac, in which case an asymmetry between N_2 and $\bar{N}_2$ is generated and should be taken into account. In both cases we have found that leptogenesis is possible for $M_1 \gtrsim 10^6$ GeV, as long as $M_2/M_1 \gtrsim 5$ and $(\lambda^\dagger\lambda)_{22} \sim 0.01 - 1$ (see Fig. 9.1). So purely flavoured leptogenesis in seesaw models with slightly broken $B-L$ provides a solution to the conflict between the upper bound on T_{RH} required to solve the gravitino problem of supersymmetric scenarios and the lower bound on T_{RH} needed for successful thermal leptogenesis. However, such heavy neutrinos are far outside the reach of present and near future colliders and do not lead to observable lepton flavour violation in non-supersymmetric frameworks.

Chapter 10

Summary and Conclusions

This thesis has been mainly focussed on the study of two mechanisms, presumably present in two different epochs in the very early Universe, whose energy scales have not yet been reached by laboratory experiments on Earth, namely *Inflation* and *Leptogenesis*. These mechanisms have been proposed in order to solve some open problems in both the particle and cosmological standard models. The first one, Inflation, is a period of accelerated expansion of the Universe meant to explain the observed homogeneity and isotropy of our Universe. The second one, Leptogenesis, generates the Baryon Asymmetry of the Universe (BAU), through the partial conversion of a lepton asymmetry previously generated. Leptogenesis is linked directly to Inflation since, even in the presence of a primordial asymmetry in the beginning of the Universe, if Inflation took place, it would have erased this asymmetry. Hence, if we believe in Inflation, it is mandatory to have a second mechanism that generates the right BAU dynamically afterwards. In the following, we present our major conclusions.

Inflation is an elegant mechanism that, on top of explaining the observed homogeneity and isotropy of our Universe, is capable of solving some other problems of the Cosmological Model such as the absence of relics in the present Universe and the generation of the perturbations that are the seeds of the structures we observe in our Universe. It is this last achievement perhaps the most important one, as they are extremely difficult to generate otherwise. The nearly scale invariance of the power spectrum of the scalar and tensor perturbations is a consequence of the dilation isometry of the de Sitter space and the approximate time-translation symmetry $t \to \tilde{t} = t + \text{const.}$ of the lagrangian of the theory. This scale invariance has been contrasted by CMB data, and it is considered one of the most important successes of Inflationary theories. This is the reason why models with no explicit time shift symmetry are hard to accommodate with observations. Nevertheless, there is no reason why a more general symmetry affecting the time component cannot be present in the underlying theory that causes Inflation. In that sense, in [1] we promote the time translation symmetry to a time reparametrization invariance $t \to \tilde{t} = \tilde{t}(t)$, and study their consequences for the observables, in an effective field theory approach. We find that, despite the non-standard behavior of the perturbations in the symmetric phase, the successful generation of perturbations is recovered once the symmetry is broken and the Universe enters in

a standard Friedmann-Robertson-Walker phase. One of the most remarkable results of this model is that all the *n-point* functions are fixed by two parameters, which are determined by the amplitude of the power spectrum and the sound speed of the perturbations. This feature gives the theory a highly predictive power.

In the last years, CMB observations have achieved an enormous precision in the measurement of the cosmological parameters, unbelievable 20 years ago. Moreover, they have put tight bounds on several parameters such as the *tensor-to-scalar* ratio, r, whose value must be very tiny, if not zero, and extremely difficult to measure. And it is possible that future CMB experiments could provide a detection for primordial tensor modes (and hence a value for r) if they are different from zero. Nonetheless, in order to extract the tensor-to-scalar ratio several assumptions are made. For instance, an underlying fiducial Cosmology is needed, usually the ΛCDM cosmological model. Effects like the reionization of the intergalactic medium and how it happened affect also the observables and they must be taken into account to extract the right value of the cosmological parameters. Usually, this reionization is taken to happen instantaneously at redshift z_r between 4 and 28. In [2] we analyze the possible consequences of a more general reionization scenario. We find that hybrid models, excluded assuming a sudden reionization, are still allowed by WMAP7 data when we relax that assumption. Another important fact we find is that the tensor-to-scalar ratio, r, barely depends on the assumed reionization history, which is very remarkable as this quantity can be used to distinguish among several models of Inflation.

CMB data also provides the most accurate measurement of the baryon-to-photon density ratio. From this measurement we can extract what is the baryon asymmetry in the Universe. The origin of this asymmetry is another open question that the standard models of particle physics and Cosmology cannot answer by themselves. One possible mechanism proposed in order to solve this issue, called Leptogenesis, generates the right baryon asymmetry through a partial conversion of a previously generated lepton asymmetry. The simplest version of this mechanism is based on seesaw models, where the standard model of particles is extended with at least two heavy sterile neutrinos which couple to the light active neutrinos to give them mass. This standard model extension provides a natural solution to the baryon asymmetry since it is possible to generate it in the decay out of equilibrium of some of the heavy sterile neutrinos, provided that there is enough CP violation in the interactions responsible for such decays. In the standard Leptogenesis scenario, there exist a lower bound on the mass of the lightest heavy neutrino state of about 10^9 GeV, the Davidson-Ibarra bound, which means that the maximum temperature of the Universe reached after Inflation or *reheating* temperature should be roughly larger than 10^9 GeV, in order to generate such particles. Such high temperature in turn, is disfavored in supersymmetric theories, as it would imply the generation of gravitinos in the very early Universe whose late decays would jeopardize successful Big Bang Nucleosynthesis.

In [3] we have explored Leptogenesis in models with almost conserved lepton number. In that case, either the heavy sterile neutrino masses are almost degenerate and these neutrinos combine to form a quasi-Dirac fermion, which causes a resonant enhancement of the CP asymmetries, or they are two Majorana fermions with a large contribution to the

L-conserving part of the flavoured CP asymmetries. Both cases escape from the Davidson-Ibarra bound and hence can lead to successful Leptogenesis at lower temperatures than the ones in the standard seesaw scenario. In the second case it is mandatory that flavour effects are at work since the total CP-asymmetry vanishes when considering only the $L-$ conserving part. Since resonant models have been widely studied, in [3] we have stick to the second case, scanning through all the allowed range of the relevant parameters; M_1; M_2/M_1, $(\lambda^\dagger\lambda)_{11}$, $(\lambda^\dagger\lambda)_{22}$ and $K_{\alpha i} \equiv \lambda_{\alpha i}\lambda^*_{\alpha i}/(\lambda^\dagger\lambda)_{ii}$, being M_1 and M_2 the masses of the lightest and next-to-lightest heavy neutrinos that produce the asymmetry, and $\lambda_{\alpha i}$ is the Yukawa coupling between the Heavy neutrino N_i and the lepton field l_α through the Higgs field H. We find a lower bound of the mass of the lightest heavy neutrino N_1 of $\sim 10^6$ GeV, alleviating the gravitino problem in supersymmetric scenarios.

Part III

Appendices

Appendix A

Khronon Inflation

A.1 Constraints and the validity of the decoupling limit

In the main text of Chapter 7 we have calculated everything in terms of π, focussing on the decoupling limit, (i.e. neglecting its effects on the metric) and then converting the results in terms of ζ. The logic behind it is that we expect the corrections coming from the effect of π on the metric to be subleading in $1/M_P^2$, and therefore negligible when $M_\lambda^2 \ll M_P^2$ and $M_\alpha^2 \ll M_P^2$. However the model we are describing is sufficiently unconventional to warrant a check of this intuitive explanation. Let us calculate the power spectrum of ζ directly in the ζ-gauge, i.e. setting to zero the π perturbations.

Starting from the action (7.9), we go through the standard procedure [56] of solving the constraint equation and plug the solution back into the action. We use the ADM splitting of the metric

$$ds^2 = -(N^2 - h_{ij}N^iN^j)dt^2 + 2h_{ij}N^i dx^j dt + h_{ij}dx^i dx^j, \tag{A.1}$$

where N and N^i are non dynamical fields and can be integrated out.

Defining $N = 1 + \delta N$ and $N^i = N_T^i + \partial_i\psi$, with $\partial_i N_T^i = 0$, the linearized constraint equations obtained by varying with respect to N and N^i respectively are given by

$$\left(1 + \frac{3}{2}\frac{M_\lambda^2}{M_P^2}\right)\left(\partial^2\psi - 3(\dot\zeta - \delta N H)\right) + \partial^2\left(\frac{\zeta}{a^2 H}\right) + \frac{M_\alpha^2}{M_P^2}\frac{\partial^2\delta N}{2a^2 H} = 0$$

$$\partial_i\left[(\delta N H - \dot\zeta)\left(1 + \frac{3}{2}\frac{M_\lambda^2}{M_P^2}\right) + \frac{M_\lambda^2}{2M_P^2}\partial^2\psi\right] = 0\,. \tag{A.2}$$

We can now solve these equations at first order in M_α^2/M_P^2 and M_λ^2/M_P^2 and plug the solutions back into the action. After some work, we obtain

$$S_\zeta = \int \mathrm{d}^3x\,\mathrm{d}\eta\left(\frac{M_\alpha^2}{2H^2}(\partial\zeta')^2 - \frac{M_\lambda^2}{2H^2}(\partial^2\zeta)^2\right)\,, \tag{A.3}$$

which is the action given in (7.11) with $\pi = -\zeta/H$ as expected. The action above will contain additional terms suppressed by powers of M_α^2/M_P^2 and M_λ^2/M_P^2.

A.2 Evolution after the field redefinition invariant phase

In this Appendix we want to verify our intuitive arguments of Section 7.3 in an explicit (toy) example. Let us add to the quadratic action (7.11) a standard 2-derivative kinetic term[1]

$$S = \int \mathrm{d}^3x\,\mathrm{d}\eta \left[\frac{M_\alpha^2}{2}(\partial\pi')^2 - \frac{M_\lambda^2}{2}(\partial^2\pi)^2 + \beta a^2 H^2 \left(\frac{M_\alpha^2}{2}\pi'^2 - \frac{M_\lambda^2}{2}(\partial_i\pi)^2 \right) \right] . \tag{A.4}$$

We need $\beta \ll 1$ for the kinetic term discussed in this paper to dominate at Hubble crossing. In this case β represents a small breaking of the field redefinition symmetry and its contribution will become relevant when a mode is sufficiently long compared to the Hubble radius. What we want to check is that, up to corrections suppressed by β, π remains constant during the out-of-Hubble evolution, until the mode becomes long enough to be dominated by the standard kinetic term. This will imply that the correlation functions calculated in the paper are actually the ones observed at late times. The equation of motion is given by

$$\partial^2\pi'' - \beta H^2 \frac{d}{d\eta}\left[a^2\pi'\right] - \frac{M_\lambda^2}{M_\alpha^2}(\partial^4\pi - \beta a^2 H^2 \partial^2\pi) = 0 . \tag{A.5}$$

Out of the Hubble radius, i.e. $(k/aH)^2 \ll 1$, there are three regimes of different evolution. For $\beta^{2/3} \ll (k/aH)^2 \ll 1$, the terms proportional to β are irrelevant and everything goes as discussed in the paper. The first term which becomes relevant is the Hubble friction and it is easy to realize that this is the only term one has to consider in addition to the original Lagrangian in the window $\beta \ll (k/aH)^2 \ll \beta^{2/3}$. Finally, in the regime $(k/aH)^2 \ll \beta$, only the terms proportional to β are relevant and π behaves as in standard inflation. It is simple to follow the evolution from one phase to the other in the long wavelength limit. First of all notice that $\pi = const$ is a good solution in any phase and in the transition regions for a mode which is well oustide the Hubble radius, i.e in the $k \to 0$ limit. This can be seen explicitly in the equation and follows from the general conservation of ζ on super horizon scales (which within our approximations implies the conservation of π as $\zeta = -H\pi$, with constant H). Moreover, the velocity becomes irrelevant, $\dot\pi \ll H\pi$, before the terms proportional to β start playing any role, and this implies that $\dot\pi$ can be neglected when matching to the next phase. There is no mode mixing and π remains constant all along. It is easy to check this behaviour numerically.

The same reasoning works if we allow β to be time-dependent, i.e. dependent on the background value of $\phi_0 = t$. This describes the fact that the field redefinition symmetry will be badly broken at the end of inflation and β will become large. It is straightforward to check that also in this case $\pi = const$ is a good solution so that, for models well ouside the Hubble radius, i.e. $\dot\pi \ll H\pi$, the field remains constant while the symmetry gets broken. Notice that the logic is exactly the same one uses in the case of standard inflation to justify the conservation of ζ through the unknown reheating phase. As in that case we expect the same arguments to be valid non-linearly in the amplitude of ζ, so that each n-point function remains the same in the out of the horizon limit.

[1] For simplicity we assume that the speed of sound of the kinetic term we added is the same as the one of the original terms.

Part IV

Bibliography

Bibliography

[1] P. Creminelli, J. Norena, M. Pena, M Simonovic, JCAP **1211**, 032 (2012).

[2] S. Pandofi, E. Giusarma, E. W. Kolb, M. Lattanzi, A. Melchiorri, O. Mena, M. Pena, A Cooray, P. Serra, Phys. Rev. **D82**, 123527 (2010).

[3] J. Racker, M. Pena, N. Rius, JCAP **1207**, 030 (2012).

[4] E. Hubble, Proc. Nat. Acad. Sci. **15**, 168 (1929).

[5] R. A. Alpher, H. Bethe, and G. Gamow, Phys. Rev. **73**, 803 (1948).

[6] R. Dicke, P. J. E. Peebles, P. Roll, and D. Wilkinson, Astrophys. J. **142**, 414 (1965).

[7] D. Baumann, TASI lectures 2009, arXiv, arXiv:0907.5424 (2009).

[8] A. Albrecht, R. A. Battye and J. Robinson, Phys. Rev. Lett. **79**, 4736 (1997).

[9] L. Pogosian, S. Tye, I. Wasserman and M. Wyman, Phys. Rev. **D68**, 023506 (2003).

[10] R. M. Wald, gr.book (1984).

[11] V. Mukhanov, pfc.book (2005)

[12] A. Einstein, AnP. **354**, 769 (1916)

[13] A. Einstein, Sitzungsber. Preuss. Akad. Wiss. phys.-math. Klasse VI, 142 (1917).

[14] A. Friedmann, ZPhy. **10**, 377 (1922).

[15] S. Weinberg, cosm.book. (2008).

[16] S. Weinberg, gcpa.book. (1972).

[17] W. de Sitter, M.N.R.A.S. **78** 3 (1917).

[18] A. G. Riess, L. Macri, S. Casertano, H. Lampeitl, H. C. Ferguson, A. V. Filippenko, S. W. Jha, W. Li and R. Chornock, ApJ. **730**, 119 (2011).

[19] E. Komatsu *et al.*, Astrophys. J. Suppl. **192**, 18 (2011).

[20] C. Wirtz, Scientia **38**, 303 (1925).

[21] K. Lundmark, Mon. Not. Roy. Astron. Soc. **85**, 865 (1925).

[22] R. A. Sunyaev and Ya. B. Zel'dovich, Comments Ap. Space Sci. **4**, 173 (1972).

[23] A. J. S. Hamilton, Lect.NotesPhys.665:415-431, 2008, arXiv:astro-ph/0503603 (2005).

[24] A. J. S. Hamilton, Lect.NotesPhys.665:433-456, 2008, arXiv:astro-ph/0503604 (2005).

[25] V. J. Martínez, LNP, **665**, 269 (2009).

[26] D. J. Eisenstein *et al.*, Ap. J. , **633**, 560 (2005).

[27] A. D. Linde, ppIt.book. (2005).

[28] G. 't Hooft, Nucl. Phys. **B79**, 279 (1974).

[29] A. M. Polyakov, JETP Lett. **20**, 430 (1974).

[30] T. W. B. Kibble, J. Phys **9A**, 1387 (1976).

[31] Ya. B. Zeldovich and M. Yu. Khlopov, Phys. Lett. **79B**, 239 (1978).

[32] Ya. B. Zeldovich, I. Yu. Kobzarev and L. B. Okun, Phys. Lett. **50B**, 340 (1974).

[33] H. P. Nilles, Phys. Rep. C **110**, 3 (1984).

[34] J. Ellis, A. D. Linde and D. V. Nanopoulos, Phys. Lett. **128B**, 295 (1983).

[35] M. Yu. Khlopov and A. D. Linde, Phys. Lett. **138B**, 265 (1982).

[36] G. Mangano *et al.*, Nucl. Phys. **B729**, 221 (2011).

[37] Ya. B. Zeldovich, Soviet Phys.-Uspekhi **95**, 209 (1968).

[38] D. Kazanas, Ap. J. **241**, L59 (1980).

[39] K. Sato, Phys. Lett. **99B**, 66 (1981).

[40] A. A. Starobinsky, JETP Lett. **30**, 682 (1979).

[41] A. A. Starobinsky, Phys. Lett. B **91**, 99 (1980).

[42] V. F Mukhanov and G. V. Chibisov, JETP Lett. **33**, 523 (1981).

[43] V. F Mukhanov and G. V. Chibisov, Sov. Phys. JETP **56**, 258 (1982).

[44] A. H. Guth, Phys. Rev. **D23**, 347 (1981).

[45] K. Sato, M.N.R.A.S. **195**, 467 (1981).

[46] A. D. Linde, Phys. Lett. **108B**, 389 (1982).

[47] A. D. Linde, Phys. Lett. **129B**, 177 (1983).

[48] A. Albrecht and P. J. Steinhardt, Phys. Rev. Lett. **48**, 1220 (1982).

[49] R. D. Peccei and H. R. Quinn, Phys. Rev. Lett., **38**, 1440 (1977).

[50] A. D. Linde, Phys. Rev. **D49**, 748 (1994).

[51] D. H. Lyth and A. Riotto, Phys. Rep., **314**, 1 (1999).

[52] D. Wands, Lect. Notes Phys. **738**, 275 (2008).

[53] J. M. Bardeen, P. J. Steinhardt, and M. S. Turner, Phys. Rev. **D28**, 679 (1983).

[54] J. M. Bardeen, Phys. Rev. **D22**, 1882 (1980).

[55] V. F. Mukhanov, H.A. Feldman and R. H. Brandenberger, Phys. Rept. **215**, 203 (1992).

[56] J. M. Maldacena, JHEP **05**, 013 (2003).

[57] N. Bartolo, S. Matarrese and A. Riotto, Phys. Rev. **D65**, 103505 (2002).

[58] F. Bernardeau and J. -P. Uzan, Phys. Rev. **D66**, 103506 (2002).

[59] C. T. Byrnes and D. Wands, Phys. Rev. **D74**, 043529 (2006).

[60] M. Alishahiha, E. Silverstein and D. Tong, Phys. Rev. **D70**, 123505 (2004).

[61] N. Arkani-Hamed, P. Creminelli, S. Mukohyama and M. Zaldarriaga, JCAP **0404**, 001 (2004).

[62] P. Creminelli, JCAP **0310**, 003 (2003).

[63] E. Komatsu and D. N. Spergel, Phys. Rev. **D63**, 063002 (2001).

[64] A. R. Liddle and D. H Lyth, lss.book (2000).

[65] S. Dodelson, mc.book (2003).

[66] U. Seljak and M. Zaldarriaga, astro-ph/9603033, **http://www.cmbfast.org**.

[67] A. Lewis and A. Challinor, **http://camb.info**.

[68] M. Kamionkowski, A. Kosowsky and A. Stebbins, Phys. Rev. **D55**, 7368 (1997).

[69] U. Seljak and M. Zaldarriaga, Phys. Rev. **D55**, 1830 (1997).

[70] N. Bartolo, E. Komatsu, S. Matarrese and A. Riotto, Phys. Rept. **402**, 103 (2004).

[71] G. Steigman, Ann. Rev. Astron. **14**, 339 (1976).

[72] A. D. Dolgov, Procedings of talk at Rencontres of La Thuile (2002) and at SpacePart (2002), arXiv:astro-ph/0207441 (2002).

[73] A. G. Cohen, A. De Rujula and S. L. Glashow, Ap. J, bf 495, 539 (1998).

[74] D. Casadei, arXiv, arXiv:astro-ph/0405417 (2004).

[75] J. Beringer *et al.* (Particle Data Group), Phys. Rev **D86**, 010001 (2012).

[76] F. Iocco, G. Mangalo, G. Miele, O. Pisanti and P. D. Serpico, Phys. Rept **472**, 1 (2008).

[77] A. D. Sakharov, JETP Lett. **5**, 24 (1967).

[78] S. L. Adler, Phys. Rev. **177**, 2426 (1969).

[79] J. S. Bell and R. Jackiw, Nuovo Cim. **A60**, 47 (1969).

[80] G. 't Hooft, Phys. Rev. Lett. **37**, 8 (1976).

[81] N. S. Manton, Phys. Rev. **D28**, 2019 (1983).

[82] V. A. Kuzmin, V. A. Rubakov and M. E. Shaposhnikov, Phys. Lett. **B155**, 36 (1983).

[83] W. Buchm´uler, Presented at PASCOS-07, arXiv:hep-ph/0710.5857 (2007).

[84] A. Riotto, J. Phys. Conf. Ser. **335**, 012008 (2011).

[85] S. Davidson, E. Nardi and Y.Nir, Phys. Rep. **466** 105 (2008)

[86] M. Fukugita and T. Yanagida, Phys. Lett. **B174**, 45 (1986).

[87] P. Minkowski, Phys. Lett. **B67**, 421 (1977).

[88] R. N. Mohapatra and G. Senjanovic, Phys. Rev. **D23**, 165 (1981).

[89] L. Covi, E. Roulet and F. Vissani, Phys. Lett. **B384**, 169 (1996).

[90] G. Engelhard, Y. Grossman, E. Nardi and Y. Nir, Phys. Rev. Lett. **99**, 081802 (2007).

[91] E. W. Kolb and S. Wolfram, Nucl. Phys. **B172**, 224 (1980).

[92] L. J. A. Harvey and M. S. Turner, Phys. Rev. **D42**, 3344 (1990).

[93] C. Cheung, P. Creminelli, A. L. Fitzpatrick, J. Kaplan and L. Senatore, JHEP **0803**, 014 (2008).

[94] P. Creminelli, A. Nicolis and E. Trincherini, JCAP **1011**, 021 (2010).

[95] P. Horava, Phys. Rev. **D79**, 084008 (2009).

[96] D. Blas, O. Pujolas and S. Sibiryakov, Phys. Rev. Lett. **104** 181302 (2010).

[97] D. Blas, O. Pujolas and S. Sibiryakov, JHEP **1104**, 018 (2011).

[98] S. Mukohyama, JCAP **0906**, 001 (2009).

[99] A. Wang, D. Wands and R. Maartens, JCAP **1003**, 013 (2010).

[100] K. Izumi, T. Kobayashi and S. Mukohyama, JCAP **1010**, 031 (2010).

[101] Y. Huang, A. Wang and Q. Wu, arXiv, arXiv:hep-th/1201.4630 (2012).

[102] D. Blas and S. Sibiryakov, JCAP **1107**, 026 (2011).

[103] C. Cheung, A. L. Fitzpatrick, J. Kaplan and L. Senatore, JCAP **0802**, 021 (2008).

[104] D. Babich, P. Creminelli and M. Zaldarriaga, JCAP **0408**, 009 (2004).

[105] L. Senatore, K. M. Smith and M. Zaldarriaga, JCAP **1001**, 028 (2010).

[106] P. Creminelli, G. D'Amico, M. Musso and J. Norena, JCAP **1111**, 038 (2011).

[107] P. Creminelli, J. Norena and M. Simonovic, arXiv, arXiv:hep-th/1203.4595 (2012).

[108] N. Dalal, O. Dore, D. Huterer and A. Shirokov, Phys. Rev. **D77** 123514 (2008).

[109] S. Matarrese and L. Verde, ApJ. **677** L77 (2008).

[110] N. Afshordi and A. J. Tolley, Phys. Rev. **D78** 123507 (2008).

[111] J. Norena, L. Verde, G. Barenboim and C. Bosch, arXiv, arXiv:astro-ph/1204.6324 (2012).

[112] E. Sefusatti, J. R. Fergusson, X. Chen and E. P. S. Shellard, arXiv, arXiv:astro-ph/1204.6318 (2012).

[113] N. Arkani-Hamed, P. Creminelli, S. Mukohyama and M. Zaldarriaga, JCAP **0404**, 001 (2004).

[114] D. Blas and S. Sibiryakov, Phys. Rev. D **84**, 124043 (2011).

[115] E. R. Harrison, Phys. Rev. **D1**, 2726 (1970); Y. B. Zel'dovich, Mon. Not. Roy. Astron. Soc. **160**, (1972); P. J. E. Peebles and J. T. Yu ApJ. **162**, 815 (1970).

[116] A. Vallinotto, E. J. Copeland, E. W. Kolb, A. R. Liddle and D. A. Steer, Phys. Rev. **D69**, 103519 (2004); A. A. Starobinsky, JETP Lett. **82**, 169 (2005).

[117] M. Zaldarriaga *et al.*, CMBPol, arXiv:astro-ph/0811.3918 (2008).

[118] M. J. Mortonson and W. Hu, ApJ. **686**, L53 (2008).

[119] S. Pandolfi *et al.*, Phys. Rev. **D81**, 123509 (2010).

[120] W. H. Kinney, E. W. Kolb, A. Melchiorri and A. Riotto, Phys. Rev. **D74**, 023502 (2006); W. H. Kinney, E. W. Kolb, A. Melchiorri and A. Riotto, Phys. Rev. **D78**, 087302 (2008).

[121] S. Dodelson, W. H. Kinney and E. W. Kolb, Phys. Rev. **D56**, 3207 (1997).

[122] A. Lewis, J. Weller and R. Battye, Mon. Not. Roy. Astron. Soc. **373**, 561 (2006).

[123] A. Lewis and S. Bridle, Phys. Rev. **D66**, 103511 (2002).

[124] W. C. Jones *et al.*, ApJ. **647**, 823 (2006); F. Piacentini *et al.*, ApJ. **647**, 813 (2006), ApJ. **647**, 833 (2006).

[125] M. L. Brown *et al.*, QUaD collaboration, ApJ. **705**, 978 (2009).

[126] C. L. Reichardt *et al.*, ApJ. **694**, 1200 (2009).

[127] H. C. Chiang *et al.*, ApJ. **711**, 1123 (2010).

[128] Planck Collaboration, arXiv:astro-ph/0604069 (2006).

[129] M. Gell-Mann, P. Ramond, and R. Slansky, Prepared for Supergravity Workshop, Stony Brook, New York, 27-28 Sep 1979.

[130] T. Yanagida, In Proceedings of the Workshop on the Baryon Number of the Universe and Unified Theories, Tsukuba, Japan, 13-14 Feb 1979.

[131] R. N. Mohapatra and G. Senjanovic, Phys. Rev. Lett. **44**, 912 (1980).

[132] S. Davidson and A. Ibarra, Phys. Lett. **B535**, 25 (2002).

[133] T. Hambye, Y. Lin, A. Notari, M. Papucci, and A. Strumia, Nucl. Phys. **B695**, 169 (2004).

[134] R. Barbieri, P. Creminelli, A. Strumia, and N. Tetradis, Nucl. Phys. **B575**, 61 (2000).

[135] T. Endoh, T. Morozumi, and Z. Xiong, Prog. Theor. Phys. **111**, 123 (2004).

[136] A. Abada, S. Davidson, F. X. Josse-Michaux, M. Losada, and A. Riotto, JCAP **0604**, 004 (2006).

[137] E. Nardi, Y. Nir, E. Roulet, and J. Racker, JHEP **01**, 164 (2006).

[138] A. Abada, S. Davidson, A. Ibarra, F. X. Josse-Michaux, M. Losada, and A. Riotto, JHEP **09**, 010 (2006).

[139] S. Blanchet, P. Di Bari, and G. G. Raffelt, JCAP **0703**, 012 (2007).

[140] S. Blanchet and P. Di Bari, Nucl.Phys. **B807**, 155 (2009).

[141] W. Buchmüller, P. Di Bari, and M. Plümacher, Ann. Phys. **315**, 305 (2005).

[142] G. F. Giudice, A. Notari, M. Raidal, A. Riotto, and A. Strumia, Nucl. Phys. **B685**, 89 (2004).

[143] J. Racker and E. Roulet, JHEP **0903**, 065 (2009).

[144] J. R. Ellis, J. E. Kim, and D. V. Nanopoulos, Phys. Lett. **B145**, 181 (1984).

[145] M. Kawasaki, K. Kohri, T. Moroi, and A. Yotsuyanagi, Phys. Rev. **D78**, 065011 (2008).

[146] L. Covi and E. Roulet, Phys.Lett. **B399**, 113 (1997).

[147] A. Anisimov, A. Broncano, and M. Pĺumacher, Nucl.Phys. **B737**, 176 (2006).

[148] A. Pilaftsis, Phys.Rev.Lett. **95**, 081602 (2005).

[149] A. Pilaftsis and T. E. Underwood, Phys.Rev. **D72**, 113001 (2005).

[150] A. Pilaftsis, Phys.Rev. **D78**, 013008 (2008).

[151] R. N. Mohapatra and J. W. F. Valle, Phys. Rev. **D34**, 1642 (1986).

[152] D. Hernandez, M. B. Gavela, T. Hambye, and P. Hernandez, PoS **EPS-HEP2009**, 289 (2009).

[153] G. 't Hooft *et. al.*, Proceedings NATO Adv. Study Inst. Ser. B Phys. **59**, 1(1980).

[154] J. Bernabeu, A. Santamaria, J. Vidal, A. Mendez, and J. W. F. Valle, Phys.Lett. **B187**, 303 (1987).

[155] M. C. Gonzalez-Garcia and J. W. F. Valle, Mod.Phys.Lett. **A7**, 477 (1992).

[156] T. Han and B. Zhang, Phys.Rev.Lett. **97**, 171804 (2006).

[157] F. del Aguila, J. A. Aguilar-Saavedra, and R. Pittau, JHEP **0710**, 047 (2007).

[158] J. Kersten and A. Y. Smirnov, Phys.Rev. **D76**, 073005 (2007).

[159] T. Asaka and S. Blanchet, Phys.Rev. **D78**, 123527 (2008).

[160] S. Blanchet, P. S. B. Dev, and R. Mohapatra, Phys.Rev. **D82**, 115025 (2010).

[161] S. Antusch, S. Blanchet, M. Blennow, and E. Fernandez-Martinez, JHEP **01**, 017 (2010).

[162] D. Aristizabal Sierra, M. Losada, and E. Nardi, JCAP **0912**, 015 (2009).

[163] C. S. Fong and J. Racker, JCAP **1007**, 001 (2010).

[164] M. Garny, A. Hohenegger, A. Kartavtsev, and M. Lindner, Phys. Rev. **D81**, 085027 (2010).

[165] M. Garny, A. Kartavtsev, and A. Hohenegger, arXiv, arXiv:hep-ph/1112.6428 (2011).

[166] E. Roulet, L. Covi, and F. Vissani, Phys. Lett. **B424**, 101 (1998).

[167] S. Blanchet, T. Hambye, and F. X. Josse-Michaux, JHEP **1004**. 023 (2010).

[168] M. C. Gonzalez-Garcia, J. Racker, and N. Rius, JHEP **11**, 079 (2009).

[169] W. Buchmüller and M. Plümacher, Phys. Lett. **B511**, 74 (2001).

[170] E. Nardi, Y. Nir, J. Racker, and E. Roulet, JHEP **01**, 068 (2006).

[171] E. Nardi, J. Racker, and E. Roulet, JHEP **09**, 090 (2007).

[172] C. S. Fong, M. C. Gonzalez-Garcia, and J. Racker, Phys.Lett. **B697**, 463 (2011).

[173] B. A. Campbell, S. Davidson, J. R. Ellis, and K. A. Olive, Phys. Lett. **B297**, 118 (1992).

[174] J. M. Cline, K. Kainulainen, and K. A. Olive, Phys. Rev. **D49**, 6394 (1994).